Records of the Australian Museum (2002) Vol. 54: 215–248. ISSN 0067-1975

The Tumbarumba Basaltic Gem Field, New South Wales: In Relation to Sapphire-Ruby Deposits of Eastern Australia

F.L. SUTHERLAND[1], I.T. GRAHAM[1], R.E. POGSON[1], D. SCHWARZ[2], G.B. WEBB[1], R.R. COENRAADS[3], C.M. FANNING[4], J.D. HOLLIS[1] AND T.C. ALLEN[1]

[1] Geodiversity Research Centre, Australian Museum, 6 College Street, Sydney NSW 2010, Australia

[2] Gübelin Gemmological Laboratory, Maihofstrasse 102, CH-6000, Lucerne, Switzerland

[3] Gemmological Association of Australia (NSW Division), 24 Wentworth Avenue, Sydney NSW 2000, Australia

[4] PRISE, Research School of Earth Sciences, Australian National University, Canberra ACT 0200, Australia

lins@austmus.gov.au

ABSTRACT. Tumbarumba gemfield in the Snowy Mountains basalt province, NSW, yields corundums, zircons and garnet, corroded by magmatic effects and abraded by alluvial transport. Sub-basaltic contours suggest present drainage profiles mimic Miocene sub-basaltic leads. Six types of corundum were identified. Blue, green, yellow (BGY) zoned sapphires (80%) contain ferrocolumbite as a main mineral inclusion and exhibit variable Fe_2O_3/TiO_2 and low Cr_2O_3/Ga_2O_3 (<1). Two sub-types differ in colour absorption spectra, one being unusual in lacking the typical Fe^{2+}-Fe^{3+} charge transfer effects found in such sapphires. Related trapiche-like corundums (5%) show higher Cr_2O_3/Ga_2O_3, possibly due to Fe-Ti oxide exsolution. Vari-coloured, diffuse-zoned and pale blue sapphires (10%) have higher Cr_2O_3/Ga_2O_3 and colour absorption characteristics intermediate between BGY sapphires and pink to red corundums with elevated Cr_2O_3/Ga_2O_3. The BGY and trapiche-like sapphires are considered magmatic, the intermediate sapphires magmatic-metasomatic (possibly through interactions with Cr-bearing serpentinite bodies) and the pink to red corundums metamorphic in origin. Zircons include low- to high-U types. The latter show {100}-{110} prism combinations (unusual in eastern Australian zircons) and suggest incompatible element enriched parental melts. The magmatic sapphires and zircons (U-Pb age 23 Ma) crystallised in deep evolved salic melts, before transport in basalt. Magmatic-metasomatic sapphires contain zircon inclusions with both older inherited U-Pb ages (up to 903 Ma) and younger magmatic U-Pb ages (27–22 Ma). Basalts represent little evolved undersaturated melts (basanites and alkali basalts), and minor near-saturated transitional melts (olivine basalts). Most generated from garnet peridotite sources, but some from spinel peridotite sources. Mantle normalised incompatible multi-element patterns suggest Oceanic Island Basalt (OIB) melts interacted with amphibole (+ apatite) veined mantle. A sapphire and zircon-bearing basalt, also carries kaersutitic amphibole, apatite, alkali feldspar, titanian mica and titanian magnetite xenocrysts from a veined metasomatised source. Olivine micro-dolerite in a plug resembles the Cainozoic basalts in freshness, but its distinct trace element pattern and Early Devonian K-Ar age (400 Ma) indicate an earlier unmetasomatised spinel peridotite source. The Tumbarumba field evolved through explosive gem-bearing basaltic activity between 27–15 Ma and peaked in basalt lava activity. Interactions of basaltic melts with amphibole-rich mantle, serpentinite bodies and metamorphic corundum deposits combined to generate multi-modal gem suites.

SUTHERLAND, F.L., I.T. GRAHAM, R.E. POGSON, D. SCHWARZ, G.B. WEBB, R.R. COENRAADS, C.M. FANNING, J.D. HOLLIS & T.C. ALLEN, 2002. The Tumbarumba Basaltic Gem Field, New South Wales: in relation to sapphire-ruby deposits of eastern Australia. *Records of the Australian Museum* 54(2): 215–248.

http://www.amonline.net.au/pdf/publications/1358_complete.pdf

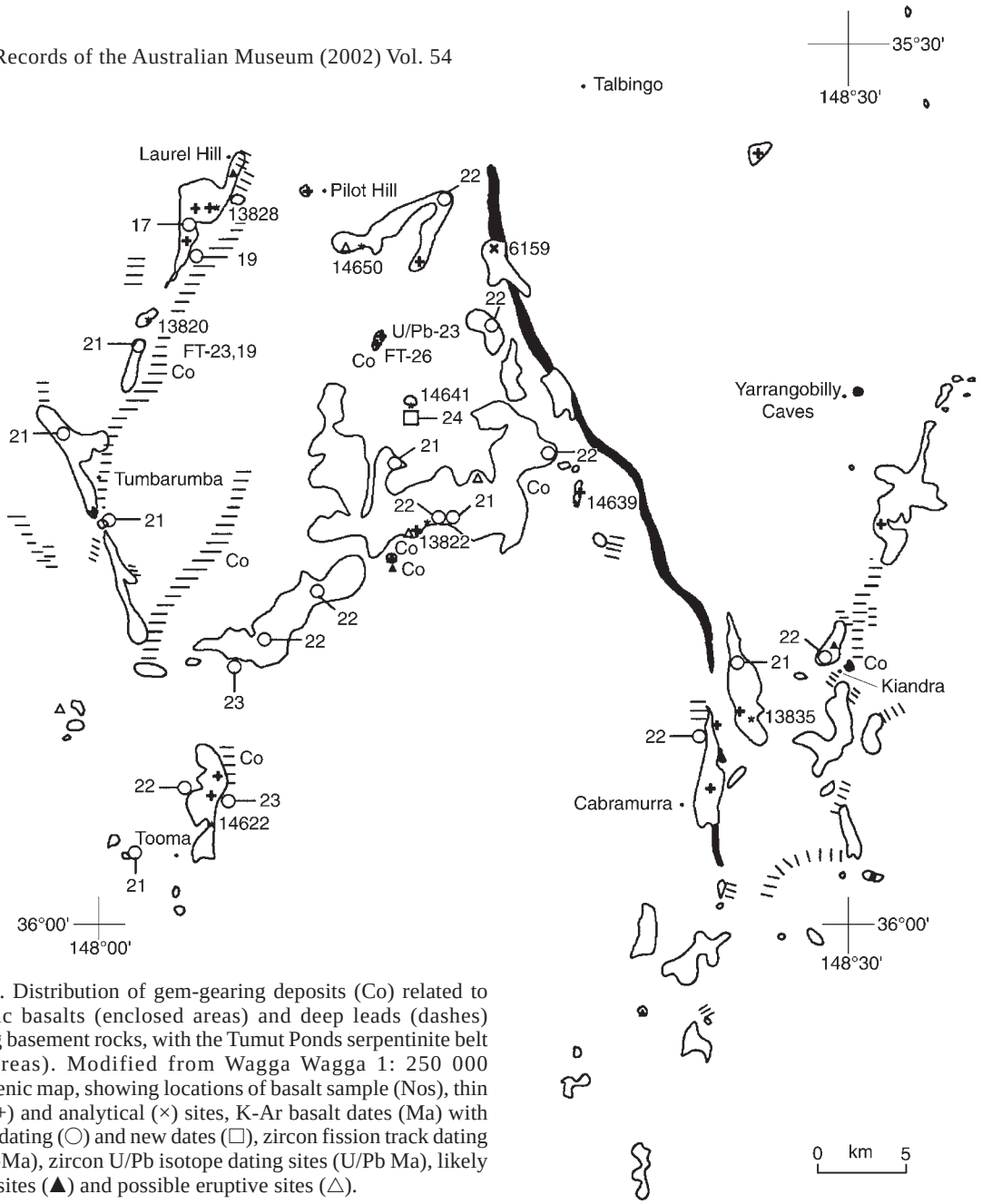

Figure 1. Distribution of gem-gearing deposits (Co) related to Cainozoic basalts (enclosed areas) and deep leads (dashes) overlying basement rocks, with the Tumut Ponds serpentinite belt (filled areas). Modified from Wagga Wagga 1: 250 000 metallogenic map, showing locations of basalt sample (Nos), thin section (+) and analytical (×) sites, K-Ar basalt dates (Ma) with previous dating (○) and new dates (□), zircon fission track dating sites (FT-Ma), zircon U/Pb isotope dating sites (U/Pb Ma), likely eruptive sites (▲) and possible eruptive sites (△).

Eastern Australia is a prime source of gem corundums derived from basaltic eruptives and the larger fields supply sapphires to international markets (Coldham, 1985; Mumme, 1988; Oliver & Townsend, 1993; Sutherland, 1996; Hughes, 1997; Neville & Gnielinski, 1998). Detailed studies of gem corundum associations and their volcanic host relationships concentrate on the larger commercial fields in New England, New South Wales (Coenraads, 1990a,b, 1994; Sutherland *et al*., 1993; Pecover, 1993, 1996; Oakes *et al*., 1996), and in central and northern Queensland (Stephenson, 1990; Krosch & Cooper, 1991a,b; Robertson & Sutherland, 1992; Pecover, 1996; Neville & Gnielinski, 1999). Recent studies of gem corundums from a medium-sized basaltic field (Barrington, NSW) firmly established that both magmatic and metamorphic corundum suites co-exist, with the latter suite including pink sapphires and rubies of potential commercial viability (Sutherland & Coenraads, 1996; Sutherland *et al*., 1998c). In addition, the precise origin of magmatic sapphires, common in eastern Australian suites, is under review (Guo *et al*., 1996a; Sutherland *et al*., 1998a; Upton *et al*., 1999). The Tumbarumba-Kiandra gem field in southern New South Wales includes both sapphire and ruby (MacNevin & Holmes, 1980). Moreover, the provider eruptives are restricted in age (26–18 Ma; Wellman & McDougall, 1974; Young & McDougall, 1993; Sutherland, 1996) so that the volcanic evolution of the field is less complex than in the larger commercial sapphire fields and the long-lived (60–5 Ma) Barrington bimodal corundum field. The current detailed study of the Tumbarumba basaltic gem field aims to further clarify two aspects of gem corundum/basalt relationships:

1 better definition of eastern Australian multi-modal corundum suites,
2 better understanding of eastern Australian magmatic sapphire origin.

The Tumbarumba gemfield lies within the Snowy Mountains basalt province (34.8–36.2°S 147.9–149.7°E; Wellman & McDougall, 1974). The lava field erupted c. 24 km^3 of alkali basalts from 23–18 Ma (Duncan & McDougall, 1989; Knutson & Brown, 1989; Young & McDougall, 1993). The area is covered by the Wagga Wagga (SI 55-15), Canberra (SI 55-16) and Tallangata (SJ 55-3) 1:250 000 Geological Series Sheets. The gemstones are found in sub-basaltic leads and later alluvial redistributions along the present-day drainage, principally along Tumbarumba Creek, Buddong Creek,

Paddy's River and near Kiandra (Fig. 1). These leads and river courses were extensively worked for gold and corundums and zircons were often recovered in the process (Clarke, 1860; Liversidge, 1888; Curran, 1897; Andrews, 1901; Gill & Sharp, 1957; Willis, 1972; Degeling, 1982). An unusual specimen of basalt containing both sapphire and zircon xenocrysts from the Tumbarumba area was drawn to Australian Museum attention in 1993 (K.G. McQueen and P.J. Brown, Geology Dept. University of Canberra). This specimen (Fig. 2a) confirmed a basaltic matrix for these gem minerals and prompted more detailed study of the gemfield and its basalts.

Fieldwork for this study was undertaken between late January–early February and early April 1997 (F.L. Sutherland, I.T. Graham & R.E. Pogson) and was assisted in the Yarrangobilly 1:100 000 Sheet area (R.S. Abell, AGSO, Canberra). Gem concentrates were recovered from three main locations; upper Tumbarumba Creek (S.A. Miller's Property); Upper Buddong Creek (Parsons Gully) and upper Paddy's River (Ruby Creek). A parcel of sapphires from Tumbarumba Creek was purchased by the Australian Museum from P.J. Brown and family, Albion Park Rail, NSW in 1996 to facilitate the study. Additional sapphires and rubies from Tumbarumba Creek were loaned for study by P.W. Millsteed, Geology Department, University of Canberra. Basalts for detailed study were collected along these drainages and in the Cabramurra-Kiandra-Talbingo areas. Gemmological properties of the corundums were investigated at the Gemini Laboratory, Australian Museum (G.B. Webb) and trace element contents and colour absorption spectra were studied through the Gübelin Gemmological Laboratory, Lucerne, Switzerland (D. Schwarz). Corundum mineral inclusions were analysed at the University of New South Wales (R.R. Coenraads) and dated using the Sensitive High Resolution Ion Micro-Probe (SHRIMP) facility, Research School of Earth Sciences, Australian National University (C.M. Fanning and P.D. Kinny). Zircons were dated through fission track analysis (Geotrack International, Melbourne) and garnets were analysed at the electron microprobe facility (EMP), Macquarie University. Basalts were dated and major elements analysed at AMDEL laboratories, South Australia, with an additional date made at the K-Ar dating facility at CSIRO, Sydney, while basalts were analysed for trace elements at the Geochemical Laboratory, University of Queensland.

Geological setting. The Tumbarumba-Kiandra deep leads and basalts (Fig. 1) occupy a dissected landscape developed in underlying Palaeozoic Lachlan Fold Belt and its granitic intrusions (Degeling, 1982; Scheibner & Basden, 1996). Metamorphic assemblages and granitic rocks found with the folded basement rocks have been described by Vallance (1953, 1954a,b). The main gem field and western basaltic leads lie within the Wagga-Omeo terrain along an anticlinorial zone and are mostly entrenched within the mid-Silurian Green Hills granite. There is minor overlap across the enclosing Ordovician flysch sequences and the Tumut Ponds Serpentinite Belt to the west (Stuart-Smith, 1990; Graham, 2000). The Tumut Ponds serpentinitic slivers form a distinctive feature, along the NNW-SSE trending Gilmore Suture and are probably related in age to the 400 Ma Coolac ophiolitic belt (Graham *et al*., 1996). The eastern basalts largely overlie the Goonumble segment on the western boundary of the Molong-Monaro Terrain. This forms a synclinorial zone composed of Early Silurian island arc volcanic rocks and pre-accretionary sedimentary sequences and Late Devonian shelf deposits that include massive limestones. However, basalts in the Round Mountain lead that passes through Cabramurra probably erupted within the Green Hills granitic body west of the Gilmore Suture. The basalts farther east in the Kiandra lead probably largely erupted within the Goonumble subterrain.

The deep leads that include gem-bearing alluvial deposits and basaltic infillings are dominated by approximately north-south trending drainage directions (Degeling, 1982). However, different interpretations exist for the direction of the original deep lead river flows; Andrews (1901) considered northerly flows were involved, while Gill & Sharp (1957) suggested the deep lead drainage was southerly, until tectonic uplifts reversed the drainages, ponding rivers to form overlying lacustrine deposits. Detailed landscape reconstruction based on extensive geochronology of the basalts (Young & McDougall, 1993) demonstrated that the major topographic features were in place by the Mid-Tertiary and that modern stream profiles are closely similar to the palaeodrainage under the basalts. Recent studies of the denudation history of the Snowy Mountains, based on apatite fission track thermochronology, suggest possible accelerated denudation from Cainozoic uplift, but the specific ages of uplift are uncertain (Kohn *et al*., 1999).

The basaltic eruptions that introduced gem corundum, zircon and garnet into the deep leads and later alluvial deposits were mostly confined valley fills with only wider overtopping of leads in places. Subsequent erosion since the Early Miocene has left the basaltic infills as small plateaus, discontinuous elongated strips and peaks and has established a new drainage divide (Gill & Sharp, 1957; Young & McDougall, 1993). The gem minerals were incorporated from the underlying lithosphere into ascending, relatively primitive basaltic melts. Many basalts erupted from their mantle sources, without prolonged residence time (see O'Reilly, 1989), although olivine-spinel-clinopyroxene assemblages (Mackenzie & White, 1970) suggest some crystal fractionation at depth took place en route (see also Fig. 4b).

Seismic studies suggest a depth to mantle of ~50 km in the region (Scheibner & Basden, 1996; Zielhuis & van der Hilst, 1996). Other studies suggest a shallower crust-mantle transition at ~30 km depth (O'Reilly *et al*., 1997). Examples of Jurassic lower crust-upper mantle assemblages beneath the Snowy Mountains are recorded in xenolith suites in basaltic breccia pipes, at Delegate (O'Reilly *et al*., 1988; White & Chappell, 1989). Isotopic dating on these xenoliths suggests granulitic facies metamorphism in the region at ~390 Ma after mafic intrusion and granitic melting (Chen *et al*., 1998). However, precise depths of present crust-mantle lithology remain uncertain as modelling depends on assumed geotherms (Sutherland *et al*., 1998b). The deep structure of the Australian continent, based on surface wave tomography, shows the Tumbarumba region lies over a zone of slow shear velocity in the mantle, extending to over 200 km depth (Simons *et al*., 1999). These slow mantle anomalies may reflect present elevated thermal zones among other possibilities, but their exact nature and status relative to Australian lithosphere at 20 Ma is conjectural.

Gem minerals

The gem minerals in heavy mineral suites include resorbed corundum (sapphire, ruby), zircon, garnet and rare pale green orthopyroxene. These, with opaque spinels and ilmenite, are derived from basaltic sources. Rutile, cassiterite, dravitic tourmaline, yellow to green monazite, biotite, topaz, small euhedral zircons and gold probably

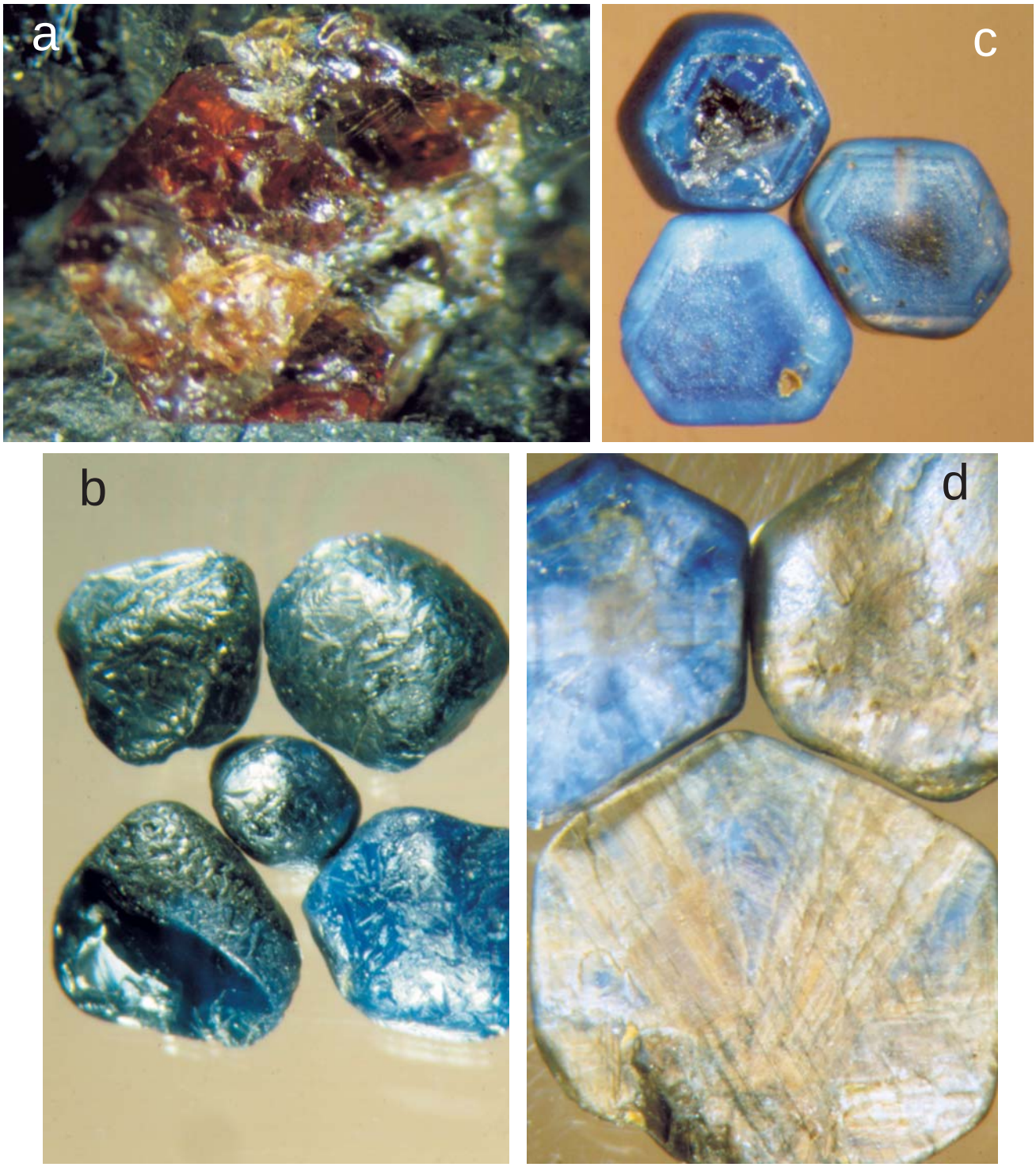

Figure 2. Gemstones, Tumbarumba field, photography G. Webb. a—Zircon xenocryst in basalt matrix, Ruby Creek. The crystal is 3 mm across. b—Strongly corroded blue sapphires, Tumbarumba Creek. Crystals to 6 mm across. c—Zoned "agate" sapphires, Tumbarumba Creek. Crystals to 6 mm across. d—Trapiche-like sapphires, with radiating silk zones, Tumbarumba Creek. Crystals to 11 mm across. e—Diffuse-zoned, vari-coloured sapphire crystals, Tumbarumba Creek. Crystals to 7 mm across. f—Pink to red corundums, Tumbarumba Creek. Crystals to 11 mm across.

come from granitic and associated vein rocks, while sillimanite crystals and serpentinitic fragments come from metamorphic sources. Diamonds were recorded with sapphires and rubies in the Tooma deep lead (Willis, 1972).

Corundums. Around one thousand corundum crystals, grains and fragments were examined by binocular microscope to sort them into different crystal groups and colours. Grains ranged up to 11 mm in size. All crystals showed magmatic corrosion (Fig. 2b–d) and small, pitted abrasions due to mechanical transport. Rare crystals show relics of dark rinds, typical of spinel reaction rims found on basaltic sapphires elsewhere (Stephenson, 1990). Main groups observed (Fig. 2b–d) were:

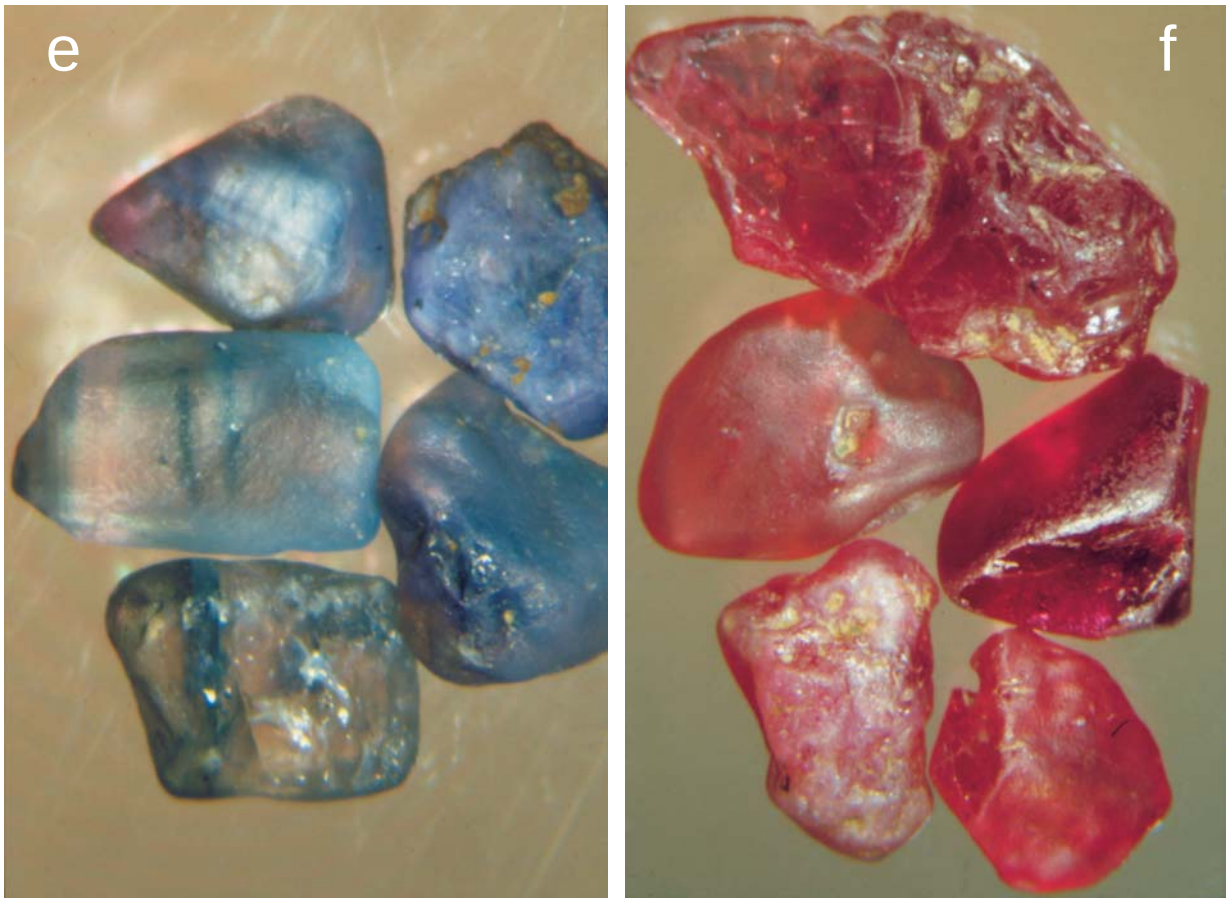

Figure 2, continued.

Group 1 Strong blue transparent crystal fragments, with pronounced blue/green pleochroism.
Group 2 Strong blue crystal fragments; some with yellow colour bands or yellow cores.
Group 3 So called "agate" sapphires; many with dark blue cores, composed of milky hexagonal outer banding.
Group 4 Particoloured blue, green crystal fragments with diffuse colour zoning.
Group 5 Large, milky blue crystal fragments with green and bronze (silk-rich) colour zoning.
Group 6 Coarse, opaque crystal fragments with silk radiating from a central core, in a trapiche-like pattern.
Group 7 Small transparent, particoloured light blue and green (± yellow) crystals and part crystals with an elongated barrel shape, showing a diffuse pale pink core.
Group 8 Small pale blue crystal fragments with undifferentiated pinkish or mauve zones.
Group 9 Pink to red crystal fragments and crystals; in one example, hexagonal colour zoning of pale pink and milky bands was observed.

Groups 1–5 resemble typical representatives of the Blue-Green-Yellow (BGY) suite of corundums from basaltic regions (Sutherland *et al*., 1998a) and make up 80% of the Tumbarumba sample. Group 6 (5%) are corundums distinctive because of their strong silk structure, but typically accompany BGY suite corundums elsewhere. Group 7 (10%) is noted for more complete crystals and is distinctive in appearance compared to the fragments found in the other groups. Groups 8–9 (5%) include types that resemble the fancy coloured sapphire and ruby corundum suite from basaltic regions (Sutherland *et al*., 1998c).

Group 9, which includes ruby, was limited to seven studied grains. One was light pink, three were bright pink, two were purple red and one red. Small rounded remnant crystal faces were visible on each grain; in one case (light pink) the bi-pyramidal crystal shape was observed. Grains ranged from 5–11 mm in length. They exhibited a medium red fluorescence when exposed to Long Wave Ultra-Violet Light but were inert under Short Wave Ultra-Violet Light. Polysynthetic twin planes were evident as well as crystals containing healing fractures, fluid inclusions and 2- and 3-phase inclusions, with some subsequent iron-staining. The red crystal was internally clear and showed a ruby spectrum using a diffraction grating spectroscope—a couplet in the red, absorption in the yellow-green and three lines in the blue. All pink crystals showed a couplet in the red, due to chromium.

Trace elements. Electron Micro-Probe (EMP) analyses of inclusion-bearing sapphires showed Fe as the main substituting element (up to 1 wt% Total FeO), with lesser Ti and in some cases minor Cr as other substitutions in the Al_2O_3 lattice (see Table 1). Rarely, sapphires contain detectable Nb, Si, Mn or Ca. To investigate the distributions of these elements and their role as colouring agents in Tumbarumba corundums, 72 crystals (CORTUM 1–72) were analysed for Fe, Ti, Cr and V by "chemical fingerprinting". This involved element analysis of main components and minor constituents with the aim of defining groups ("populations"), e.g., gemstones originating from a specific genetic environment or a specific geographic region and identification of individuals by objective and reproducible methods. This employed Energy-dispersive X-ray fluorescence (EDXRF) using a Spectrace 5000 EDXRF system, in a method developed between the University of Basel

(W.B. Stern) and the Gübelin Gemmological Laboratory (D. Schwarz). This method is a useful tool for investigating geological affinities of natural corundums (Stern, 1984; Sutherland *et al*., 1998c; Schwarz *et al*., 2000; Schwarz & Stern, 2000). The main chromophores for corundum are Fe and Ti, ± Cr, while V is generally below the detection limit of the method (± 0.005 wt% V_2O_3) and has little input into Tumbarumba corundums apart from one group.

In trace element variations, the corundums fall into five main types (Table 2).

Type 1 Typical blue, green, yellow corundums (Groups 1–5) that show high Fe, variable Ti, noticeable Ga and negligible Cr and V contents.

Type 2 Trapiche-like, silk structured sapphires (Group 6) that show similar trace element ranges to the BGY sapphires, but modified by abundant Ti and Fe exsolution effects.

Type 3 Blue, green, pink diffuse zoned corundums (Group 7) that also show high Fe, low-moderate Ti, but have noticeable Ga and Cr Contents.

Type 4 Paler blue to white zoned sapphires (Group 8) that show relatively low Fe, moderate to high Ti, quite low Ga, but have noticeable Cr and V contents.

Type 5 Dark pink to purple red ruby (Group 9) with significant Cr, but which includes low and high Fe variants that also differ in Ti, Ga and V contents.

The most useful trace element discriminant for separating corundums of magmatic and metamorphic origin (Schwarz *et al*., 2000) are correlation diagrams that plot Cr_2O_3/Ga_2O_3 against Fe_2O_3/Cr_2O_3 or Fe_2O_3/TiO_2 (Fig. 3a,b). Magmatic corundums in general show higher Ga and lower Cr contents than metamorphic corundums, apart from some Ga-enriched metasomatic corundums. Metasomatic corundums can be distinguished using a correlation diagram that plots TiO_2/Ga_2O_3 against Fe_2O_3/Cr_2O_3 (Fig. 5) where they give Fe_2O_3/Cr_2O_3 ratios between 20–110. Magmatic corundums typically give Cr_2O_3/Ga_2O_3 ratios below 1 and Fe_2O_3/Cr_2O_3 ratios between 70–800. Most of the blue, green and yellow zoned colour groups from Tumbarumba (Cr_2O_3/Ga_2O_3 0.10–0.50; Fe_2O_3/Cr_2O_3 >100; Fe_2O_3/TiO_2 4–80) fall in the magmatic field, which is typical for many eastern Australian sapphire suites. "Trapiche-like" Type 2 corundums, however, show intermediate Ga_2O_3/Cr_2O_3 (0.35–2.0), extend to Fe_2O_3/Cr_2O_3 <100 and have relatively restricted Fe_2O_3/TiO_2 (9–35). The pale blue, green and pink hues Type 3 corundums show trace element contents intermediate to those of the typical magmatic and metamorphic types, with some overlap in Cr_2O_3/Ga_2O_3 ratios (0.15–30). This makes their precise assignments uncertain. In contrast, rare Tumbarumba pale blue, mauve to pink Type 4 and pink-red Type 5 corundums extend to higher Cr_2O_3/Ga_2O_3 typical of metamorphic ratios (1–25), but trend to lower Fe_2O_3/TiO_2

Table 1. Ferrocolumbite inclusion and sapphire analyses, sapphire (S2), Tumbarumba gem field.

wt% oxide	crystal 1	crystal 2	crystal 3	host sapphire
TiO_2	4.43	4.56	4.12	0.01
Al_2O_3	0.04	0.06	0.03	99.49
Cr_2O_3	0.00	0.00	0.02	
FeO	12.84	12.65	12.75	0.97
MnO	5.41	5.59	5.76	
MgO	0.88	0.91	0.88	
CaO	0.03	0.04	0.02	
ZrO_2	1.23	1.44	0.96	
Nb_2O_5	73.18	72.33	72.93	0.07
Ta_2O_5	1.71	1.20	1.59	
ThO_2			0.11	SiO_2 0.01
total	99.75	98.78	99.17	100.55
cations	(based on 6 oxygens, and partitioning of FeO to FeO/Fe_2O_3)			
Ti	0.1843	0.1908	0.1725	
Al	0.0025	0.0037	0.0017	
Cr	0.0000	0.0000	0.0011	
Fe^{2+}	0.5942	0.5623	0.5712	
Fe^{3+}	0.0000	0.0260	0.0219	
Mn	0.2535	0.2635	0.2714	
Mg	0.0722	0.0754	0.0732	
Ca	0.0015	0.0024	0.0011	
Zr	0.0330	0.0391	0.0259	
Nb	1.8304	1.8186	1.8345	
Ta	0.0257	0.0182	0.0241	
Th	0.0000	0.0000	0.0014	
total	2.9973	3.0000	3.0000	

1 $(Fe_{0.59}\ Mn_{0.25}\ Mg_{0.07})_{0.91}\ (Nb_{1.83}\ Ta_{0.03}\ Ti_{0.18}\ Zr_{0.03})_{2.07}O_6$
2 $(Fe_{0.59}\ Mn_{0.26}\ Mg_{0.08})_{0.93}\ (Nb_{1.82}\ Ta_{0.02}\ Ti_{0.19}\ Zr_{0.04})_{2.07}O_6$
3 $(Fe_{0.59}\ Mn_{0.27}\ Mg_{0.07})_{0.93}\ (Nb_{1.83}\ Ta_{0.02}\ Ti_{0.17}\ Zr_{0.03})_{2.05}O_6$

Analyst: R.R. Coenraads.

Table 2. Geochemical trace element ranges (wt%), Tumbarumba corundums.

type	description	Fe_2O_3	TiO_2	Ga_2O_3	Cr_2O_3	V_2O_3
Type 1A*	blue, green ± yellow, white, colour zoned	1–2	0.02–0.15	0.02–0.035	<0.005	<0.01
Type 1B*	blue, green ± yellow, white, colour zoned	1.0–2.1	0.01–0.35	0.020–0.040	<0.01	<0.01
Type 2	opaque, blue, dark trapiche-like silk	1–2	0.08–0.21	0.015–0.030	<0.01–0.03	<0.01–0.015
Type 3	blue, green, pink, diffuse zoned	0.8–1.5	0.01–0.22	0.015–0.025	0.01–0.04	<0.01–0.015
Type 4	blue, light blue, white colour zoned	0.40–0.65	0.07–0.24	0.01–0.025	0.015–0.035	0.01–0.03
Type 5	dark pink, purple red					
	low Fe	0.06	0.1	0.02	0.25	0.02
	high Fe	0.7	0.05	0.005	0.15	<0.005

* Type 1A and 1B show different Fe colour absorption patterns (see text).

Type 1A (15 specimens, CORTUM 13,23,27,30,31,36,37,38,48,56,64,65,66,67,68)
Type 1B (14 specimens, CORTUM 10,12,21,22,39,40,41,42,43,50,60,69,71,72)
Type 2 (8 specimens, CORTUM 15,16,17,18,19,57,58,59)
Type 3 (19 specimens, CORTUM 4,5,6,7,8,9,11,14,20,24,32,33,34,51,52,53,54,55,63)
Type 4 (6 specimens, CORTUM 1,2,3,25,46,70)
Type 5 (2 specimens, CORTUM 44,45)

(1–10). The pale blue sapphires have relatively low Cr_2O_3/Ga_2O_3 values (1–3) compared to the ruby values (>10).

Colour absorption spectra. Polished corundums were studied with a Perkin Elmer Lambda 9 spectrophotometer at the Gübelin Gem Lab. Ultraviolet-visible-near infrared spectra (UV-vis-NIR, 280–880 nm range) absorption behaviour was recorded from selected stones, with polarised spectra being taken on crystals orientated normal to the c-axis (D. Schwarz analyst).

The BGY "magmatic" (Type 1) group shows two distinct sub-groups in their absorption spectra.

Type 1A spectra are combination spectra dominated by the Fe^{3+}-line groups 375 and 475 nm. This basic absorption spectrum becomes superimposed by intense absorption bands, assigned to Fe^{2+}-Ti^{4+} charge transfer processes (maxima around 600 nm, with polarisation ⊥ c > // c, and ~700 nm, with polarisation // c = ⊥ to c). There is also Fe^{2+}-Fe^{3+} pair absorption (maximum ~870–880 nm, with polarisation ⊥ c > // c). These spectra are typical for BGY sapphires elsewhere (Sutherland *et al*., 1998c; Schwarz *et al*., 2000).

In contrast, Type 1B spectra do not show the typical absorption bandss in the NIR region related to Fe^{2+}-Fe^{3+} charge transfer transitions (Fig. 6a). This unusual combination of chemical and absorption features does not seem to have been previously described in the literature.

The trapiche-like (Type 2) sapphires are almost opaque, so that absorption spectra could not be recorded. This also applies to some of the more opaque (Type 1) sapphires.

The blue, green, pink (Type 3) sapphires show quite unusual absorption behaviour in the UV-vis-NIR range (Fig. 6b). Strong Fe^{3+}-line groups are representative at 375 and 475 nm and are accompanied by pronounced absorption bands ~550 nm and in the NIR. The latter are related to

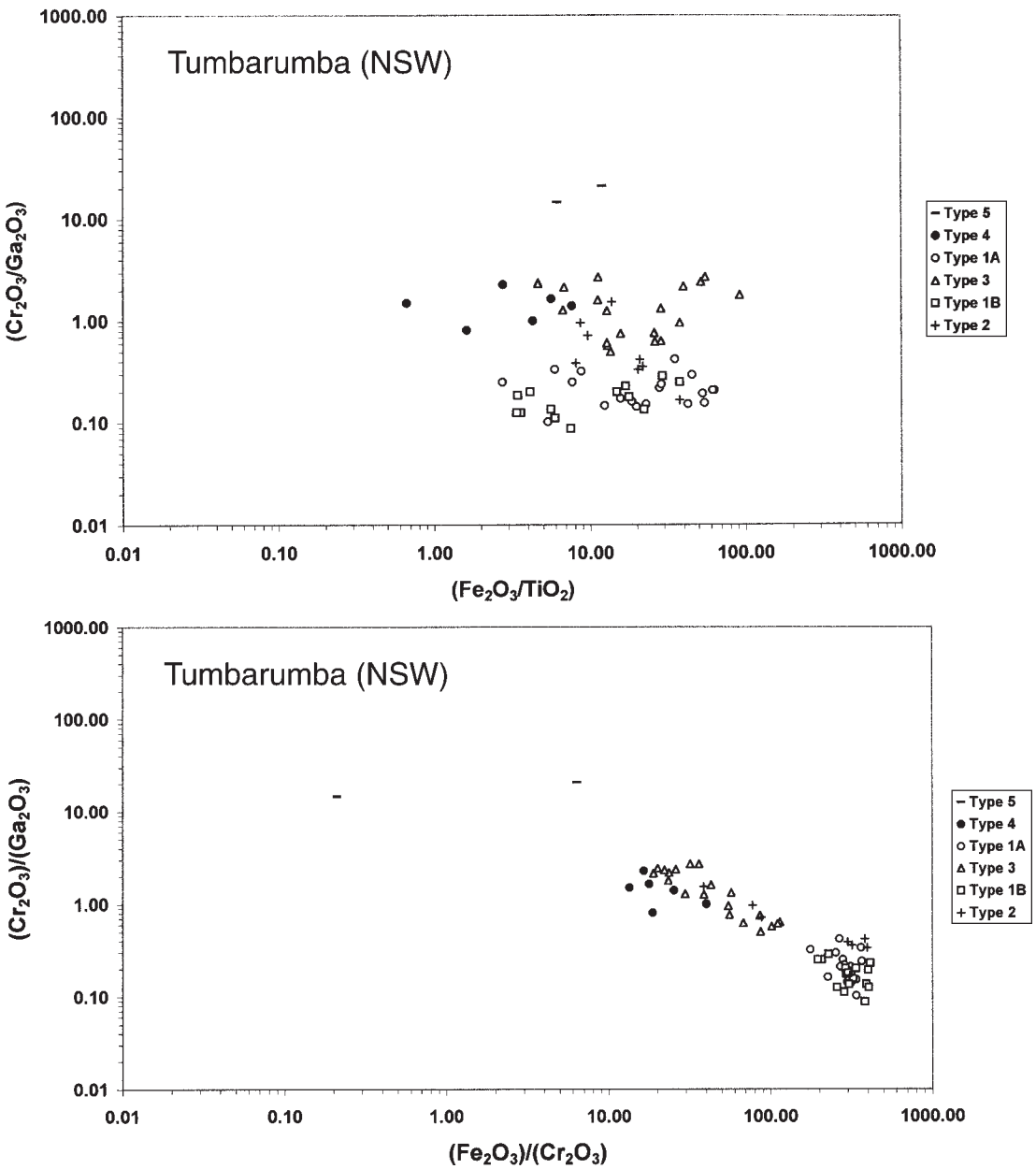

Figure 3. Chemical ratio variation diagrams, Tumbarumba corundums. Type 1A (○), Type 1B (□), Type 2 (+), Type 3 (△), Type 4 (●), Type 5 (-). a—Cr_2O_3/Ga_2O_3 against Fe_2O_3/Cr_2O_3. b—Cr_2O_3/Ga_2O_3 against Fe_2O_3/TiO_2.

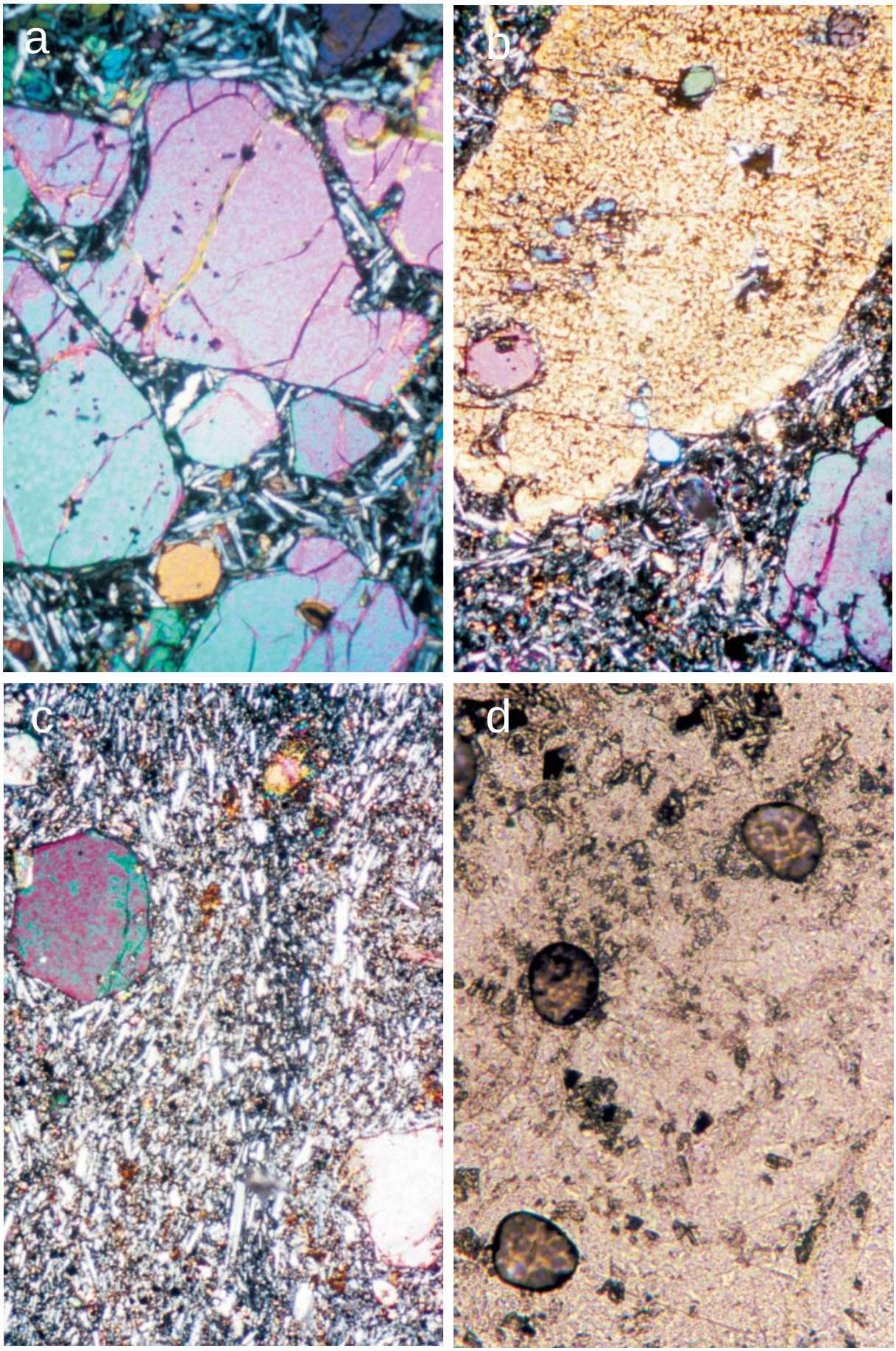
a
b
c
d

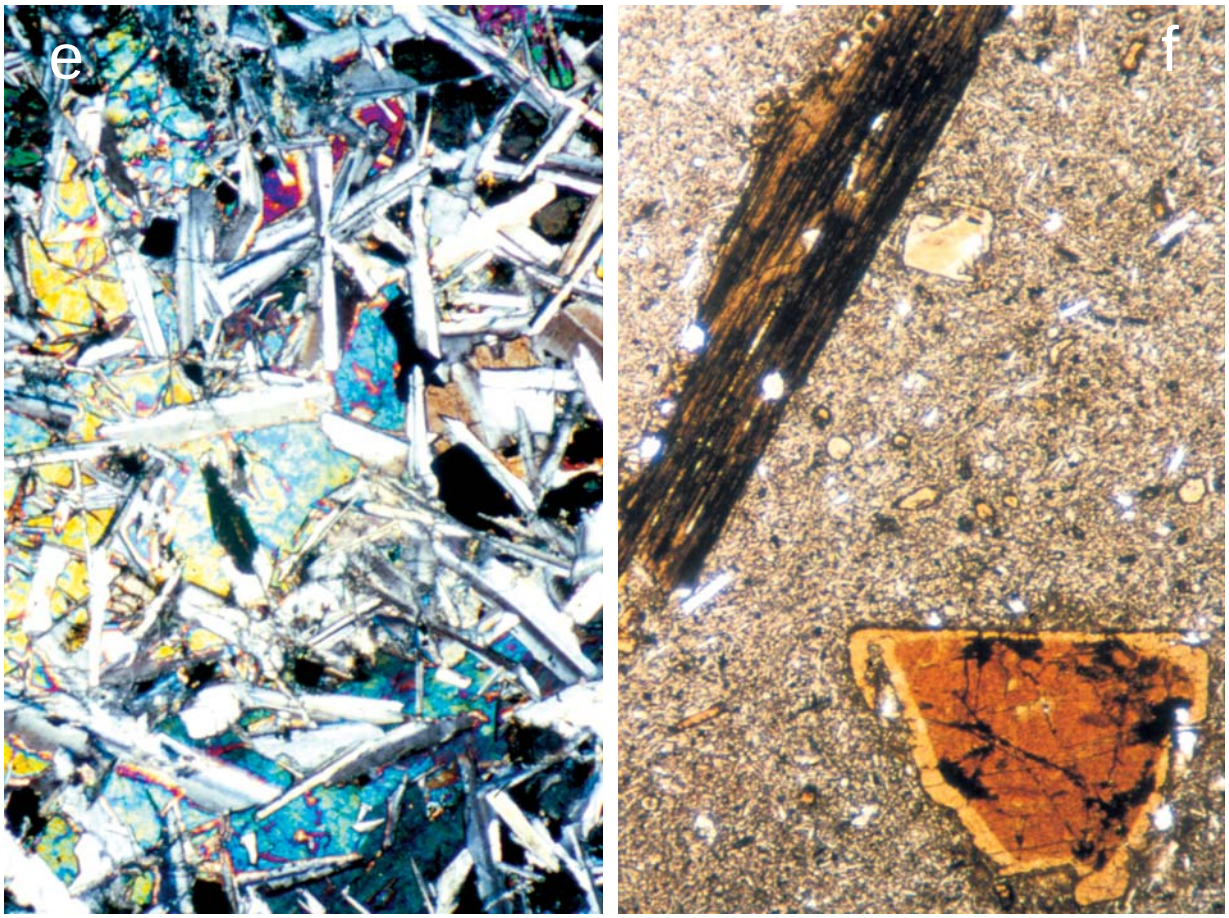

Figure 4. Photomicrographs of Tumbarumba basalts (F.O.V. = Field of View width). a—Olivine phyric alkali basalt, Yorkers Creek (DR14639). F.O.V. 2.5 mm. b—Augite xenocryst, with included olivine and reacted sieved interior, and overgrowth rim, Tooma (DR14662). Field of view (F.O.V) width 1.25 mm. c—Olivine and augite microporphyritic, flow-banded basanite, Jimmies Hill (DR14641). F.O.V. 2.5 mm. d—Feldspathic (sodian plagioclase) segregation, with rounded vesicles, in alkali basalt, Laurel Hill (DR13828). F.O.V. 3.75 mm. e—Olivine micro-dolerite, Ruby Creek (DR13822). F.O.V. 2.5 mm. f—Kaersutite, biotite and apatite xenocrysts in transitional hawaiite, Ruby Creek (D48682). F.O.V. 3.75 mm.

Fe^{2+}-Fe^{3+} charge transfer transitions and the absorption in the 500–600 nm range is caused by Cr^{3+} as well as by Fe^{2+}-Ti^{4+} charge transfer transitions. This absorption may be more intense than the Fe absorption.

The paler blue "metamorphic" (Type 4) sapphires show absorption spectra that lack pronounced features. Normally a rising "background" absorption towards the UV-region is present. Cr^{3+} and Fe^{2+}-Ti^{4+} charge transfer absorption bands are only weakly developed, as are Fe^{3+}-line groups. The Fe^{2+}-Fe^{3+} charge transfer absorption in the NIR as typically seen in magmatic sapphires is absent.

The pink to red "metamorphic" (Type 5) corundums provide absorption spectra dominated by Cr^{3+} bands. The low-Fe ruby shows an almost pure Cr^{3+} absorption pattern, whereas the spectrum of the high-Fe ruby has an intense absorption shoulder in the UV at ~320 nm (related to Fe) and a distinct Fe^{3+} line group at 375 nm.

Mineral inclusions. Exsolved iron and titanium oxides, commonly aligned along crystal directions, prevail in many of the sapphire groups. Some sapphires contain discrete syngenetic or protogenetic crystals and several were sliced and polished to expose such inclusions for analysis. Determinations used a automated Cameca SX 50 CAMEBAX Electron Micro-Probe (EMP), equipped with 4 wave length-dispersive spectrometers (WDS) and an energy-dispersive spectrometer (EDS) attachment, in the Material Sciences Facility, University of New South Wales, Sydney. Operating conditions included an accelerating voltage of 15kV, a sample current of 20nA, PAPS software for processing raw counts and an ASTIMEX standard block.

The main syngenetic mineral analysed was ferrocolumbite, in euhedral, elongate opaque crystals. Three separate crystals within a sapphire (S3) showed a narrow compositional range (Table 1), approximating $(Fe_{0.59}\,Mn_{0.26}\,Mg_{0.07})_{0.92}\,(Nb_{1.83}Ta_{0.03}Ti_{0.18}Zr_{0.03})_{2.06}O_6$. This composition is typical of ferrocolumbite inclusions in basaltic "magmatic" sapphire suites (Guo *et al*., 1996a; Sutherland *et al*., 1998a). It is low in Ta and in this respect matches ferrocolumbite inclusions in Jizerská Louka, Czech Republic sapphires (Malíková, 1999). Orange inclusions in the edge of another sapphire (S2) contain high TiO_2 (84–85 wt%), with variable amounts of Al_2O_3 (6–7%), BaO (3–4%), P_2O_5 (2–3%) and FeO (2–3%). The main mineral present matches anatase, with some Fe-oxide, when examined by laser Raman spectroscopy (M. Garland, Geology Department, University of Toronto, pers. comm. 1999) and the Ba, Al and P may represent a gorceixite-like phase. These inclusions may mark breakdown and metasomatic alteration of original rutile. Other orange-red grains, associated with tension-like fractures, have subhedral shape and form a granular mass with a rough surface. The

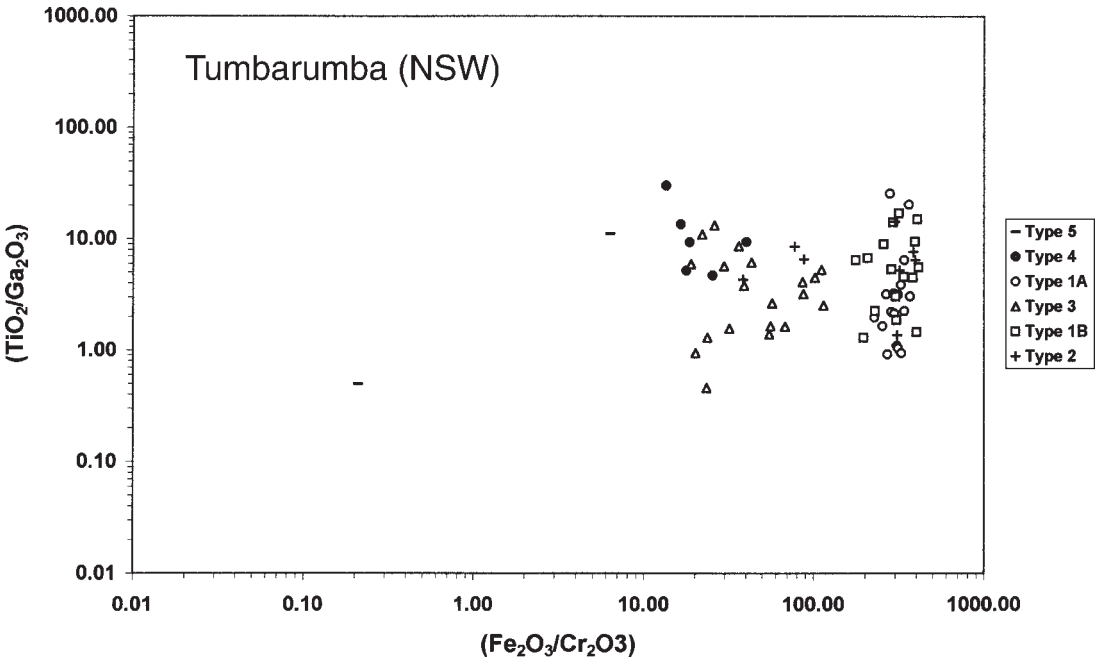

Figure 5. Chemical ratio variation diagram, Tumbarumba corundums. Types as for Fig. 3. TiO_2/Ga_2O_3 against Fe_2O_3/Cr_2O_3.

granular mass takes poor polish and shows low reflectivity. It is Fe-rich and may represent a primary iron oxide, altered by fluids invading along the surrounding cracks. A small inclusion of feldspathic glass was also identified by EDS and has a composition approaching anorthoclase.

Other analysed inclusions include ferrocolumbite (CORTUM 11, 20, 46), ilmenorutile (CORTUM 28), zircon (CORTUM 46, 63) and thorian monazite (CORTUM 46). Ferrocolumbite compositions (7 analyses) range between 71–75% Nb_2O_5, 11–17% FeO, 1.5–8% MnO, 3–5% TiO_2, <0.5–2% Ta_2O_5, 1–2% ZrO_2, 0–2% SiO_2, 0.5–1.5%MgO and 0–1% Al_2O_3. Ferrocolumbites in Type 1 sapphires are enriched in FeO compared to MnO in ferrocolumbite in a Type 3 sapphire. Ilmenorutile (2 analyses) contains between 41–44% Nb_2O_5, 24–32% TiO_2, 13–18% FeO, 2–4% Ta_2O_5, 1–2% SiO_2 and some Zr substitution for Nb. Zircons in Type 3 sapphires (2 analyses) contain minor FeO and TiO_2 (up to 4%) and traces of HfO_2, ThO_2, UO_3 and Sc_2O_3 (<0.5%). Thorian monazite in Type 3 sapphires (2 analyses) contains 24–25% Ce_2O_3, 21–23% ThO_2, 11–13% La_2O_3, 10–11% Nd_2O_3 and minor UO_3, Sm_2O_3, Gd_2O_3 and Pr_2O_3 (<4%).

Zircon megacrystst. Zircons range up to 8 mm long and show a variety of colours and crystal habits. Three main groups were separated from concentrates examined under the binocular microscope, viz:

- darker orange brown and red grains
- colourless to pale yellow grains
- brightly polished pale grains.

The darker grains dominate the Parsons Gully and Ruby Creek samples, while the paler and brightly polished grains are more prevalent within the Tumbarumba Creek samples. The zircon in basalt is a euhedral prismatic orange-brown crystal, 3 mm across, with fractured surface (Fig. 2a).

Crystal features. Surface and crystallographic features of the zircon suites were studied in detail (J.D. Hollis). Strong magmatic resorption and mechanical abrasion are common on the larger crystals, particularly in the Tumbarumba Creek and Parsons Gully suites. Many resorbed zircons exhibit surface "slits". These typically develop by later etching within a regolith to form baddeleyite (ZrO_2) rinds, which erode off leaving elongate indentations. The abrasive wear on the large crystals is typical of zircons that travel at least 20–30 km from their release site in high energy, large river systems, based on Victorian studies. However, small zircons (<2 mm fraction) show lesser abrasion, with some crystals (<0.5 mm) being practically unabraded, suggesting a degree of protection from abrasion. The zircon suites exhibit very high proportions of resorbed crystals, peaking in size distribution in the >2 mm + range. The relatively low proportion of smaller crystals reflects a typical resorption pattern where small zircons were largely dissolved.

Only the Ruby Creek suite preserves zircons with sufficient crystal characteristics to separate them into different groups. Three groups are recognised, with notation after Dana (1932):

1 Orange-red zircons; with forms largely 1st order pyramids {111} and prisms {110}, with minor 2nd order prisms {100}. Some crystals range into 2nd order prisms {100}, combined with major or minor development of 1st order pyramids {111} and ditetragonal pyramids {311}
2 Mauve zircons; with 1st order pyramids {111} and prisms {110} ± minor 2nd order prisms {100}.
3 Paler highly resorbed zircons; with 1st order pyramids {111} and prisms {110} ± ditetragonal pyramids {311} and 2nd order prisms {100}.

In general, Tumbarumba zircons predominantly exhibit 1st order prism forms ranging into 1st and 2nd order prism combinations. Ditetragonal pyramids tend to develop mostly with the prism combinations. The Tumbarumba suites are relatively unusual among eastern Australian basaltic suites with their lack of pure 2nd order prism crystals, and in this aspect they are closest to Boat Harbour, Tasmania, zircons in their morphology (Hollis & Sutherland, 1985).

Geochemistry. Detailed analyses of zircons were not made, but U contents were measured during fission track dating of the three main zircon groups (Table 3). The darker coloured groups yielded moderate U contents (95–879 ppm, av. 387 ppm), the pale coloured group generally had higher U (36–1433 ppm, av. 486 ppm), while the bright polished group was low in U (37–130 ppm, av. 103 ppm). This suggests separate zircon sources for the groups, in keeping with differences in fission track ages. An orange brown crystal used for U-Pb isotope dating (Table 4), showed high U (1744 ppm) and Th (6050 ppm) with low U/Th ratio (0.29).

Garnet. Bright pink, transparent garnet grains are abundant as broken fragments in the gem concentrates. They form small, magmatically corroded grains and rare composite aggregates up to 5 mm across. They resemble the pink corundums in the concentrates and without detailed inspection are sometimes mistaken for them. Crystal faces are rarely preserved and some grains are coated with a fusion crust of dark Fe and Mn oxide material.

Geochemistry. The crystals and a composite garnet microxenolith were polished and analysed by EMP (Table 5). Representative analyses show that the garnets are manganese-bearing almandines ($al_{68–75}$ $py_{12–20}$ $sp_{4–15}$ $an_{3–4}$). The microxenolithic garnetites contain minor accessory minerals including quartz, calcite and muscovite. The garnet composition and accessory phases suggest derivation from a metamorphic crustal assemblage before incorporation into basalt melt.

Sub-basaltic drainage

The gem minerals represent minor alluvial components within sub- and inter-basaltic lead systems. To better understand their origin, pre-basaltic drainage channels were analysed along the lines used in previous studies in the Central Volcanic Province in New South Wales (Coenraads, 1990a,b). The sub-basaltic topography was analysed at a scale of 1:25 000 (on the Yarrangobilly, Ravine, Cabramurra, Tumbarumba, Tooma, Batlow and Courabyra map sheets) using geology mapped by Graham (2000). The geological boundaries between the basalts and older basement rocks, supplemented by field observation of direct contacts, were overlain on the topography. Elevations for each mapped boundary were then plotted and contoured. Source rocks for the gemstones found in the sub-basaltic deep leads must lie up palaeo stream unless they have been removed from the catchment area by erosion. This study allows for more detailed appraisal of the gem-related palaeodrainage systems in the Tumbarumba-Cabramurra area than in the previous general reconstruction of Young & McDougall (1993).

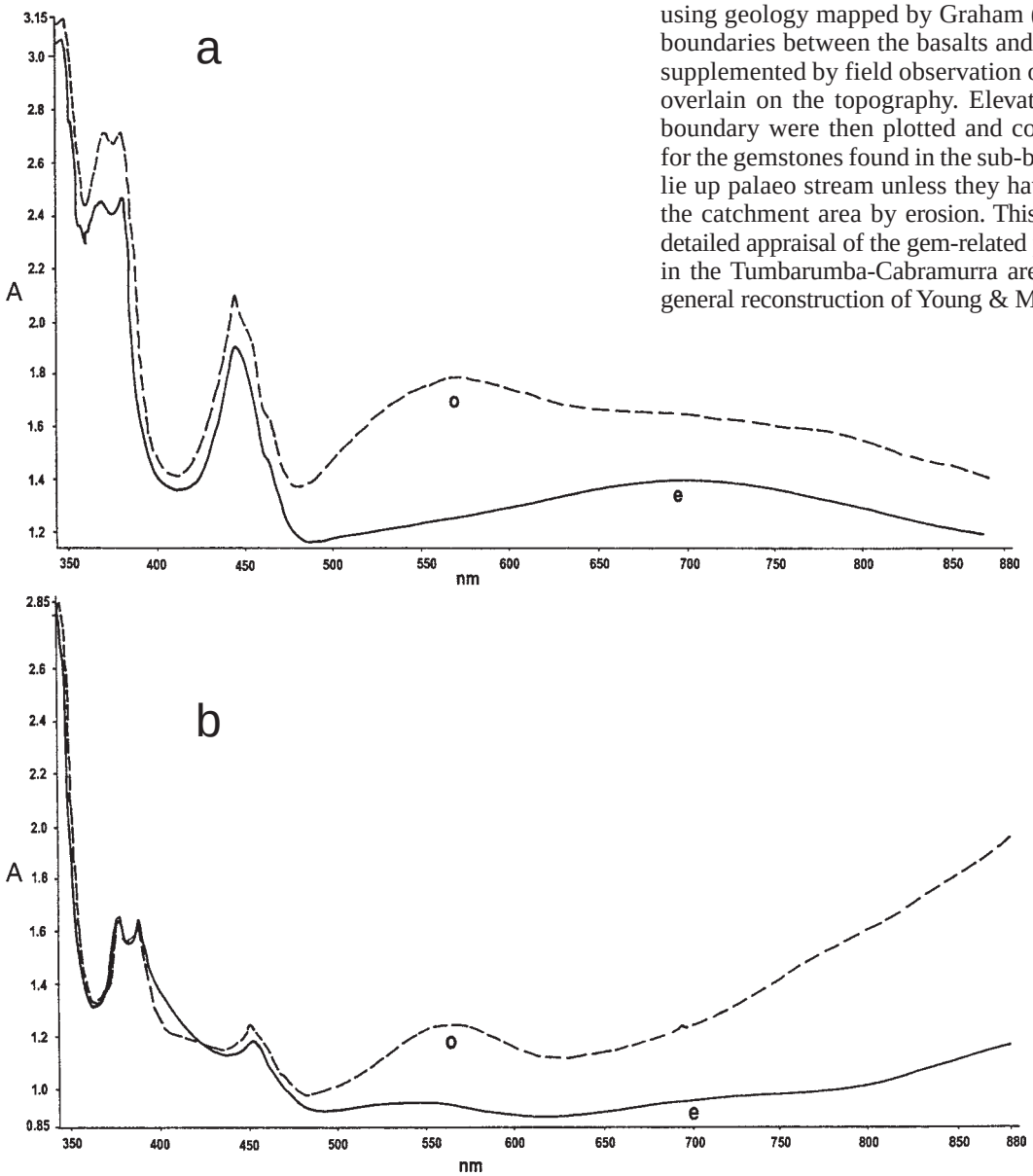

Figure 6. Representative colour absorption spectra (amplitude, A, plotted against wavelength in nm), unusual corundum types: a—Type 1b sapphire, ordinary ray (dashed line) and extraordinary ray (solid line). Blue green sapphire (CORTUM 50). b—Type 3 sapphire, with o- and e-rays as in Fig. 6a. Blue sapphire (CORTUM 08).

Table 3. Zircon fission track results, Tumbarumba-Cabramurra area.

number of grains	Ns	Ni	Na	ratio	RHOs	RHOi	age (Ma) ± error	U ppm (av.)
Parsons Gully, Buddong Creek *(sub-basaltic lead)*								
dark red grains: 4	283	534	100	0.525	3.23E+06	6.09E+06	26.0±1.1	149–505 (av. 290)
Tumbarumba Creek, Miller's property *(sub-basaltic lead)*								
dark red grains: 8	154	215	69	0.760	3.533E+06	4.933E+06	22.8±1.0	95–819 (av. 361)
pale grains: 8	237	312	77	0.770	4.902E+06	6.439E+06	23.6±0.9	153–1433 (av. 486)
bright polished grains: 9	52	83	100	0.610	8.193E+05	1.322E+06	18.6±1.2	37–161 (av. 103)

Determinations from Geotrack Reports No. 30 (Buddong Creek, compiled by P.F. Green & I.R. Duddy, 1985) and No. 655 (Tumbarumba Creek, compiled by P.F. Green, 1997). Standard (RHOD) and induced track RHOi densities were measured on external detector faces and fossil track densities (RHOs) on internal mineral surfaces. Ages were calculated using a Zeta of 87.9 (Buddong Creek) and 87.7±0.8 (Tumbarumba Creek) for dosimeter glass U3. Ns is the number of spontaneous tracks, Ni the number of induced tracks and Na area of units of counted tracks. RHOD (cm^{-2}) is 1.119E+06 (Buddong Creek) and 6.858E+05 (Tumbarumba Creek). Ages represent pooled ages and errors are quoted as ±1σ.

Yarrangobilly 1:100 000 synthesis. The detailed analyses of basaltic leads from the seven 1:25 000 map sheets were combined at 1:100 000 scale (Yarrangobilly Sheet 8526) to provide an overview of the sub-basaltic palaeochannels and their catchments (Fig. 7).

The highest regions of this area lie along the Great Dividing Range (Cabramurra 1:25 000 Sheet, 35º55'S 148º25'E) at elevations still exceeding 1600 masl. Flat topped basalt hills and abandoned gold diggings preserve sections of Miocene palaeochannels that once flowed from the palaeohighs south of Cabramurra. Substantial palaeochannels descending to the north include the Cabramurra (1560 to 1320 masl, with over 80 m thickness of basalt), Kiandra- Dunn's (1500 to <1400 masl, with basalt >190 m thick at Dunn's Hill) and Section (1480 to 1240 masl) palaeochannels. Since then, this palaeohigh has been deeply dissected by the Tumut River and its tributaries draining to the south and west, and the Yarrangobilly River and its tributaries draining to the north and west. The present divide here runs east of Cabramurra and west of Kiandra north towards Yarrangobilly.

Another prominent palaeohigh existed around the Granite Mountain area (Courabyra 1:25 000 Sheet, 100E 456N) and still remains at >1400 masl. Several palaeochannels drain radially away from this high land. The Rutherford (from 1240 masl) and Buddong (from 1180 masl) palaeochannels descend northeasterly from the Burra Ridge palaeohigh before joining up (at ~900 masl, with basalt up to 200 m thick). The Honeysuckle palaeodrainage trends northward (from 1120 to 1000 masl) towards the Rutherford-Buddong palaeochannel. Several palaeochannels drained southward from the palaeohigh including Sparks Plain, Granite, Bull & Damper and Paddy's palaeochannels (from >1300 to <550 masl, with basalt up to 180 m thick). The first named channels joined the continuation of Paddy's channel as the main outlet. The largest area of basalt was ponded within the tributary channel junctions with Paddy's channel. This basalt mass is less severely dissected than other basalt infillings in the region. The relatively flat area of basalt forms the swampy headwaters to several present day drainages that flow radially off this basalt plateau.

The north-south trending Burra Ridge palaeohigh (Tumbarumba 1:25 000 Sheet, 010E 480N) still exceeds 1200 masl. This separates Paddy's palaeochannel from Tumbarumba palaeochannel, which continues as the major southerly palaeochannel after this junction. Tumbarumba palaeochannel is traceable over 50 km (descending from 1000 to 440 masl, with basalt up to 80 m thick). The present topography is now largely inverted by well-developed lateral stream activity and the infilling channel remnants are now largely visible as a series of linear flat-topped remnant basalt mesas. The straight sections of this course appear to be fault controlled (Wagga 1:250 000 Geological Sheet).

The palaeodrainage reconstruction as presented here applies to drainages largely in place before initial damming and sealing by the earliest lava flows. As lavas progressively filled the channels they would affect stream courses and some lavas would overtop the lower adjacent divides. The main overtopping took place in upper Paddy's drainage where several courses had interfluves bevelled into relatively subdued palaeotopography. Potential overtopping from the Rutherford infilling also exists towards the adjacent Buddong tributary channel, west through Pilot Hill towards the distant Tumbarumba channel and south towards Paddy's channel. An example of diversion from a well-established channel may be represented in the lower Tumbarumba channel where the highest basalt flow in the infilling north of Tooma petrographically resembles basalts overlying lead deposits to the west and south of Tooma.

Table 4. Reconnaissance U-Pb isotope dating, zircon megacryst, Tumbarumba gemfield.

grain	colour	U (ppm)	Th (ppm)	$^{206}Pb/^{238}U \pm 1\sigma$	age±1σ (Ma)	Pb*	%cPb
B2	orange brown	1744	6050	0.00362±18	23.3±1.2	12	2.4

$^{206}Pb/^{238}U$ refers to radiogenic ^{206}Pb which was estimated by correcting the measured $^{207}Pb/^{206}Pb$ in each case by the amount required to yield concordant Pb/U ages, using an assumed common $^{207}Pb/^{206}Pb$ of 0.9618 (Broken Hill ore Pb). Pb* refers to the total radiogenic Pb as measured (in ppm). %c Pb refers to the percentage of common (non radiogenic) ^{206}Pb in the total measured ^{206}Pb. Analyst P.D. Kinny, SHRIMP facility, Australian National University.

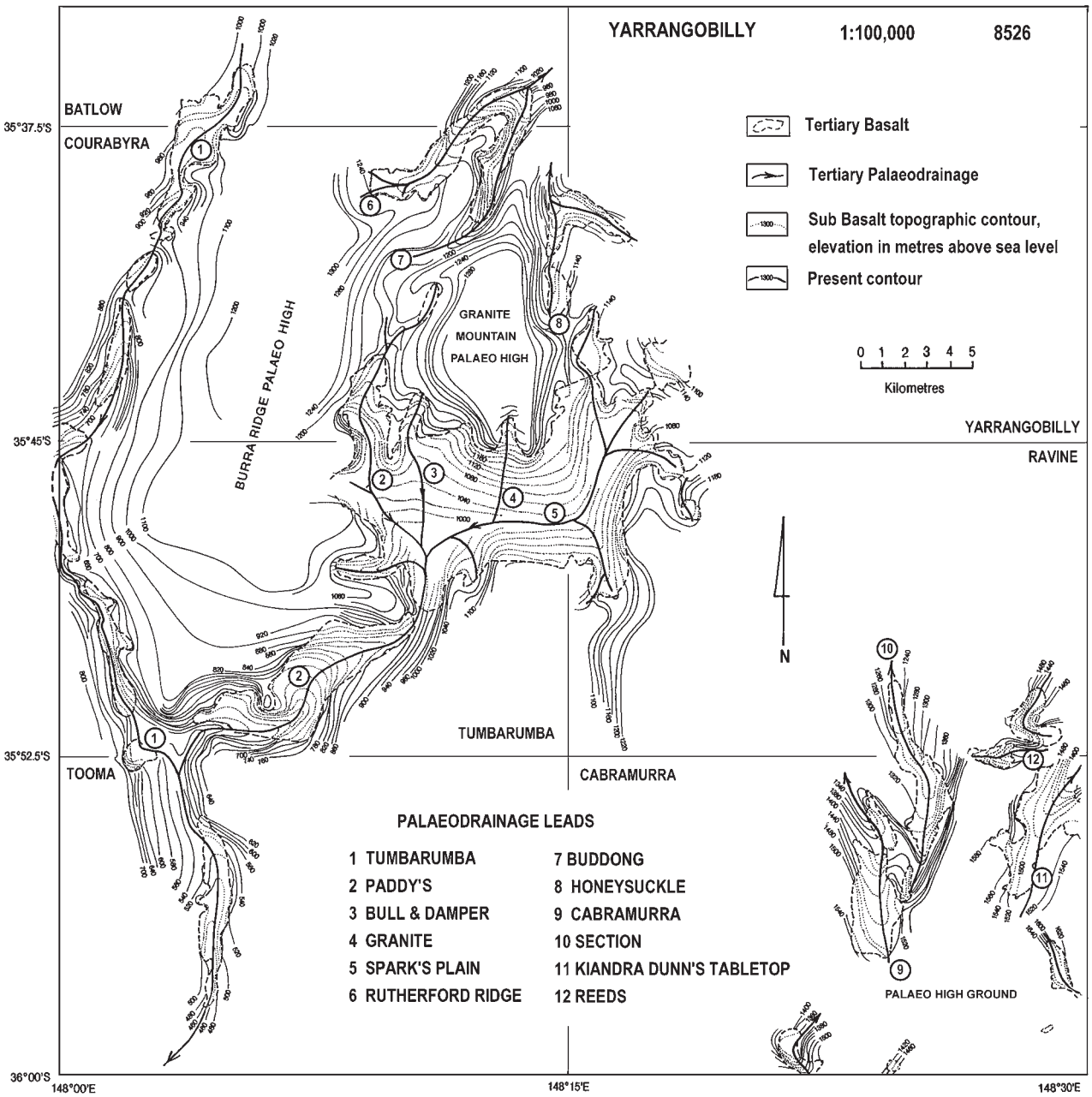

Figure 7. Sub-basaltic paleodrainage related to basalt lava exposures, Tumbarumba-Kiandra region (Yarrangobilly 1:100 000 sheet). Palaeochannels (thick lines) showing direction of drainage flow (arrows) are based on sub-basaltic contours (thin lines) shown at 400 m contour intervals.

Basalts

Basalts infill two main drainage areas, which mark separate eruptive foci (Figs. 1, 7). Western basalts, with largely southerly trending thalwegs, extend from Laurel Hill, Rutherford Ridge and Bago Range through Tumbarumba and Bago Plains to Tooma. Eastern basalts, with largely northerly trending thalwegs, extend from 25 km south of Cabramurra though Cabramurra and Kiandra towards Yarrangobilly Caves.

Distribution. The western basalts form dissected strips within a 140 km^2 area. Eruptive sources probably underlie Laurel Hill (dykes in flow, 2 km S of Laurel Hill), Rutherford Ridge and Bago Range (topographic basalt highs) and near Ruby Creek (basalt dyke ? and volcaniclastic beds). Basalt flows from Bago Range (>1300 m elevation) and Rutherford Ridge (>1260 m) descend to Bago Plains and join Laurel Hill (>1000 m) and Tumbarumba (>550 m) flows at Paddy's River, to continue to Tooma (>440 m). Basalts are 80 m thick east of Rutherford Ridge, 180 m at Bago Plains, 170 m at Paddy's River and under 80 m in the Laurel Hill-Tumbarumba-Tooma lead. Up to four flows are observed in exposed sections. Columnar cooling joints are well developed on Tumbarumba-Batlow Road (Courabyra 1:25 000 Sheet 965563), at Paddy's Falls (lower flow), in Tumbarumba Basalt Quarry (upper part) and on Tumbarumba-Tooma Road near Tooma (lowest flow in sequence, passing into sub-horizontal platy jointing). Flow contacts are exposed overlying weathered granite at Laurel Hill, protruding into dark siltstones 4 km S of Laurel Hill and in the three-flow Tooma sequence where flows successively overlie weathered granite, interbasaltic quartz

grits and clays and then a weathered amygdaloidal flow top. Deep lead deposits containing rounded quartz and dacitic metavolcanic fragments were observed under flows extending from 3 km S of Laurel Hill as far as 5 km S of Tooma. Drill holes to 70 m depth west of Tumbarumba intersected two flows with intervening sands and silts and underlying carbonaceous siltstones and weathered granite. The cores (R. Condon, pers. comm. 1997) suggest local undulating pre-basaltic topography.

The eastern basalts form elongate remnants aligned along two major infills each up to 30–35 km long and 20 km across (Gill & Sharp, 1957). Eruptive sources were suggested 12 km S of Cabramurra (plug), 3 km ENE of Cabramurra (dyke) and 11 km S of Kiandra (plug) and 2.1 km SW of Kiandra (plug; Mackenzie & White, 1970). Flow sequences reach 30–100 m thick and up to 4 flows were recognised in the section west of Cabramurra. Well-developed cooling columns are present at several localities (Lafeber 1956; Gill & Sharp, 1957). These columnar basalts are subject to spontaneous cracking within columns due to hydrothermal alteration effects imposed within the lava during cooling (Lafeber, 1956). Flow contacts were well-exposed at Kiandra, where compact basalt overlies lacustrine and fluviatile sediments of a deep lead (Andrews, 1901). The basalts were considered to be the source of alluvial sapphires rather than redistribution from the underlying deep lead as was previously suggested by Curran (1897).

Petrology. Some 30 basalts from the Tumbarumba-Kiandra region (samples DR13808–13836; 14638–14669) were thin sectioned for examination by petrological microscope. The main mineralogy includes olivine, clinopyroxene, plagioclase feldspar and opaque iron oxides with associated minor alkali feldspar, feldspathoid(s), apatite, biotite, chlorite, hornblende, zeolite, carbonate, clay, goethite and opal-chalcedony. Many rocks have porphyritic, microporphyritic or glomeroporphyritic textures and fluidal flow textures appear in some rocks (Fig. 4a–c). Approximate estimates of phenocrysts and groundmass phases and extent of alteration in the rock are listed in Table 6. Olivine largely alters to chlorite, magnetite and goethite, but "iddingsite" and siderite alteration was noted in a quenched basalt (Barron, 1987). Clinopyroxene is largely augite, zoned to titanian augite, and plagioclase ranges from calcian to sodian compositions ($An_{70–35}$). Opaque oxides include ferrian and titanian spinels and ilmenite. Analcime is an alteration phase in more undersaturated rocks and nepheline- and analcime-bearing basanites, some with late-stage phonolitic globules composed of sanidine, nepheline, clinopyroxene and magnetite are described from the Kiandra-Cabramurra area (Lafeber, 1956; Mackenzie & White, 1970). A range of crustal and mantle xenoliths appear in some flows, e.g., a flow on Elliot Way, 20 km W of Tumbarumba (Tumbarumba 1:25 000 Sheet 120389) contains sporadic fragments of Palaeozoic quartzites, granites and pyroxenite-gabbro and mantle lherzolites and pyroxenites.

Pyroclastic and altered volcaniclastic sediments and regoliths were sampled and sectioned from the Tumbarumba-Tooma area during investigations by the NSW Department of Mineral Resources in 1984–1987 (G. Oakes, S.R. Lishmund, L.M. Barron data; Barron, 1987). A lithic volcanic mudstone at a basalt flow base near Ruby Creek (Tumbarumba 1:25 000 Sheet 619 579) contained clasts of highly vesicular basalt, olivine and pyroxene-phyric basalt and microlitic basalt as well as fragments of olivine, feldspar, spinel and pyroxene in a red fine-grained muddy matrix. Red multi-generation peaty fragmental rock exposed in fresh cuts at Permanent Creek contained iron-stained lithic fragments, including altered basalt (?), feldspar, augite (?) and olivine (?) set in a clay matrix. A micaceous muddy reworked volcaniclastic deposit underlies basalt (Tooma 1:25 000 Sheet 975 230) within the Tooma lead (Barron, 1987). It includes material derived from granite, micas that are well separated and unbent and local high contamination by reworked (?) airfall crystal/vitric rhyolitic tuff. These basal (?) and interbedded volcaniclastic sediments and pyroclastics in the basalt sequences suggest explosive phases during eruption of the basaltic lavas. The presence of rhyolitic tuff is further considered in the Discussion section on evolution of the Tumbarumba gemfield (Early Miocene activity, 24–18 Ma).

The survey of basalt types shows a dominance of alkali-olivine basalts and basanites based on petrographic assemblages. Phyric rocks commonly include olivine-dominant, olivine and augite-dominant and olivine, augite and plagioclase-dominant types. In some sequences lower flows are more strongly olivine-phyric (DR14639), in others, upper flows are olivine-phyric (DR13828). Olivine

Table 5. Garnet xenocryst and microxenolith analyses, Tumbarumba gem field.

wt% oxide	xenocryst range	average (3 grains)	xenolith range	average (3 grains)	xenocryst range	xenolith range
SiO_2	37.96–38.34	38.12	37.01–37.59	37.24	al 68.7–74.6	al 73.5–74.5
TiO_2	0.00–0.06	0.03	0.01–0.02	0.02		
Al_2O_3	20.94–21.08	21.02	20.63–20.78	20.72	py 17.2–19.4	sp 12.1–14.7
Cr_2O_3	0.01–0.04	0.03	0.01–0.05	0.03		
MgO	4.17–4.81	4.49	1.91–2.48	2.14	sp 4.0–8.9	py 7.9–8.5
CaO	1.10–1.44	1.24	1.07–1.09	1.08		
MnO	1.69–3.89	3.08	6.15–6.25	6.20	an 3.1–4.1	an 3.0–3.2
FeO	31.99–33.93	32.66	33.26–33.89	33.48		
NiO	0.01–0.08	0.05	0.00–0.00	0.00	u 0.0–0.1	u 0.0–0.2
Na_2O	0.00–0.03	0.02	0.00–0.03	0.01		
total	100.19–100.93	100.68	100.32–100.92	100.60	gr 0.0–0.0	gr 0.0–0.0

Electron microprobe analyses, Cameca CAMEBAX unit, CSIRO, Sydney. Abbreviations: al-almandine, py-pyrope, sp-spessartine, an-andradite, u-uvarovite, gr-grossular. Analyst: B.J. Barron.

Table 6. Summary of basalt characteristics, Tumbarumba-Snowy Mountains Region.

	phenocryst minerals (modal)					ground mass	alteration	R.L.	section	
~%	oliv.	aug.	plag.	qtz.	composites	~%	degree	(m)	number	loc.
west of Tumbarumba: Ruby Creek (RC), Yorkers Creek (YC)										
40	•					60	minor	1220	14639	YC
25	•	•				75	major	1000	13823	RC
MD	•	•	•				minor	950	13822	RC
south of Tumbarumba: Tumbarumba basalt quarry (TB), Tooma (TO)										
15	•				•	85	major	610	14646	TB
15	•	•			•	85	minor	460	14662	TO
15	•	•	•	•	•	85	minor	480	14664	TO
15	•	•	•	•	•	85	minor	550	14669	TO
northeast of Tumbarumba: Jimmies Road (JR), Rutherford Ridge (RR), Buddong Creek, (BC), Pilot Hill (PH), Parson's Gully (PG)										
40	•	•	•		•	60	major	1200	13819	PG
20	•	•			•	80	minor	1220	13817	PG
5	•	•			•	95	negligible	1360	14641	JR
30	•	•			•	70	negligible	1275	14650	RR
25	•	•	•	•	•	75	negligible	1100	14652	BC
30	•	•			•	70	major	1150	14653	PH
40	•	•			•	60	major	1150	14655	PH
north of Tumbarumba: Miller's Property (MP), Laurel Hill (LH)										
10	•	•			•	90	minor	860	13820	MP
20	•	•			•	80	minor	990	13833	LH
30	•		•		•	70	minor	990	13826	LH
20	•	•			•	80	minor	1060	13830	LH
30	•	•			•	70	minor	1000	13828	LH
Snowy Mountains Region: Yarrangobilly (YB), Cabramurra (CA), Talbingo Ruby Creek (TR), Kiandra (KI)										
20	•		•			80	minor	1150	Y13	YB
30	•	•	•		•	70	minor	1200	Y26	YB
5			•			95	minor	>1000	DR1	YB
20	•		•		•	80	major	1290	13813	TR
30	•		•			70	major	1522	13810	KI
30	•	•			•	70	minor	1325	13834	CA
40	•	•			•	60	minor	1540	13832	CA
10	•	•			•	90	major	>1400	13811	KI
30	•				•	70	minor	1325	13835	CA
25	•	•	•			75	minor	1390	13836	CA

Thin section numbers are Australian Museum DR registration numbers, except for Y13, Y26 and DR1 (R.A. Osborne, University of Sydney). Abbreviations: MD, micro-dolerite; oliv., olivine; aug., augite; plag., plagioclase; qtz., quartz.

and augite glomeroporphyritic and micro-glomeroporphyritic basalts are found in most sequences. The phenocrystic basalts contrast with more uniformly textured olivine basalts. Basalts with predominant sodian plagioclase, typical of hawaiite-mugearite associations are generally absent, although microlitic plagioclase of An_{40} is recorded in a quenched basalt (Barron, 1987). Basalts with low Ca pyroxenes or black iron-oxide charged glassy mesostases denoting distinct tholeiitic affinities were not observed. However, rare basalts show transitional characteristics, including absence of titanian colour enrichments in pyroxenes and/or presence of an opaline mesostasis. In some sections flows become less mafic and more feldspathic up through the sequences, but this is not a consistent feature throughout the sequence, suggesting the presence of eruptive cycles.

An unusual texture is present in alkali–olivine basalt (DR13828) from a columnar jointed flow near Laurel Hill. Here, typical olivine, clinopyroxene, plagioclase, opaque oxide-bearing basalt (see Table 7C) is interspersed with feldspathic veinlets to > one cm across (Fig. 4d). These segregations largely consist of sodian plagioclase passing into albite, with subsidiary magnesian fayalite and augitic clinopyroxene. They commonly contain a central vesicle or a few small vesicles and resemble micro-miarolitic structures. The veinlets are sub-horizontal within the columns and expand in thickness towards the column margins.

Olivine micro-dolerite from the Ruby Creek plug (DR13822) has a coarser texture in which calcic plagioclase forms 50% of the rock in prismatic subhedral grains ranging up to 1.5 mm long (Fig. 4e). Augite (30%) forms subophitic to ophitic intergrowths with plagioclase. Some clinopyroxene completely encloses khaki-brown primary amphibole inclusions. Olivine (15%) forms euhedral to subhedral ovoid grains and aggregates between plagioclase laths and is partly replaced by fine-grained chlorite and magnetite. Opaque angular and irregular grains of ferrian oxides and minor mesostasis and carbonate form the remainder.

Some basalt fragments found within gem-bearing alluvial deposits represent a different basalt than those observed in local basalt flows within the catchment. This includes the sapphire-zircon bearing basalt from Ruby Creek, which also

Table 7A. Major elements and CIPW norms, Tumbarumba-Cabramurra basalts.

oxide	DR	DR	DR	DR	DR	DR	DR	DR	IG	SL	SL
wt%	14639	13822	13835	14650	13820	14662	13828	14641	159	61	63
SiO_2	44.1	47.2	44.9	43.1	43.7	43.6	44.8	45.3	46.15	43.70	43.60
TiO_2	1.54	1.08	1.93	1.97	2.53	2.11	2.31	2.68	1.77	2.47	2.42
Al_2O_3	11.9	17.1	14.4	14.4	14.7	14.5	15.0	17.0	14.96	14.20	16.10
Fe_2O_3	2.48	1.93	2.32	2.26	2.28	2.28	2.52	2.34	3.43	3.20	5.30
FeO	8.93	6.96	8.35	8.13	8.21	8.21	9.07	8.42	7.32	7.90	5.30
MnO	0.19	0.16	0.17	0.17	0.18	0.17	0.17	0.19	0.17	0.15	0.15
MgO	16.80	9.61	10.30	9.71	9.55	9.28	8.81	6.27	10.08	10.70	7.75
CaO	7.93	11.90	9.62	10.90	10.00	10.10	9.01	9.13	8.79	9.80	8.06
Na_2O	2.47	2.48	3.89	4.10	3.32	3.97	3.47	3.89	2.85	3.00	3.30
K_2O	0.96	0.12	1.43	1.54	1.56	1.63	1.33	1.71	0.69	1.26	1.35
P_2O_5	0.56	0.07	1.10	1.40	1.42	1.41	1.16	0.94	0.66	1.20	1.50
L.O.I.	0.70	1.10	0.49	1.50	1.39	1.45	1.00	0.80	2.99	2.90	4.50
total	98.56	99.71	98.90	98.19	98.84	98.71	98.65	98.67	99.86	100.48	99.33
Mg#	0.77	0.71	0.69	0.68	0.68	0.67	0.63	0.57	0.67	0.68	0.62
$Mg\# = Mg^{2+}/Mg^{2+} + Fe^{2+}$											
CIPW Norms (anhydrous norms calculated using $Fe_2O_3/FeO + Fe_2O_3 = 0.2$)											
Or	5.74	0.71	8.51	9.23	9.37	9.81	7.97	10.23	4.21	7.63	8.41
Ab	14.98	21.11	14.88	7.51	14.99	11.98	21.13	20.15	24.88	15.64	26.28
An	18.76	35.39	17.72	16.57	20.94	17.25	21.72	24.16	26.81	22.09	26.50
Ne	3.34		9.89	15.00	7.35	12.05	4.67	7.13		5.63	1.72
Di	13.85	18.96	18.59	23.37	16.14	19.69	12.88	12.59	10.84	15.87	4.32
Hy		0.61							4.78		
Ol	34.42	17.39	19.84	17.00	18.69	17.52	19.73	14.01	20.37	22.49	21.13
Mt	3.64	2.82	3.39	3.32	3.36	3.37	3.70	3.43	2.59	2.67	2.57
Il	2.96	2.06	3.69	3.79	4.89	4.08	4.45	5.15	3.47	4.81	4.85
Ap	1.34	0.17	2.62	3.36	3.42	3.40	2.78	2.25	1.61	2.91	3.75
An%	56	63	54	69	58	59	51	55	52	59	50
D.I.	24.16	21.8	33.3	31.7	31.7	33.8	33.8	37.5	29.10	28.9	36.4
Type (J&D)	Alkali ol basalt	Olivine basalt	Basanite	Basanite	Basanite	Basanite	Alkali ol basalt	Basanite	Olivine basalt	Basanite	Alkali ol basalt
Type (LM)	Basanite	Basalt	Basanite	Basanite	Basanite	Basanite	Basanite	Basanite	Basalt	Basanite	Basanite

An% = (An/[An+Ab])×100. D.I. differentiation index Σq or ab ne, lc; Type (J&D), basalt type, based on normative mineralogy after Johnson & Duggan (1989); Type (LM), basalt type, based on Total Alkali-Silica (TAS) diagram after Le Maitre (1989). IG 159 analysis by Macquarie University Laboratories, Sydney. SL61, SL62 analyses by NSW Mineral Resources Laboratories, Lidcombe, Sydney.

carries conspicuous xenocrysts, unobserved elsewhere in the Tumbarumba-Kiandra region (Fig. 2a).

The zircon-corundum-bearing basalt (DR48682) contains rare peridotite xenoliths up to 1.5 cm across and corroded xenocrysts of kaersutitic amphibole (5%), sparse apatite, and rare potassian anorthoclase, titanian biotite and titanian magnetite up to 5 mm across (Fig. 4f). The olivine in the peridotite is partly altered through oxidation of Fe, but is Mg-rich and is intergrown with aluminian diopside and kaersutitic amphibole. It may represent metasomatically altered lherzolite. The kaersutite shows khaki brown to pale yellow pleochroism and crystal cores mantled by narrow rims, with a reaction margin of fine-grained granular opaque iron oxide. Compositions vary between crystals (SiO_2 39–41%, TiO_2 4–6%, Al_2O_3 14–16%, Fe_2O_3 15–19%, MgO 8–9%, CaO 9–10%, Na_2O 1–2%, K_2O 1–2%), but core and rim compositions are generally similar. Larger crystals exhibit a crystallographic controlled prismatic phase (rhönite?), zeolite-replaced enclaves (barian phillipsite?) and intergrown apatite. Apatite xenocrysts have a cloudy pink grey colour and are also intergrown within heavily iron-oxide altered titanian biotite blades (up to 7 wt% TiO_2). The apatite resembles lherzolite mantle apatite described by O'Reilly & Griffin (2000). The basalt groundmass is dominantly composed of plagioclase laths (~An_{50}) with accessory magnetite-ulvospinel, some anorthoclase and feldspathic glass and rare small olivine crystals (~$Fo_{70–80}$). It approaches a transitional hawaiite in character.

Geochemistry. A range of fresh basalt types were selected for analysis after thin section examination (Tables 7A–C). Analyses were made at AMDEL Laboratories, Adelaide, using an alkaline fusion and Inductive Coupled Plasma (ICP) Mass Spectrometry for major elements (± 5% accuracy) and HF acid digest and ICP-MS for trace elements including rare earth elements (REE) (± 10% accuracy). Three unpublished analyses from other sources, with more limited trace element determinations, are also listed (I. Graham, Macquarie University Laboratory, Sydney; S. Lishmund, NSW Dept. Mineral Resources Laboratory, Sydney). Additional major element and restricted trace element analyses of Cabramurra-Kiandra basalts (Lafeber, 1956; Mackenzie & White, 1970; Knutson & Brown, 1989) were also considered in the overall synthesis.

Major element analyses (Table 7A) show a range of primary to slightly evolved basalts, based on Mg# (0.77–

Table 7B. Trace element analyses, Tumbarumba-Cabramurra basalts.

element (ppm)	14639	13822	13835	14650	13820	14662	13828	14641	159	61	63
Ni	550	160	260	190	195	200	165	62	245	258	170
Cr	460	350	410	250	250	290	240	60	350	283	199
Zn	115	83	110	120	120	115	125	120	74	95	88
Cu	105	91	60	74	75	70	66	64	56	98	66
V	170	220	180	180	200	170	190	220	162	197	174
Y	18	21.5	23	28	24.5	25	23.5	25.5	24	25	29
Sc	< 5	15	25	15	15	20	25	25		24	25
Rb	14	9	21	30	16.5	22.5	13.5	19.5	10	15	22
Sr	650	160	1200	1700	1800	1700	1450	1250	884	1307	1386
Ba	280	< 20	700	1000	850	950	550	700	437	639	865
Zr	110	60	170	170	180	190	170	220	218	233	296
Hf	4	7	3	7	3	4	3	15		< 3	< 3
Ga	15	16.5	19.5	19	20.5	23	18.5	20	14	20	18
Nb	57	2.5	120	175	80	135	22	150	57	81	104
Ta	5	6	7	6	7	9	7	8			
Th	4.6	0.5	11.5	19	10.5	13.5	6.5	7	5	7	9
U	0.9	0.1	2.2	3.1	2.3	2.8	1.4	1.3	1	< 1	< 1
La	39.5	3.6	89	120	110	125	83	67		100	109
Ce	59	8.5	120	160	155	170	120	110		138	164
Pr	7	1.65	11	18.5	15	15	12	14			
Nd	24.5	7.5	35.5	61	47	48.5	40.5	49		65	72
Sm	4.3	2.4	8	9	10	10	8.5	7.5			
Eu	1.60	1.05	2.6	3.3	3.4	3.3	2.9	2.8			
Gd	3.9	2.9	6	7	7.5	7.5	6.5	6			
Tb	0.56	0.51	0.85	0.96	1.05	1.05	0.91	0.84			
Dy	3.1	3.3	4.7	4.8	5.5	5.5	4.9	4.4			
Ho	0.7	0.84	0.81	1.05	0.89	0.91	0.83	0.96			
Er	1.55	1.95	2.2	2.3	2.3	2.4	2.2	2.2			
Tm	0.2	0.3	0.3	0.3	0.3	0.35	0.3	0.3			
Yb	1.35	1.95	1.85	2.0	1.85	1.95	1.80	2.0			
Lu	0.23	0.32	0.30	0.33	0.29	0.31	0.28	0.32			

0.57). Using CIPW norms and a Differentiation Index (DI) diagram (Johnson & Duggan, 1989), the rocks classify into basanites (<5% ne, >5%ab) and alkali olivine basalts (<5% ne, <5% hy). Using a Total Alkali ($Na_2O + K_2O$)—Silica (SiO_2) classification (TAS diagram; Le Maitre, 1989) most rocks are basanites with minor basalts. Quenched basalt from Ruby Hill (SL63) shows higher volatile content (4.5 wt%) than the other basalts (0.7–3.0 wt%) and is transitional to hawaiite (An 50%). Ruby Creek micro-dolerite (DR13822) has highest SiO_2 (47.2%) and CaO (11.9%) and lowest K_2O (0.12%) and P_2O_5 (0.07%), which with low hy (0.6%) suggests transitional olivine basalts. This rock however proved Palaeozoic in age (see Table 9). Talbingo basalt (IG159) is also low in K_2O (0.69%) and P_2O_5 (0.66%) and with 4.8% hy approaches transitional olivine basalt. Some of the major analytical totals are slightly low. This

Table 7C. Locality data, analysed rocks, Tumbarumba-Cabramurra basalts.

DR14639	Coarse grained olivine-rich alkali basalt flow, Yorker's Creek, 1120 m R.L., Ravine 1:25 000 Sheet (GR 193 395)
DR13822	Coarse olivine basalt (micro-dolerite) plug (?), Ruby Creek, 950 m R.L., Tumbarumba 1:25 000 Sheet (GR 075 352)
DR13835	Basanite flow, Link Road, west of Ravine Junction, 1325 m R.L., Cabramurra 1: 25 000 Sheet (GR 274 287)
DR14650	Vesicular olivine-pyroxene phyric basanite, Rutherford Ridge, 1275 m R.L., Courabyra 1:25 000 Sheet (GR 060 539)
DR13820	Vesicular olivine-pyroxene phyric basanite, 0.7 km NE of Courabyra-Adelong road junction, 860 m R.L., Courabyra 1:25 000 Sheet (GR 947 507)
DR14662	Columnar olivine-pyroxene phyric basanite, lowest flow, Bald Hill, Tooma-Tumbarumba Road, 460 m R.L., Tooma 1:25 000 Sheet (GR 971 202)
DR13828	Columnar olivine alkali basalt flow, Laurel Hill camp, Adelong Road, 1000 m R.L., Courabyra 1:25 000 Sheet (GR 965 563) *
DR14641	Flow banded olivine-pyroxene phyric basanite, W side Jimmies Road, near Granite Mountain, 1360 m R.L., Courabyra 1:25 000 Sheet (GR 090 458)
IG159	Massive olivine basalt flow, near Talbingo, 1030 m R.L., Yarrangobilly 1:25 000 Sheet (GR 139 545)
SL61	Basanite flow, Ruby Creek, 1060 m R.L., Tumbarumba 1:25 000 Sheet (GR 096 374)
SL62	Olivine alkali basalt flow, above Ruby Creek, 1010 m R.L. Tumbarumba 1:25 000 Sheet (GR 073 359)

* DR13828 Main mineral phases, approximate compositions: Olivine ($Fo_{65–80}$ $Fa_{20–35}$), augite-diopside ($Wo_{29–47}$ $En_{23–45}$ $Fs_{20–47}$), plagioclase ($An_{51–62}$ $Ab_{34–41}$ $Or_{2–6}$), anorthoclase ($Ab_{55–65}$ $Or_{15–25}$ $An_{15–20}$), ulvospinel ($Usp_{69–72}$ $Mf_{13–19}$ $Mt_{3–11}$ $Hc_{3–7}$ $Chr_{0–2}$).

may reflect trace element enrichments as these rocks show relatively high Sr and Ba compared to other related eastern Australian basalts (see Knutson & Brown, 1989: table 3.6.1).

Trace elements analyses (Table 7B) show the primary basalts (Mg# 0.77–0.67) have relatively higher Ni (160–550 ppm) and Cr (250–460 ppm) than more evolved basalts (Mg# <0.67; Ni 62–170 ppm, Cr 60–240 ppm). The highest Zr content (296 ppm) is found in evolved basalt which borders on hawaiite (SL63). Most of the more primitive alkali basalts have relatively low K/Ba (14.2–17.0), Rb/Sr (0.01–0.02), K/Nb (73–162) and Zr/Nb (0.97–2.25). However olivine-rich Yorkers Creek basalt (DR14639) shows higher K/Ba (28.5), while near-transitional Talbingo basalt (IG159) shows lower K/Ba (13.1) and higher Zr/Nb (3.82) than in the typical range. Two basalts are significantly different in trace element ratios to the mainstream basalts. Laurel Hill alkali basalt (DR13828) is significantly low in Nb (22 ppm), resulting in high Zr/Nb (7.73) and K/Nb (502) and low Nb/Ta (3.1). Ruby Creek micro-dolerite (DR13822) is exceptionally low in Sr, Rb, Ba, Zr, Nb and light to middle REE, leading to markedly high Zr/Nb (24.0), K/Nb (400), K/Ba (49.8) and Rb/Sr (0.06) and noticeably low Zr/Hf (8.6), Nb/Ta (0.32), La/Yb (1.8) and Ce/Y (0.40).

Incompatible element patterns for the basalts are compared using multi-element plots, normalised to primitive mantle values (Fig. 8). Normalising values are taken from Sun & McDonough (1989) to allow direct comparison with such plots from other eastern Australian basalt fields (O'Reilly & Zhang, 1995). Primary Tumbarumba-Cabramurra basanites and alkali basalts show highly differentiated patterns with marked depletions in Rb, K, Hf, Y and some heavier REE and enrichments in Th, Nb, Ta, P and light to middle REE (Fig. 8a,b). This type of pattern is attributed to the presence of amphibole and apatite in mantle sources, with their components entering into Oceanic Island Basalt (OIB)-like melts (O'Reilly & Zhang, 1995).

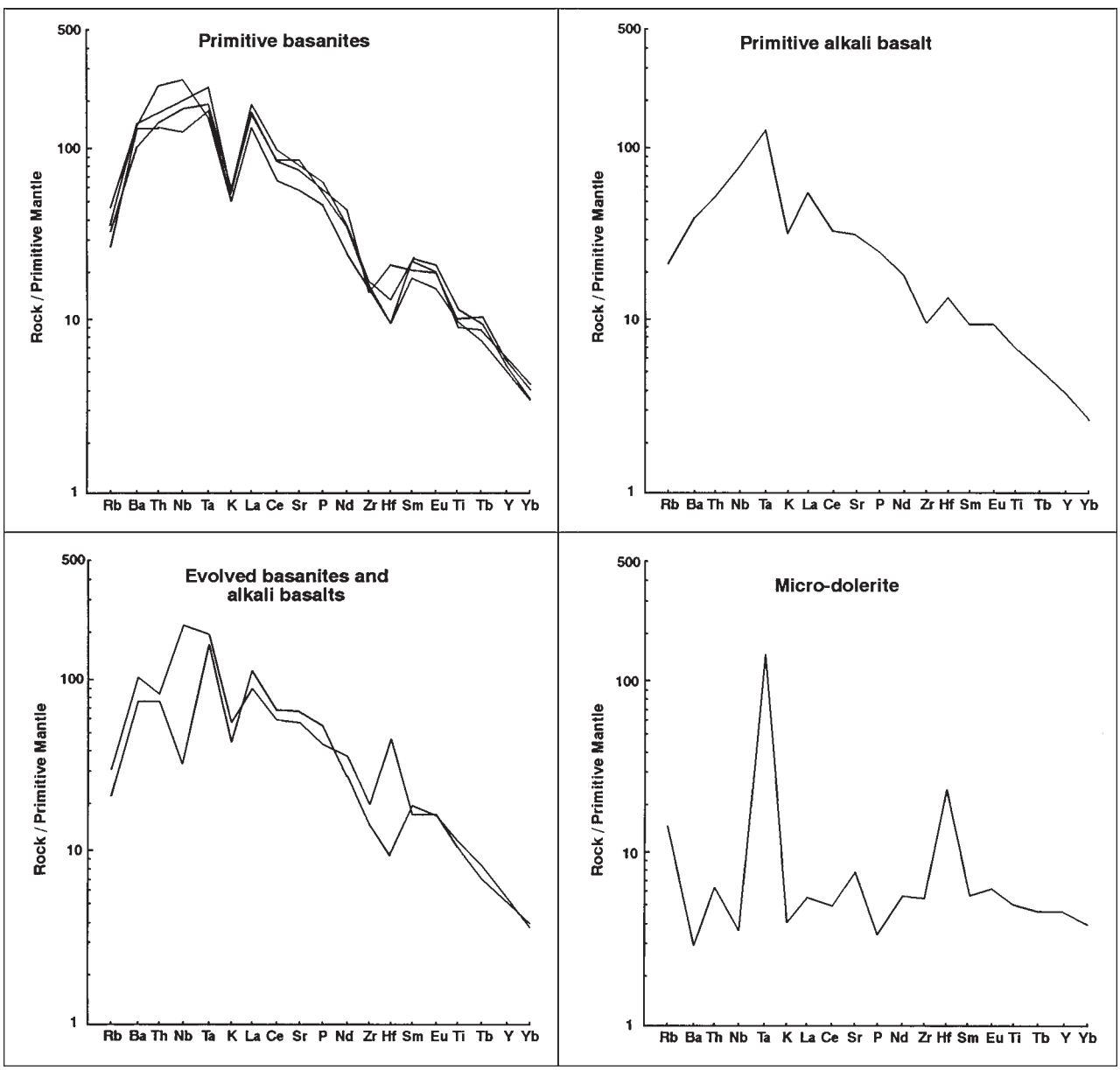

Figure 8. Normalised incompatible element plots, Tumbarumba basalts. a—primary-near primary basanites (DR13820, 13835, 14650, 14662); b—primary alkali basalt (DR14639); c—mildly evolved basanites and alkali basalt (DR13828, 14641); d—primary olivine micro-dolerite (DR13822).

Some variations in the patterns can be noted, e.g., for olivine-phyric alkali basalts (DR14639) and olivine and augite-phyric basanite (DR14650), where Hf is enriched relative to Zr. The evolved basanites and alkali basalts retain some characteristics of the more primitive patterns, but show additional variability (Fig. 8c). Jimmies Road basanite (DR14641) shows strong Hf enrichment and depletion in Th, while Laurel Hill alkali basalt (DR13828) shows marked Nb and Th depletion. The precise contributions of sources, fractionation and contamination in element variations in the alkaline lavas are uncertain, but all seem to carry strong imprints of amphibole (and apatite)-enriched sources and garnet-in residue partial melting.

Ruby Creek micro-dolerite (DR13822) exhibits a multi-element array that contrasts markedly with the other rocks (Fig. 8). It is strongly depleted in many incompatible elements such as Ba, Th, Nb, Zr, K and P and is enriched in a few elements, particularly Ta, Hf and to small extent Ba and Sr. This has high Mg# (0.71) and must derive from a very different garnet-free source to the amphibole-imprinted source for the other basalts. Basalts, with only limited trace element analyses (IG159, SL61, SL63) provide partial multi-element arrays that mostly conform to amphibole (apatite) source patterns, although relatively subdued in the Talbingo basalt (IG159).

Geochronology

Xenocrystic zircons in Tumbarumba basaltic corundum associations not only allow more complete dating beyond the radiometric basalt results, but also help to reinforce the basalt dating. Fission track dating of these basalt-released zircons provides "reset" ages corresponding to the eruptive event and has proved highly effective in establishing gemstone/basalt relationships in other eastern Australian fields (New England, Barrington, North Queensland; Sutherland *et al*., 1993, 1999; Sutherland & Fanning, 2001). U-Pb isotope dating of these zircons and rare zircon inclusions in the sapphires helps to clarify sapphire/basalt melt formation, although precise mechanisms remain in contention (Coenraads *et al*., 1990; Guo *et al*., 1996a; Sutherland *et al*., 1998a). Considerable K-Ar dating is already available for the basalts (21 dates; Young & McDougall, 1993) giving a solid framework to interpret the zircon dating, so that new basalt dating in this study was confined to isolated basalts of topographic interest.

Zircon fission track dating. Two zircon samples (Parsons Gully, Tumbarumba Creek) were dated by Geotrack International, Melbourne, using standard methods (Gleadow *et al*., 1976; Green, 1981, 1985; Hurford & Green, 1983) and statistical smoothing and discrimination techniques (Galbraith, 1981, 1988). Dark red grains were selected from the Parson Gully sample and subsets of dark grains, pale grains and bright polished grains were selected from the Tumbarumba Creek sample.

The results (Table 3) suggest 3 or 4 possible pooled ages may be present within the zircon suites at the 1σ error level (26.0±1.1, 22.8±0.9, 23.6±0.9, 18.6±1.2 Ma). However, the intermediate ages are within error and results at the 2σ level provide substantial overlap within error (26.0±1.6, 22.8±1.3, 23.6±1.3, 18.6±1.7 Ma), so the age groups may not be separable. Nevertheless, the data shows a significant spread in single grain fission track ages, so that the colour grouping may not accord strictly with age grouping. Therefore, the data was further analysed by a radial plot using statistical principles and methods outlined by Galbraith & Green (1990). The analysis (Geotrack Report #655, Australian Museum) gave estimated modal ages, with confidence limits (c.l.) for the following components.

1 26.6 Ma (29.3–24.2 95% c.l.); U 36–1070 (av. 311) ppm from 9 grains
2 21.6 Ma (23.4–19.8 95% c.l.); U 53–1433 (av. 510) ppm from 10 grains
3 15.6 Ma (19.0–12.8 95% c.l.); U 36–396 (av. 197) ppm from 6 grains
4 2.0 Ma (4.9–0.8 85% c.l.); U 95 ppm from 1 grain

The youngest age is represented by only a single grain and is not considered significant for the main "reset" zircon ages, as it may merely represent isolated local fire or lightning strike heating events. The three main episodes show some relative difference in av U contents, which reinforces the suggested age separations.

U-Pb isotope dating. This method investigated formation ages of zircon megacrysts and inclusions in sapphires in relation to the basaltic eruptions.

U-Pb zircon megacryst dating. A zircon megacryst from Parsons Gully (B2) was dated using a special treatment of the SHRIMP isotope data, needed to accommodate the geologically "young" age of these zircons (Coenraads *et al*., 1990). The measured ^{207}Pb was used to estimate the proportion of non-radiogenic Pb present in the zircon. The resultant ^{206}Pb/^{238}U age (Table 4) when compared at 2σ uncertainty, (23.3±1.7 Ma) lies within the 2σ error of fission track ages for similar zircons in the Parsons Gully—Tumbarumba Creek suites (26.0±1.6 and 23.6±1.3 Ma). The result implies zircon crystallisation was closely related in time to basaltic magmatic processes, assuming no Pb loss took place during heating from magmatic transportation.

U-Pb zircon in sapphire dating. SHRIMP analyses (based on techniques outlined in Sutherland & Fanning, 2001) for zircon inclusions in two Type 3 sapphires (C46, C63) are presented in Table 8. Six grains in C46 (U936–1578 ppm; Th 193–428 ppm; Th/U 0.18–0.46) gave an age range 392±4 to 264±3 Ma; this scatter in ages suggests these may represent inherited zircons from the Palaeozoic fold belt. Three grains in C63 also showed scatter in ages, 903±10 to 22.6±0.4 Ma, but each grain yielded coherent younger ages in the range 27.6±0.3 to 22.6±0.4 Ma. The younger results showed higher Th/U (0.73–1.74) than the older spread of ages (903–67 Ma; Th/U 0.34–0.64). The younger ages are geologically meaningful at the 2σ level (28±0.4–23±0.6 Ma) falling within the eruptive age range of zircon megacrysts and basalts from the region (28–16 Ma) and the older scattered ages may indicate inherited zircon within these grains.

Basalt K-Ar dating. Two basalts were dated in this study, using conventional K-Ar dating techniques (AMDEL Laboratories, Adelaide; CSIRO Laboratories, Sydney). One basalt (DR14641) represents an isolated high level flow cap on Jimmies Hill (1340 masl); the other (DR13822) an isolated plug in Ruby Creek (950 masl).

Table 8. Summary of SHRIMP U-Pb zircon results for Tumbarumba sapphires.

sample no. grain · spot	$^{204}Pb/^{206}Pb$	f_{206}	f_{206} %	total $^{238}U/^{206}Pb$	±	total $^{207}Pb/^{206}Pb$	±	radiogenic $^{206}Pb/^{238}U$	±	age (Ma) $^{206}Pb/^{238}U$	±
C46											
1 · 1	0.000041	1.15E-02	1.15	19.96	0.240	0.0619	0.0007	0.0495	0.0006	311.6	3.7
2 · 1	0.000014	5.03E03	0.50	15.88	0.179	0.0588	0.0004	0.0627	0.0007	391.7	4.3
3 · 1	0.000100	1.77E-03	0.18	22.16	0.328	0.0535	0.0005	0.0451	0.0007	284.0	4.1
4 · 1	0.000015	2.61E-03	0.26	23.84	0.262	0.0537	0.0004	0.0418	0.0005	264.2	2.9
5 · 1	0.000010	0.00216	0.22	23.09	0.261	0.0536	0.0005	0.0432	0.0005	272.7	3.0
C63											
1 · 1	0.000835	1.35E-02	1.35	230.10	2.747	0.0572	0.0011	0.0043	0.0001	27.6	0.3
1 · 2	0.001057	1.01E-02	1.01	275.60	3.941	0.0544	0.0020	0.0036	0.0001	23.1	0.3
1 · 3	0.000040	0.00589	0.59	7.08	0.086	0.0723	0.0005	0.1404	0.0017	846.7	9.7
2 · 1	0.003739	0.0923	8.23	87.58	1.134	0.1124	0.0014	0.0105	0.0001	67.2	0.9
2 · 2	0.000567	0.00806	0.81	279.98	3.621	0.0529	0.0017	0.0035	0.0001	22.8	0.3
3 · 1	0.001894	0.01531	1.53	280.33	4.887	0.0586	0.0038	0.0035	0.0001	22.6	0.4
3 · 2	0.000011	1.26E-03	< 0.01	6.66	0.080	0.0677	0.0004	0.1503	0.0018	902.7	10.2

Uncertainties given at the one σ level. f_{206} % denotes the percentage of ^{206}Pb that is common Pb
Correction for common Pb made using the measured $^{238}U/^{206}Pb$ and ^{207}Pb ratios following Tera & Wasserburg (1972) as outlined in Compston *et al*. (1992). **U, Th, Pb* contents (ppm)** (* = total radiogenic Pb).
C46: 1.1 U 936, Th 428, Th/U 0.48, Pb 34; 2.1 U 1048, Th 193, Th/U 0.18, Pb 49; 3.1 U 1191, Th 353, Th/U 0.30, Pb 40; 4.1 U 1081, Th 320, Th/U 0.30, Pb 33; 5.1 U 1139, Th 409, Th/U 0.36, Pb 37.
C63: 1.1 U 1454, Th 1227, Th/U 0.84, Pb 6; 1.2 U 861, Th 627, Th/U 0.73, Pb 3; 1.3 U 623, Th 212, Th/U 0.34, Pb 71; 2.1 U 867, Th 552, Th/U 0.64, Pb 7; 2.2 U 812, Th 1219, Th/U 1.50, Pb 3; 3.1 U 301, Th 524, Th/U 1.74, Pb 1; 3.2 U 573, Th 230, Th/U 0.40, Pb 72.

The results (Table 9) show that:

1 Jimmies Hill basalt at 23.7±0.3 (2σ) Ma is the oldest dated Cainozoic lava and the related Bago Range basalt high point is the oldest preserved eruptive lava sequence.
2 The Ruby Creek olivine-microdolerite at 397±9.5 (2σ) Ma is unrelated to the gemfield basalts, but is linked to the plagioclase-bearing intrusions of the Devonian ophiolitic belts (Graham *et al*., 1996, 1998).

Discussion

The Tumbarumba basaltic gem field is notable for a diverse range of corundums, including ruby. However, good gem quality sapphires are scarce, while ruby is rare (Curran 1897; MacNevin & Holmes 1980; this study). Thus the field does not favour commercial prospects. Nevertheless, the corundum (and associated zircons) studied here have considerable scientific significance for the origin of these gem minerals in a wider context.

Corundum types. Tumbarumba corundums show a wide-range in colour, crystal and growth characteristics (Group 1–9). Colour combinations, inclusion mineralogy and chemical fingerprints demonstrate that many of these groups correspond to bimodal magmatic and metamorphic groups identified in some basalt fields (Barrington, West Pailin; Sutherland *et al*., 1998c). Groups 1–5, in particular, show blue, green and yellow colour zoning, syngenetic inclusions (ferrocolumbite), trace element ratios (Cr_2O_3/Ga_2O_3 <1) and related colour absorption spectra that typify BGY magmatic-origin corundums (Type 1 corundums). Groups 8–9, equally clearly, show the pastel colour range and passage through pink into red colours, with higher Cr_2O_3/Ga_2O_3 (>1) and colour absorption spectra that typify metamorphic-origin corundums (Type 4–5 corundums). Tumbarumba metamorphic corundums, however, only partially overlap into the Barrington metamorphic field. The pale blue to mauve-pink colour range extends into lower Cr_2O_3/Ga_2O_3 and Fe_2O_3/TiO_2 ratios (Type 4 corundums). This type also shows more obvious colour zoning than Barrington examples. In fragments they can resemble outer parts of "agate" sapphires, but lack the intense blue cores found in those magmatic types. The strong pink, purple red, red range within the Tumbarumba metamorphic suite overlaps the Barrington field and shows higher Cr and Cr-controlled colour absorption spectra (Type 5 corundums). Tumbarumba ruby, however, extends into purer Cr, Fe-poor absorption spectra than observed at Barrington.

Overall, Tumbarumba corundum suites are not sharply bimodal, as they include suites (Groups 6 and 7) with intermediate trace element and colour absorption characteristics that smear the picture (15%). These intermediate groups include the BGY-like, "trapiche" exsolution (Type 2) sapphires, the vari-coloured diffuse zoned, well-crystallised (Type 3) sapphires and pale blue (Type 4) sapphires.

Corundum crystallisation. The predominant magmatic BGY sapphires have differing interpretations for their formation in the literature, but two main models include:

1 Crystallisation through a hybrid meeting of carbonatitic and silicic melts at mid-crustal levels and T ~400°C (Guo *et al*., 1996a).
2 Crystallisation in syenitic melts generated under deeper crustal to shallow mantle conditions at T 680–900°C, in the presence of hydrous phases such as amphiboles and mica (Australia, Sutherland *et al*., 1998a; Scotland, Upton *et al*., 1999). Such melt

compositions which would calculate normative corundum and zircon are designated as salic compositions (Le Maitre, 1989).

Some points against shallow level carbonatite-silicic melt mixing as a general process for BGY corundum formation are:

i lack of syngenetic mineral inclusions such as carbonates that would reflect carbonatitic input.
ii presence of Nb-bearing syngenetic mineral inclusions (ferrocolumbite, uranopyrochlore), which although found in carbonatites have compositional fields that more closely match these minerals in more silicic parageneses.
iii finds of corundum-bearing xenoliths in basalts (Australia, Scotland) that have syenitic character.
iv oxygen isotope values for corundums and associated minerals (Scotland) that suggest crystallisation in a magmatic reservoir at 800°C and which preclude an origin in crustal lithologies such as meta-sedimentary and evolved high level magmatic bodies.
v corundum crystallisation in syenites (Scotland), which may involve fugitive loss of alkalis and carbonatitic residues from salic melts, rather than direct carbonatitic-silicic magmatic intermingling.
vi general lack of silicic melts associated with eastern Australian basaltic gemfields.

Tumbarumba BGY magmatic sapphires (Type 1) conform with a salic paragenesis in the composition of observed inclusions (ferrocolumbite) and lack of carbonate inclusions expected for carbonatitic or some metamorphic/metasomatic paragenesis. The corundum, zircon, amphibole, feldspar megacryst assemblage in the Ruby Creek basalt also gives circumstantial support for an amphibole-related syenitic association. Some BGY sapphires show change in their crystallisation features during or after growth. Deep blue cores in many "agate-like" sapphires mark an early growth, probably at higher temperatures when corundum can accommodate greater Fe contents (Upton *et al*., 1999). Intense blue colours were considered to largely mark Fe^{2+}-O-Fe^{3+} super-exchange rather than Fe^{2+}-O-Ti^{4+} charge transfer effects (Matson & Rossman, 1988; Upton *et al*., 1999). However, this current and other studies indicate Fe^{2+}-Ti^{4+} charge transfer effects are comparable to or even higher in their intensity in Tumbarumba and other sapphire suites (see also Schwarz *et al*., 2000). The outer "agate"-like milky and light blue growth zones indicate later Fe-depleted oscillatory crystallisation of corundum, due to changes in temperature, pressure, chemical composition or reduction-oxidation effects.

Metamorphic-type Tumbarumba corundums (Types 4 and 5) resemble the Barrington fancy coloured sapphire-ruby suite in some general crystal characteristics. However they lack abundant co-existing mineral phases to better define their parental association and only partially overlap the Barrington metamorphic geochemistry (Figs. 3, 5). Barrington metamorphic corundums crystallised at 780–940°C (based on sapphirine-spinel geothermometry; Sutherland & Coenraads, 1996) and similar temperatures may apply at Tumbarumba. The trace element differences, however preclude any definite correlation and their crystallisation at Tumbarumba involved a chemistry more depleted in Fe relative to Ti and slightly depleted in Cr relative to Ga. The light blue (Type 4) sapphires plot separately to the pink-red (Type 5) corundums in chemical variation diagrams (Figs. 3, 5) suggesting different metamorphic parameters for their origins. Type 4 sapphires, in fact, plot within the field for metasomatic sapphires from Madagascar (Schwarz *et al*., 2000), which raises the possibility for a metasomatic-metamorphic origin.

The enigmatic vari-coloured Tumbarumba intermediate sapphires (Type 3) pose problems for genetic origin. Their Fe, Ti and Ga ranges match "magmatic" sapphires, but Cr is unusually high for such sapphires. Consequently, their absorption spectra show prominent Cr^{3+}+ Fe^{2+}-Ti^{4+} absorption.

1 They may be magmatic in origin, but represent special types associated with Cr-enriched melts (hence higher Cr/Ga). Growth banding typical in magmatic types (Type 1) may not be a completely reliable criterion at Tumbarumba in assigning origin, as it also appears within an apparent metamorphic type (Type 4). Cr-bearing serpentinites near Tumbarumba provide a potential Cr-enriching interactor at depth.
2 They may be metamorphic in origin, but represent special metasomatic types associated with Ga-enriched fluids (hence lower Cr/Ga). Such metasomatic corundums occur in some skarn deposits (Schwarz *et al*., 1996). The presence of granitic intrusions, massive limestones and skarns in the Silurian sequence east of the Gilmore Suture provides potential support for such metasomatic processes near Tumbarumba. However, known exposures seem geographically separated from the gem field, unless the sequences extend westward below the serpentinite belt bounding the field.

Relatively high Ga can occur in metasomatic sapphires (Schwarz *et al*., 1996) but these show lower Fe and Cr contents and their inclusions are more in line with metamorphic corundums (e.g., calcite, phlogopite/biotite, apatite). Magmatic crystallisation from evolving salic melts that interacted with a Cr-bearing source (serpentinite?) seems the most likely origin for this unusual type.

The trapiche-like sapphires (Type 2) exhibit pronounced exsolution due to cooling after crystal growth. Zones of silk radiate from central cores cutting across earlier growth zones and intersect prism faces in hexagonal sections. These sapphires differ from trapiche sapphires described by Schmetzer *et al*. (1996), where the radial arms contain phlogopite inclusions rather than exsolved rutile-hematite inclusions, and also differ from trapiche rubies, which form by a change in growth mechanism (Sunagawa *et al*., 1999). The Tumbarumba examples resemble trapiche-like sapphires found elsewhere in eastern Australia (Sweeny, 1996; Neville & Gnielinski, 1998; authors' observations) and in Scotland (Upton *et al*., 1999), where zones intersect second order prism faces {1120}. Cr_2O_3/Ga_2O_3 ratios are mostly higher (except for CORTUM 58) than is typical for BGY corundums, requiring explanation. Trace element contents determined largely on clearer zones away from the heavily included silk zones would sample corundum from which Fe and Ti had migrated into the crystal-controlled exsolution zones. Gallium, with stable trivalent

Table 9. Summary new whole rock K-Ar dating, Tumbarumba-Cabramurra basalts.

sample number	Status	Ref.	%K#	$^{40}Ar^{*}$(×10 $^{-10}$ moles/g)	$^{40}Ar^{*}/^{40}Ar_{total}$	age±1σ
DR14641	A	1	1.51	0.62433	08.894	23.7±0.2
DR13822	A	2	0.11	0.84825	0.5985	397.4±6.7

DR14641 Basanite, Jimmies Road, Granite Mountain (35°43.5'S 148°12.3'E)

DR13822 Olivine micro-dolerite, Ruby Creek (35°49.4'S 148°11.5'E)

Status A: potassium-bearing phases are fresh. Ref. 1—AMDEL laboratories, A. Webb analyst. Ref. 2—CSIRO Division of Petroleum Research, H. Zwingmann analyst. # mean K value used in age calculations. * denotes radiogenic ^{40}Ar. Age in Ma with error limits given for the analytical certainly at one standard deviation.
Constants: ^{40}K = 0.01167 atom%; $\lambda\beta = 4.962\times10^{-10}y^{-1}$; $\lambda\varepsilon = 0.581\times10^{-10}y^{-1}$

valency would probably follow Fe^{3+} into hematite, as supported by trace element data from Ambondromifehy, Madagascar magmatic sapphires where Fe and Ga show positive correlation with each other (Schwarz *et al.*, 2000). This would alter trace-element values in the residual zones. Alternatively, the trapiche-like structure typifying Type 2 corundums may be a composite phenomenon that developed in both Type 1 and Type 3 corundums, so that some corundums would range into higher Cr_2O_3 (CaO 0.03 wt%, CORTUM 15) and V_2O_3 (Ca 0.015 wt% V_2O_3, CORTUM 19) contents. This alternative would suggest closely linked paragenesis for Type 1 and Type 3 corundums.

Zircon types. Tumbarumba zircons range from pale, anhedral low-U types into better crystallised types that show higher U contents. This is typical of zircon megacrysts from eastern Australian basalt fields, which exhibit wide variations in crystal and chemical features (Hollis & Sutherland, 1985; Robertson & Sutherland, 1992; Worden *et al*., 1996; Sutherland, 1996; Sutherland & Fanning, 2001). The Tumbarumba zircons however, are notable for {110}-{100} prism combinations, a relatively rare feature in eastern Australian suites. This combination is common in Boat Harbour, Tasmania, zircons, but sapphire is relatively rare there. It also appears in a distinctive zircon suite within the Barrington, NSW, gemfield, but this suite is restricted in its abundance, geographical and temporal range compared to the other zircon suites in that field (Sutherland & Fanning, 2001).

Zircon crystallisation. The U-Pb isotope dating on a Tumbarumba zircon indicates crystallisation was probably related to basaltic magmatism. However, the strong resorption of megacrysts suggests this crystallisation was unrelated to the carrier basaltic melts. Zircon can crystallise in some mafic melts (SiO_2 48–60wt%) and these zircons typically have high Th/U (up to 2.3; Heaman *et al*., 1990). Tumbarumba zircons extend to high Th/U (3.47, Table 4), but inclusion studies on zircon megacrysts from elsewhere in Australia favour involvement of evolved salic melts similar to melts associated with corundum crystallisation (Coenraads, 1992). This is consistent with zircon (± corundum)—bearing syenitic xenoliths found in basalts elsewhere (Scotland, Upton *et al*., 1999). The Tumbarumba zircons would develop in salic melts, where Zr-saturation was maintained essentially under non-peralkaline, metaluminous conditions (Watson, 1979; Linthout, 1984).

The morphology developed by Tumbarumba zircons would reflect a variety of factors including temperatures, melt composition and volatile content (see Speer, 1982). The {100} prism forms found in Tumbarumba zircons were initially equated with higher temperature, less evolved melts, with lower U, Th (Pupin & Turco, 1974; Pupin, 1980). However, later studies of zircon crystallisation showed that more complex interactions determined the final morphology of crystal growth. The relative growth of {100} and {110} prism forms are mainly controlled by zircon-supersaturation of the melt and may vary during zircon growth due to cooling effects (Vavra, 1990). In contrast, growth of steep pyramidal {211} forms are dampened by adsorption of incompatible elements. The restrained presence of this form among Tumbarumba crystals suggests host melts with moderately high to high incompatible element concentrations.

The development of {100} and {110} prism combinations found at Tumbarumba may also reflect growth blocking, from U, Th adsorption and substitution of Zr^{4+} and Si^{4+} by Y $(REE)^{3+}$ + P^{5+}, favouring {110} expression (Benisek & Finger, 1993). Adsorption effects may also further control pyramidal forms, with {110} forms being adsorption-sensitive relative to {121} growth and {100} growth being favoured due to adsorption of H_2O inhibiting growth of {110} forms (Vavra, 1994). In contrast, {100} prism development depends largely on cooling rates.

Considering the multiplicity of factors involved in developing zircon crystal forms, only general characteristics of the Tumbarumba host melts can be construed here. The preponderance of {110} prism forms among the combined prism forms favours melts with high zircon-saturation and incompatible element levels, particularly enriched in U, Th relative to Zr. Development of {100} prisms and ditetragonal {311} pyramids among crystals suggest some melts involved lower zircon-saturation and incompatible element contents. The general absence of {100} prisms suggest crystallisation under slow cooling rates. These suppositions depict highly alkaline felsic melts evolving under late-stage, slowly cooling conditions. The Tumbarumba zircons converge in some features towards those of zircon inclusions found in Australian sapphires, which have dominant {110} prism forms and strong enrichments in elements such as U, Th, Hf and REE (Guo *et al*., 1996a,b; Sutherland *et al*., 1998a). Zircon megacrysts in eastern Australia with similar morphologies to Tumbarumba zircons (Boat Harbour, Barrington) contain 0.7–1.1 wt% Hf (Sutherland, 1996; Sutherland *et al*., 1998a). This matches

the range for zircon found in syenitic xenoliths that lack corundum (0.6–1.1 wt% Hf, Scotland; Hinton & Upton, 1991). In comparison, zircons found in corundum-bearing xenoliths (Scotland, Thailand) contain 1.3–3.0 wt% Hf (Hinton & Upton, 1991; Sutherland *et al*., 1998a). Thus, the zircon-crystallising melts at Tumbarumba were evolving towards corundum-crystallising conditions.

Distribution of gemstones. Zircons and corundums concentrate in relatively restricted sections of drainages descending through the basaltic infillings around Tumbarumba. Of eight main palaeochannels reconstructed under the eastern basalts (Fig. 7), the main gem deposits are confined to only three palaeochannels. The greatest concentrations were found in the present upper Buddong, Ruby Creek and Tumbarumba Creek drainage.

Gemstone delivery. Zircon fission track dating indicates gemstones were introduced early in the eruptive cycle (26 Ma), before substantial basaltic flows infilled the leads (19–24 Ma). However multiple deliveries (15–23 Ma) were interspersed with and followed the basaltic infilling. The time-space pattern of delivery suggests local pyroclastic eruptions were important providers. This would yield patchy sources from which hardy gemstones would be easily winnowed and concentrated into local drainages. Some sources would become re-exposed much later, after erosional removal of sealing basalt covers. Many gemstones not only exhibit magmatic corrosion from their eruptive delivery, but show significant abrasion and fragmentation from alluvial processes. The wear on zircons matches alluvial travel equivalent to over 30 km based on research into zircons traced back to their originating points in Victorian drainages (J.D. Hollis data). This raises the possibility of gemstone travel into the area from more distant outside sources, such as the Cabramurra-Kiandra uplands. However, such degrees of abrasion could result equally from continued recycling into fresh channels following disruptions to and erosion of earlier deposits, which may also involve changes in drainage fall and hydraulic forces. Recycling material two or three times would produce equivalent wear and reduce actual transport distances to under 20–25 km, well within the perimeter of the main gem field.

The best preserved zircon crystals were found at Ruby Creek. This suggests a local source, especially as pyroclastic and volcaniclastic horizons occur in the area. However, gemstones are scarce in Paddy's River to the west, so the source was not extensive. Gemstones in a Buddong Creek tributary include strongly abraded "early age" zircons (26 Ma) and shed from a small basaltic lead. This suggests derivation from a source that lay towards Rutherford Ridge in the north part of the basalt field. Gemstone deposits appear in Tumbarumba Creek 4 km south of its headwaters towards Laurel Hill and suggest a flanking rather than a northerly source. One possibility is that the gemstones were reworked from the high level deep lead deposits exposed on the west side, but this lead held little sapphire when under active mining (Curran, 1897). Alternatively, the gemstones may derive from an eastern source from poorly exposed lead or pyroclastic deposits that now lack basalt cover. The palaeodrainage reconstruction (Fig. 7) allows potential input for a lead diverted into the Tumbarumba drainage from Rutherford Ridge, skirting around the Storm Lookout palaeohigh via a basalt remnant at Pilot Hill.

The upper Tumbarumba Creek palaeodrainage includes complex leads formed at different levels and probably represents separate ages of channel disposition. The gemstones concentrate in young, low-level Quaternary deposits and show considerable wear, except for the brightly polished youngest pale, low-U zircons (<19 Ma). These zircons suggest some late-stage eruptive input, possibly from the nearby Laurel Hill centre. They probably entered the drainage after its basaltic infilling and are unlikely to herald a significant corundum contribution. Gemstones are recorded within Tumbarumba lead deposits (23–21 Ma) much farther south near Tooma. Whether this material travelled 30–40 km downstream from the upper Tumbarumba sources, arrived into the lead from the Ruby Creek source, via the lower Paddy's Lead (20–25 km), or even entered the lead from a nearer source (e.g., Mannus Creek tributary lead; Young & McDougall, 1993) is uncertain on present information.

Basalt petrogenesis. Basalts in the Snowy Mountain fields largely represent undersaturated, near-primary magmas based on Mg# and compatible element contents. Similar petrological ranges appear in some other southeastern Australian basaltic gemfields (Oberon, Barrington, Kandos, NSW; Weldborough, Tasmania), although some fields contain more olivine nephelinites (Morris, 1986; Sutherland *et al*., 1989; O'Reilly & Zhang, 1995; Sutherland & Fanning, 2001). Other larger, or more diversely aged basaltic gemfields than the Snowy field (eastern Central Province, Southern Highlands, NSW; Hoy, Qld.) include a wider range of more evolved alkali to transitional basalts (Stephenson, 1989; Sutherland *et al*., 1993; Coenraads, 1994; O'Reilly & Zhang, 1995). Primary and near-primary basanites and alkali to transitional olivine basalts dominate the Snowy basalts (over 70% of basalts analysed here compared to <20% at Oberon). Primary basanites, alkali and transitional basalts, as in the Snowy examples, represent a range in degrees of partial melting in mantle sources. Estimates based on complete partitioning of K_2O or P_2O_5 from the source into the melt (see Morris, 1986) are not used here due to uncertainties introduced by later work (Sun & McDonough, 1989; O'Reilly & Zhang, 1995) on precise modelling of mantle compositions, abundances of various elements and magmatic processes. However, they probably fall within the range of partial melting determined for similar melts elsewhere using incompatible element enrichment factors (basanite 4–6%, alkali basalts 6–11%, transitional basalts 7–12%; Beccaluva *et al*., 1998; Zou *et al*., 2000).

The primary basanites (13835, 14650, 13820, 14662) show high light REE to heavy REE ratios (La/Yb_N 34–46, using chondrite normalising factors after Sun & McDonough, 1989). This, and their high Ce/Y_N ratios (13–18) indicate melts derived from garnet peridotite mantle, with heavy REE and Y being retained in residual garnet. Similar ratios (La/Yb_N 26–39) were noted for alkaline melts generated from garnet lherzolite mantle (Beccaluva *et al*., 1998) and these were significantly higher than ratios for melts derived from overlying spinel lherzolite mantle (La/Yb_N 3–24). Slightly evolved basanite (14641) and alkali basalt (13828) also show relatively high La/Yb_N (24–33) compatible with incomplete melting of a garnet peridotite source. In contrast, primary alkali basalt (14369) shows significantly lower La/Yb_N (21) and Ce/Y_N (8) and probably represents more complete garnet melting or perhaps even melting of spinel

peridotite mantle (alkali basalts, La/Yb_N 11–18; Beccaluva *et al*., 1998).

Accessory mantle phases (amphibole, mica, apatite) influence incompatible element profiles of basaltic melts. Tumbarumba basalts show low K_2O/Na_2O ratios (0.34–0.47) and low Rb/Sr (0.009–0.022) signifying titanian amphibole was a major donor over titanian mica to the alkali element budget in the melts (Wilkinson & Le Maitre, 1987). This is compatible with relative xenocryst abundance in the Ruby Creek basalt (kaersutite > apatite > mica). Titanian amphibole enrichment within the garnet peridotite source for Tumbarumba primary melts feeds into their high Ti/V ratios (64–75) which match ratios for mantle kaersutites (Ti/V 61–90; Wass, 1980). Alkali basalt (14639) sourced from garnet-poor mantle, however, shows lower Ti/V (54) indicating some amphibole depletion. An amphibole (+ apatite) imprint (depleted Rb, K, Zr and enriched Th, Nb, Ta, La and high P; O'Reilly & Zhang, 1995) typifies most of the basalts suggesting extensive amphibole in the underlying mantle. The lower Ba/Sr over Ba ratios (av. 0.00008) for Tumbarumba basalts compared to some other fields (e.g., Oberon, av. 0.00096) supports amphibole dominance over phlogopite as a main additional phase. This is also compatible with moderate Ba and Sr (cf Ba and Sr contents in vein amphibole and phlogopite in garnet lherzolite; Ionov & Hofmann, 1995) and high Ta and Nb enrichment and high light (La, Ce) and middle (Eu) REE enrichment over heavy REE, typical in amphibole-bearing mantle peridotites (McDonough & Frey, 1987; O'Reilly & Zhang, 1995; Eggins *et al*., 1998). The amphibole imprint is less clear in some transitional olivine-basalts, probably due to dilution through higher degrees of partial melting of the source or even amphibole depletion by earlier melting in the source. Relative Nb depletion in one alkali basalt (13828) is anomalous, but this partly evolved, internally segregated rock incorporates a feldspathic, presumably Nb-poor, residue within its make up.

Primary olivine basalt (13822) differs markedly in its incompatible element pattern to other Tumbarumba patterns in its extremely flat light to heavy REE profile and very low La/Yb_N (1) and Ce/Y_N (1) values. Melting of spinel peridotite is favoured over an unusual garnet-free mantle assemblage. The rock is extremely low in K_2O/Na_2O (0.05), moderately high in Rb/Sr (0.056) and low in Ti/V (29) suggesting a source impoverished in both amphibole and mica. The mantle-normalised incompatible element pattern is typical of enriched Mid-Ocean Ridge Basalt (MORB), with relatively flat profile, particularly if the variations in Ta and Hf ratios are often introduced in the analytical process (Sun & McDonough, 1989).

High Mg# alkaline melts with amphibole/apatite imprints, as in the Snowy lavas, were recently described elsewhere in eastern Australia as having HIMU-like trace element arrays (Barrington, NSW; Cooktown, Qld; Zhang *et al*., 2001). These melts were attributed to lithospheric sources rather than asthenospheric sources of true HIMU (high radiogenic lead component) melts which show elevated $^{206}Pb/^{204}Pb$ isotope ratios. However, Snowy primary melts have key element ratios (Zr/Nb 1.0–2.3, La/Nb 0.69–1.38, Ba/Nb 4.9–10.6, Ba/Th 53–81, Rb/Nb 0.13–0.25, K/Nb 73–162, Ba/La 7.1–8.3) that show minimal overlap with values for Tasmanian-Southern Ocean HIMU-related basalts (Zr/Nb 3.1–4.6, La/Nb 0.54–0.62, Ba/Nb 5.0–7.2, Ba/Th 64–99, Rb/Nb 0.32–0.72, K/Nb 111–261, Ba/La 9.3–12.6; Lanyon *et al*., 1993). The Snowy melts resemble Barrington amphibole/apatite signature melts in these ratios (Sutherland & Fanning, 2001) suggesting HIMU-like is an inappropriate term for them.

Partial melting calculation. In order to refine a melting model for the Tumbarumba basalts, quantitative partial melting calculations were undertaken, using two methods: (a) major element mass balance; and (b) incompatible element modelling. Both methods require the estimation of primary magma compositions. Major element compositions of primary magmas were adjusted by mass balance mixing calculations, in which theoretical compositions of Mg-rich olivine (Fo_{89}) and clinopyroxene ($En_{45.5}Fs_{5.5}Wo_{49}$) were added to Tumbarumba basalt analyses to allow for effects of fractional crystallisation. For each basalt, increasing quantities of the two minerals were "mixed in", until the modelled magma composition was appropriate for equilibration with Fo_{89} during partial melting. In determining the equilibrium compositions, a widely used $K_{Mg/Fe2+}^{ol/liq}$ value of 0.3 was applied, following Roeder & Emslie (1970). Weight percentages of ol+cpx fractionation predicted by the models vary between 7% and 20%. Incompatible element contents for the primary magmas were obtained by "reversing" the effects of modelled olivine and clinopyroxene fractionation, using partition coefficients from the literature, and the fractionation equations of Shaw (1970).

The calculation of degrees of partial melting by major element mass balance entails: creating mantle modes for potential bulk mantle and mineral compositions; repeating these calculations using a primary magma composition as an extra phase, in order to find the degree of partial melting; and then comparing the results of each experiment, i.e. mode and mode+melt, to obtain the melting proportion of each mineral in the melting process. Satisfactory mass balance solutions are those resulting in squared residuals of <1. Tables 10 and 11 list melting calculations for Tumbarumba primary magmas, based on six possible mantle mineralogies, namely garnet and spinel lherzolites±phlogopite±kaersutite. Low clinopyroxene contents (5.2–12.5 wt%) combined with low garnet contents (2.1–11.5 wt%) may reflect the presence of metasomatic phases. The most accurate melting models are probably those which produce degrees of melting of >2–3 wt%, and in the order: basanite < alkali olivine basalt < olivine basalt. For some mantle types and bulk compositions (garnet, garnet-phlogopite [b], and garnet-amphibole lherzolite [a, b]), these conditions fail whilst for other types, solutions were not found for some or all primary magma compositions (garnet-phlogopite [b], spinel-phlogopite, and spinel-amphibole lherzolite). Both spinel and spinel-amphibole lherzolites returned feasible solutions; although the former (anhydrous) mantle type is unlikely on the basis of trace element evidence (see below). On the basis of absolute and relative degrees of melting (Table 11), the most feasible source type is garnet-phlogopite lherzolite (a), based on bulk mantle and mineral compositions cited by Comin-Chiaramonti *et al*. (1997). However, no unequivocal evidence is provided by these calculations to discount other modal mineralogies in the source region(s) of the Tumbarumba basalts. In particular, spinel-amphibole lherzolite is still a possible source, although lacking solutions for several primary magmas. It is conceivable that the magmas involved input from both phlogopite- and kaersutite-bearing lherzolites.

Table 10. Modal mineralogy and melting proportions of mantle types.

mantle assemblage		Olivine	Opx	Cpx	Garnet	Spinel	Kaersutite	Phlogopite
Spinel	mode	58.06	25.96	12.45		3.53		
lherzolite	melt prop	0.33	7.64	72.90		19.13		
	SD	0.30	5.10	4.85		0.49		
Garnet	mode	59.80	21.10	7.60	11.50			
lherzolite	melt prop	0.21	7.59	29.64	62.56			
	SD	0.19	4.90	4.30	1.64			
Spinel	mode	59.27	24.90	8.68		2.14	5.02	
amphibole	melt prop	1.08	14.36	17.43		3.23	63.90	
lherzolite (a)	SD	1.16	5.62	5.87		2.71	8.21	
Garnet	mode	59.70	20.22	6.46	9.53		4.09	
amphibole	melt prop	3.74	14.36	28.92	43.23		3.74	
lherzolite (a)	SD	0.66	5.62	0.61	1.06		0.66	
Garnet	mode	65.66	24.23	3.47	2.18		4.47	
amphibole	melt prop	1.59	6.86	13.68	24.37		53.50	
lherzolite (b)	SD	1.06	2.05	2.53	4.66		3.62	
Spinel	mode	58.18	25.18	12.33		3.27		1.05
phlogopite	melt prop	11.00	13.17	52.42		12.97		10.44
lherzolite	SD	15.52	18.59	24.98		3.34		5.78
Garnet	mode	60.29	16.94	9.78	5.98			7.00
phlogopite	melt prop	1.14	3.08	25.55	13.36			56.87
lherzolite (a)	SD	0.75	6.37	9.68	18.90			31.05
Garnet	mode	65.35	22.36	5.23	5.65			1.42
phlogopite	melt prop	0.89	0.89	26.19	68.33			3.71
lherzolite (b)	SD	0.58	0.58	3.22	4.89			4.82

Modal mineralogy of each mantle type is calculated using major element mass balance and also given are the melting proportions (and their standard deviations) which produce the degrees of partial melting listed in Table 11. All values in wt%. All mineral compositions are from McKenzie & O'Nions (1991), except that for amphibole, which is an average value for kaersutite xenocrysts from this study and those used in models GAL (b) and GPL (b), which are from Comin-Chiaramonti *et al*. (1997). In most models, the bulk mantle composition used is that of the bulk Earth (McKenzie & O'Nions, 1991). The only exceptions are models GAP(b) and GPP(b), which are based on an analysis of a garnet-phlogopite xenolith (Comin-Chiaramonti *et al*., 1997). Suffix (a) stands for mantle based on the bulk Earth composition given by McKenzie & O'Nions (1991); and (b) for mantle compositions based on a garnet-phlogopite lherzolite from Comin-Chiaramonti *et al*. (1997).

Table 11. Degrees of partial melting for Tumbarumba primary magma compositions.

sample	garnet lherzolite	garnet-amphibole lherzolite (a)	garnet-amphibole lherzolite (b)	garnet-phlogopite lherzolite (a)	garnet-phlogopite lherzolite (b)	spinel lherzolite	spinel-amphibole lherzolite
14639	6.60	3.00	4.20	2.81	7.79	8.13	6.82
13835	5.10	2.99	1.97	6.27	5.92	6.74	6.12
14650	5.60	0.50	1.95	–	5.45	7.28	–
13820	5.57	1.55	2.72	3.85	5.04	7.10	–
14662	5.30	1.16	2.86	–	5.58	6.94	6.34
13828	5.49	1.85	4.62	4.97	6.66	7.01	9.59
14641	4.65	1.21	1.71	4.05	5.87	6.23	7.79
159	4.86	1.80	2.29	4.60	6.23	6.49	–
61	6.02	1.24	4.73	4.13	6.35	7.46	3.95
63	4.50	2.14	1.41	3.53	8.14	6.04	–
averages							
basanite alkali basalt	5.37	1.44	2.66	4.57	5.70	6.96	6.05
basalt	5.53	2.33	3.41	3.77	7.53	7.06	8.21
olivine basalt	4.86	1.80	2.29	4.60	6.23	6.49	–
average basalt	5.36	2.20	3.13	3.98	7.20	6.92	–

14639 alkali basalt, 13835 basanite, 14650 basanite, 13820 basanite, 14662 basanite, 13828 alkali basalt, 14641 basanite, 159 olivine basalt, 61 basanite, 63 alkali olivine basalt.
Degrees of partial melting are calculated by major element mass balance (see Table 10). All values in wt%.

Degrees of partial melting were estimated by analysing variations in the concentration of incompatible elements during the melting process. Melting curves (Fig. 9) were created for various mantle types, using the batch melting equations of Shaw (1970). Bulk mantle compositions and partition coefficients were obtained from the literature (see Fig. 9 caption), while the modes and melting proportions used were those formulated by major element analysis. These melting curves may be compared to the trace element contents of modelled primary magmas, as follows:

La/Yb vs Yb. When creating the curves a typical "enriched" or "primitive" mantle composition (Sun & McDonough, 1989) could not provide La/Yb ratios for reasonable degrees of melting. Therefore, a second set of curves was created, based on the composition of a cryptically metasomatised mantle xenolith from southeastern Australia (O'Reilly & Griffin, 1988). The latter curves predict approximately 10% melting of garnet lherzolite, or 5–8% melting of garnet-phlogopite and/or garnet-amphibole lherzolite. They also allow input into some alkali basaltic magmas of a 1–2% melt of modally metasoma-

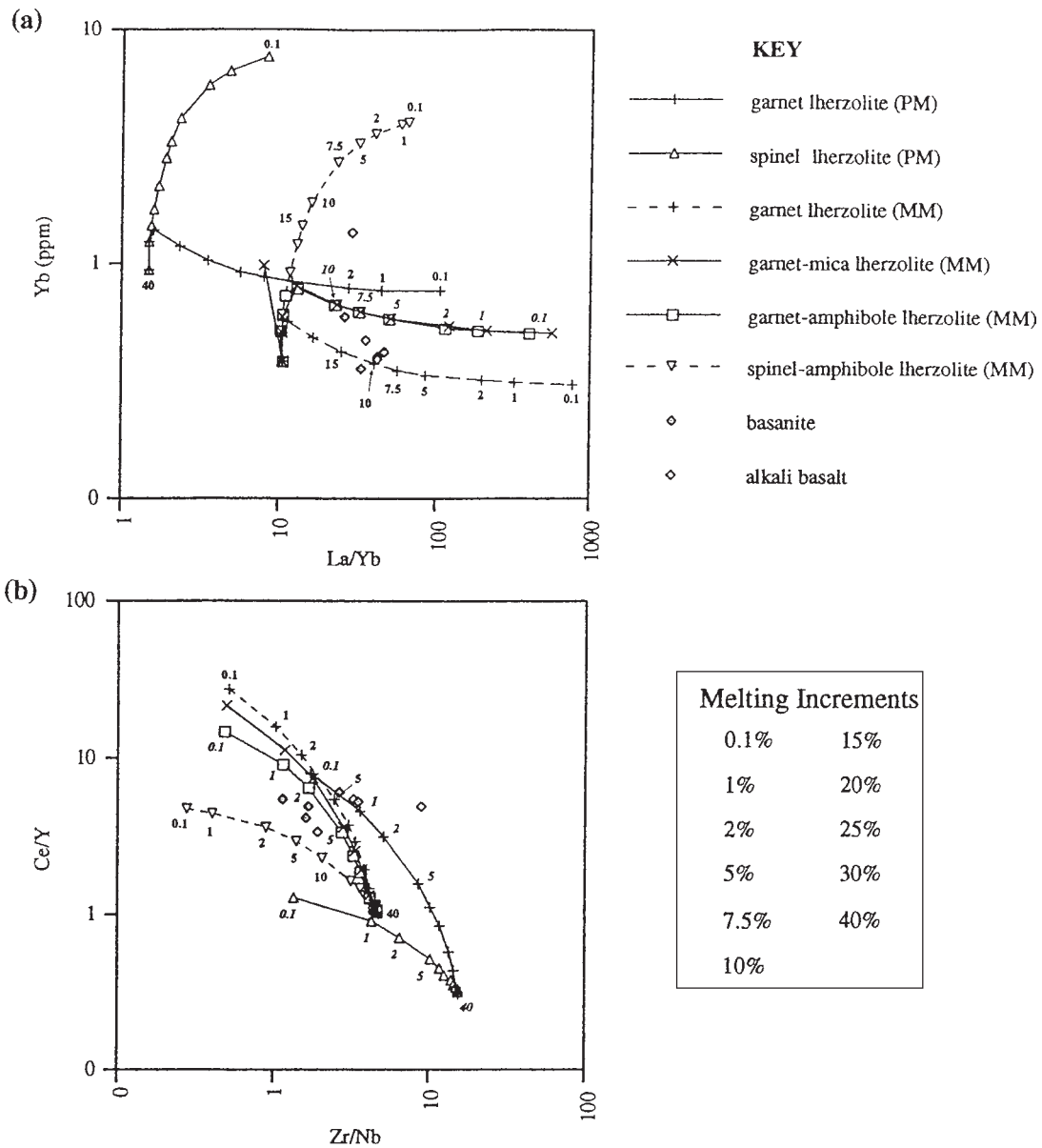

Figure 9. (a,b) Comparison between trace element concentrations in theoretical Tumbarumba primary magmas, and calculated curves for non-modal batch partial melting. See text for explanation. Each curve represents a different combination of mantle type and bulk trace element composition. PM = primitive mantle (Sun & McDonough, 1989); MM = metasomatised mantle (sample WGBM 15, O'Reilly & Griffin, 1988). Curve increments are listed in the Key, as well as being shown on the diagrams. The method for calculating trace element compositions of "primary" magmas is detailed in the text, with mineral/melt partition coefficients for olivine and cpx being obtained from: Ablay *et al*. (1998), Ewart & Chappell (1989), Kostopoulos & James (1992), McKenzie & O'Nions (1991), Nielsen (1998) and Panter *et al*. (1997). Source of partition coefficients used in the melting calculations are: all olivine, cpx, opx, garnet and spinel from Kostopoulos & James (1992), except for the REE (McKenzie & O'Nions 1991); all amphibole and kaersutite from Ionov *et al*. (1997), except REE for phlogopite (McKenzie & O'Nions, 1991).

tised spinel lherzolite. In general, basalts were produced by slightly higher degrees of melting than basanites.

Zr/Nb vs Ce/Y. These curves predict 3–7% melting of garnet lherzolite (metasomatised bulk composition), and/or 2–5% melting of modally metasomatised garnet lherzolite. Again they allow mixing with a 1–2% melt of metasomatised spinel lherzolite. The maximum degree of melting of garnet lherzolite based on the "primitive mantle" bulk composition is only 0.1–1%. Basanites are characterised by lower degrees of melting than alkali basalts.

These findings suggest the Tumbarumba source was dominated by cryptically and/or modally metasomatised, high LREE/HREE (HREE-poor) garnet lherzolite, with possible input of metasomatised spinel lherzolite. It is difficult to choose unequivocally between amphibole and mica as the main metasomatic phase; but on balance, based on the major element calculations, phlogopite seems the dominant phase. This, however, contradicts other evidence such as low Ba/Sr ratios, which suggests dominant amphibole. Again, this may mean the Tumbarumba magmas involved both phlogopite- and kaersutite-dominant mantle sources.

Comparison of the Tumbarumba primary magmas with experimental melts of hydrous mantle peridotites (Kushiro, 1990) permits estimation of the pressures and temperatures controlling partial melting, particularly using variations in the Si and Mg content of magmas (after Kushiro, 1990; Scarrow & Cox, 1995; Hoang & Flower, 1998; Allen, 1999). The results give the following average temperatures: basanite 1269°C; alkali basalt 1311°C; olivine basalt 1237°C. Average pressures/depths are: basanite 23.2 kb (75 km); alkali basalt 22.4 kb (73 km); olivine basalt 19.4 kb (64 km). These values indicate melting near the garnet-spinel transition (Sutherland *et al*., 1998b) and the region where the "H_2O-undersaturated" solidus of Kushiro (1990) intersects the boundary of the phlogopite stability field (Hoang & Flower, 1998). They also suggest melting within or above the Low Velocity Zone in lithospheric mantle, which probably lies at >120 km below the Snowy region.

Evolution of Tumbarumba Gemfield. Dating of gem minerals and basalts suggests this gemfield mainly evolved over some 10 million years from Late Oligocene to Middle Miocene time (27–15 Ma).

Late Oligocene activity (27–24 Ma). Zircon and associated corundums were discharged explosively as xenocrysts in undersaturated volatile-rich basaltic melts. This activity centred in the northwest region. It followed initial low volume mantle melting, which crystallised zircon and corundum from evolved salic melts within the mantle/crust boundary. Two main potential mechanisms could generate magmatic zircon and corundum crystallisation under mantle conditions. One involves minor melting of amphibole (± garnet)-bearing mantle to provide relatively aluminous basaltic melts (Sutherland *et al*., 1998a). These would fractionally crystallise, leaving residual liquids which then evolved towards salic compositions capable of crystallising zircon and corundum between 700–900°C and 0.7–1.1 Gpa. Alternatively, the salic melts formed with volatile fluxing and metasomatism of lithospheric mantle, yielding small fraction trachytic melts (Upton *et al*., 1999). These evolved to peraluminous corundum-crystallising conditions, between 700–970°C, perhaps involving fugitive alkali and carbonate loss.

The mantle-derived salic melts proposed here for crystallising Tumbarumba magmatic gemstones receive some support from alkaline, aluminous silica-rich glasses found in mantle xenoliths from basaltic fields, including eastern Australian examples. However, interpretation of these glasses has been a contentious subject. Some workers link them to melts derived from melting amphibole-bearing mantle (Schiano & Clocchiatti, 1994; O'Connor *et al*., 1996). Others, however, equate them with mixing of introduced basaltic melts and siliceous melts produced by orthopyroxene reactions (Wilshire & McGuire, 1996; Neumann & Wulff-Pedersen, 1997), or with metasomatic reactions related to ephemeral alkali-rich carbonatites (Wiechert *et al*., 1997; Coltorti *et al*., 1999), or even with diffusion of sodium into partially molten peridotite (Lundstrom, 2000). Other workers consider they only represent localised *in situ* melting of mantle phases and were produced by high temperature (1010–1100°C) decompressive melting during rapid transport of xenoliths (Chazot *et al*., 1996; Eggins *et al*., 1998; Yaxley & Kamenetsky, 1999). Clearly a range of processes may be involved. Experimental work on more extreme silicic glass compositions (Draper & Green, 1997) suggested low degree melts of such compositions could co-exist and circulate within mantle assemblages, particularly harzburgitic mantle. However, phlogopite would be the main hydrous equilibrium phase, rather than amphibole, and this may not match Tumbarumba shallow mantle. Another study suggested that in eastern Australia carbonatitic melts produced amphibole, phlogopite and apatite metasomatism and this may release a fugitive alkaline, aluminous silicic melt (Yaxley *et al*., 1998).

Several potential mechanisms thus exist for salic melt generation in the Tumbarumba mantle during initial Oligocene melting. A comparison of low-volume melt glasses in deeper garnet-spinel transitional peridotite (2.5 GPa) with those in shallower spinel peridotite (1 GPa) showed that at the lower pressure melts were more siliceous and alkaline in composition (Schiano *et al*., 2000). On this basis, the salic gem-forming melts under Tumbarumba would probably crystallise in shallow spinel peridotite mantle at P <1 GPa (i.e. <35 km depth).

Not all magmatic gemstone crystallisation at Tumbarumba need stem from the initial Late Oligocene melting. Low-volume melting conditions suitable for salic zircon and corundum formation may develop repeatedly around waxing and waning of episodic basaltic magmatism (Sutherland *et al*., 1993; Sutherland *et al*., 1998a; Sutherland & Fanning, 2001). Similarly, expulsion of the rarer metamorphic corundums and garnet could mark fortuitous intersections of basaltic magma with crustal metamorphic assemblages at any stage of eruptive activity.

The precursor mantle melting and explosive basaltic activity may have accompanied tectonic activity, which dammed and possibly reversed drainages, to give the sediments now preserved in deep leads (Gill & Sharp, 1957). This tectonism would follow conjectured faulting, tilting and downwarping proposed along the adjacent continental margin (Brown, 2000), which affects coastal basalts older than 28 Ma (Spry *et al*., 1999). The timing of such tectonism, however, remains in debate (Young/Brown, 2000).

Early Miocene activity (24–18 Ma). Basaltic lava flow activity developed more fully after 24 Ma. Lavas emanating from the earlier regions of gem-bearing eruptions descended drainages flowing off the Granite Mountain palaeohigh, overtopping Paddy's palaeochannel and extending south to Tooma. Basanites and alkali basalts in these sequences indicate some 5–8% partial melting within the underlying metasomatised garnet peridotite mantle.

Lava flow activity became widespread across the Tumbarumba-Kiandra region by 22 Ma. This activity peaked, with near-saturated basalts being generated as degrees of partial melting in the mantle exceeded 10%. Melting rose into the overlying spinel peridotite mantle, with reduced imprints of amphibole and other hydrous phases. The rhyolitic tuff in the upper Tooma sequence (between 22.8–21.3 Ma) presents an enigmatic feature. It suggests local silicic activity, as the nearest known Early Miocene rhyolitic centres are minor bodies over 450 km north (Wingham; Sutherland, 1999), while larger central volcanoes lie over 600 km north (Nandewars, Tweed Shield; Duncan & McDougall, 1989).

Following this peak magmatism, western activity partly subsided, allowing an interlude of explosive gem-bearing activity, providing the second zircon fission track age peak (22–21 Ma). Further lava flow activity then topped up the Tumbarumba lead descending from Laurel Hill and western Paddy's lead to Tooma. Some eastern lava flow activity also took place, e.g., dyke and lower entrenched basanite flow, 8 km NE of Cabramurra. This later undersaturated magmatism marked relatively low degrees of partial mantle melting (around 4–6%).

Early-Middle Miocene activity (18–13 Ma). The late Tumbarumba magmatism seems to largely reflect explosive gemstone-bearing activity, marking the third zircon fission track age peak (16–15 Ma). This phase produced the magmatically polished and little abraded low U-zircons, which probably crystallised from less evolved alkaline melts. The unusual vari-coloured intermediate character corundums may belong here, as their more complete crystals suggest less re-working than for the other fragmentary corundum types. Minor alkaline melt pockets interacting with Cr-bearing wall rocks (serpentinite bodies?) may explain their origin, but their late development requires confirmatory age dating.

Overall synthesis (27–15 Ma). Some sapphires (Type 3) contain zircons with suspected inherited U-Pb ages (C46) which range up to the age of serpentinite bodies, suggesting formation later than, and possibly involving, those intrusions. Other sapphires (C63) contain zircons that provide ages comparable to the Miocene basaltic events and may indicate formation with that melting episode. Type 1 magmatic sapphires remain undated, lacking identified zircon. However, it is hoped to use the abundant ferrocolumbite inclusions as a dating technique in further investigations. Magmatic and metasomatic gemstone eruption (27–15 Ma) overlapped basaltic lava field magmatism (24–19 Ma). Lava fields, such as the Snowy field, have been equated to either sporadic diapiric mantle upwellings of OIB-related magmas, or to melting associated with long standing asthenospheric plumes (O'Reilly & Zhang, 1995; Zhang & O'Reilly, 1997; Sutherland, 1998). Distinction between short term mantle diapirs and longer term diapirs and plumes is not always clear, as long term plume traces can exhibit discontinuous activity and involve both silicic central volcanoes and basalt lava fields (Sutherland, 1998; Sutherland & Fanning, 2001). If the Snowy field is plume-linked, then a migration in volcanism related to Australian plate motion should show up in adjacent lava fields.

During the Snowy field evolution, the Australian plate was moving northeasterly (0.63°/My from 30–20 Ma, 0.55°/My from 20–10 Ma; Sutherland, 1998). Comparison of the adjacent Snowy and Grabben Gullen basalt ages along this trend are shown in Figure 10. The Grabben Gullen basalt ages are adopted from Bishop *et al*. (1985), deleting the youngest ages which they discounted due to alteration effects. The ages suggest a shift between the two fields compatible with Australian motion (using an averaged 0.6°/My from 26–18 Ma). However Grabben Gullen dating is less complete than Snowy dating and lacks zircon fission track dating, while some uncertainties lie in Australia's precise plate motion because of differences in Indian and Pacific Ocean hotspot paths. Further testing of a mantle plume model needs to include the Oberon field, northeast of Grabben Gullen. However, only one basalt is dated there (18 Ma), although zircon fission track dating suggests activity extended beyond 27 Ma (F.L. Sutherland, unpublished data). Basalt fields with related migratory age are not obvious south of the Snowy field, so at best a migratory model would fit a short term (<20 Ma) mantle diapir. The thermal event peaked under Tumbarumba at 22 Ma, marked by maximum basalt generation and possible minor rhyolitic activity.

The post-eruptive evolution of the gemfield mainly reflects erosion. Since the Palaeogene, plateau surfaces, including the basaltic surfaces, were lowered by 2–5 m/My and major streams incised their courses by 5–18 m/My (max. 30 m/My), producing present profiles strikingly similar to pre-basaltic profile (Young & McDougall, 1993). The original gemstone deposits were eroded on exposure and now represent recycled heavy mineral concentrations in the recent drainage, within alluvial terraces and river beds.

Gemfield comparisons. Tumbarumba gemfield carries magmatically resorbed corundums and zircons that feature in many eastern Australian basaltic fields (Sutherland, 1996). Tumbarumba corundums, however show a particularly wide range of magmatic, metamorphic and metasomatic (?) types. Some of the sapphire types have unusual characteristics and there are two variants of ruby. This suite is more complex than other bimodal Australian suites (Barrington). Multi-modal suites are not confined to Tumbarumba, as similar intermediate character corundums also appear elsewhere (Swanbrook, New England, NSW; Myrniong, Victoria; Sutherland *et al*., 1999) and large spreads in corundum characters are noted across some regions (Victoria—Birch & Henry, 1997).

Amphibole-endowed mantle features under several other basaltic gemfields besides Tumbarumba (e.g., New England—Wilkinson & Hensel, 1991; Barrington—Sutherland & Fanning, 2001). Such fields show closely similar incompatible element ranges and are summarised in Table 12. Other basaltic fields with minor gem deposits (e.g., Southern Highlands, Monaro) also include a proportion of basalts that indicate localised amphibole-mantle sources (O'Reilly & Zhang, 1995; Roach, 1999). Thus, ample titanian amphibole in mantle regions may be a

Table 12. Comparative key mantle-normalised incompatible element ranges, selected primary Na-rich basalts, eastern Australian sapphire fields.

basalt field no. analyses	Snowy[a] 6	Barrington[b] 10	Oberon[c] 7	New England[d] 3	Hoy, Qld[e] 3	NE Tas[f] 1
SiO_2	43.1–46.2	41.4–46.5	43.2–45.7	44.0–44.7	42.0–44.9	44.6
MgO	9.3–16.8	9.0–12.3	8.8–12.9	8.0–9.5	9.6–12.4	8.7
Ka_2O/Na_2O	0.24–0.47	0.19–0.37	0.20–0.45	0.45–0.48	0.39–0.49	0.31
K_N	23–54	25–53	29–54	33–54	40–57	26
P_N	25–65	24–62	17–32	27–65	27–65	19
Zr_N	10–17	10–21	14–27	13–24	15–21	14
Nb_N	80–190	52–132	56–122	59–98	59–126	59
Rb_N	16–48	16–50	22–46	33–36	30–50	25
Th_N	59–141	35–188	–	24–71	24–94	30
Ta_N	122–220	49–195	–	–	–	–

[a] this paper (4Bsn, 2AOB). [b] O'Reilly & Zhang (1995) and Sutherland & Fanning (2001) (3 Ne, 5Bsn, 2AOB). [c] Morris (1986) (5Bsn, 2AOB). [d] Coenraads (1994) (3AOB). [e] Sutherland & Robertson (unpublished data) (1Ne, 2AOB). [f] Sutherland *et al*. (1989) (1AOB). $_N$ primitive mantle normalised values, based on Sun & McDonough (1989). Ne, Nephelinite; Bsn, Basanite; AOB, Alkali Olivine Basalt.

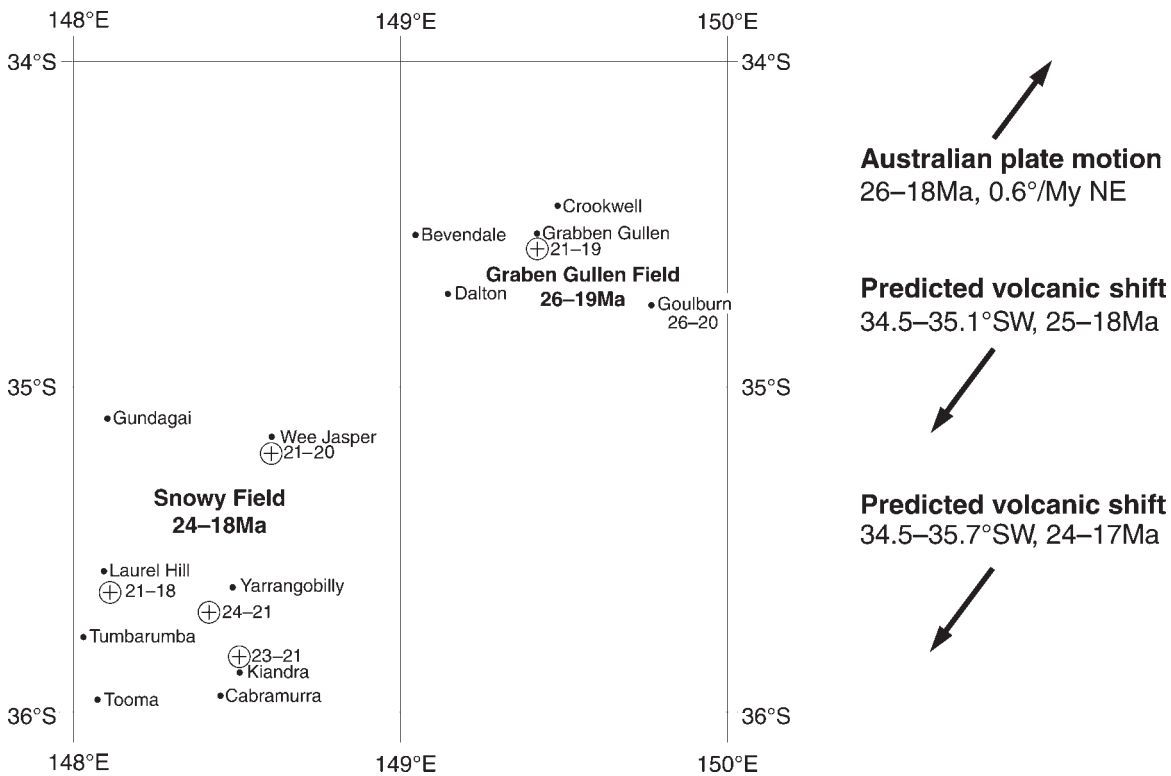

Figure 10. Comparative post-Eocene basalt ages, Southern Tablelands–Snowy Mountains region, New South Wales, Australia. Age data for Grabben Gullen field from Bishop *et al*. (1985) and for Snowy field from Wellman & McDougall (1974), Young & McDougall (1993) and this paper. The diagram sets out entries in approximate geographic relationship. ⊕ indicates sapphire/zircon gemstone locality. Arrows indicate directions of plate motion and predicted volcanic shift.

factor in developing minor melts that crystallise zircon and corundum before mobile basaltic melts disrupt and carry up gem debris from their sources. Titanian mica may be more plentiful in some sources and contribute to the medium-K primary basalts found within several gemfields (Oberon—Morris, 1986; New England—Wilkinson & Hensel, 1991; Hoy—F.L. Sutherland & A.D. Robertson, unpublished data; Southern Highlands—O'Reilly & Zhang, 1995). Mixed mica-amphibole-enriched mantle sources for zircon and corundum crystallising melts, indeed, were proposed under Scottish basalt fields (Upton *et al*., 1999).

Trace element ratios (Cr_2O_3/Ga_2O_3 vs Fe_2O_3/TiO_2) for Tumbarumba corundum suites (Fig. 3) can be compared with those from several eastern Australian basaltic fields (Sutherland & Schwarz, 2001). The magmatic Tumbarumba corundums occupy the usual BGY corundum envelope for many suites, although one variant lacks the typical strong Fe^{2+}-Fe^{3+} charge transfer colour absorption. The trapiche-like corundums range into higher Cr_2O_3/Ga_2O_3, but limited data on these "exsolution" corundums elsewhere restrict detailed comparisons. Metamorphic Tumbarumba corundums only show minor overlap with the Barrington

(higher Fe_2O_3/TiO_2) and Wellington (higher Cr_2O_3/Ga_2O_3) metamorphic envelopes. The high-Fe Tumbarumba ruby falls within and the low-Fe ruby just outside the Barrington envelope. The Wellington pink corundums are geochemically distinct and may derive from corundum-fassaite-garnet granulite assemblages, found as xenoliths in Jurassic breccia pipes (Sutherland & Schwarz, 2001).

Tumbarumba zircons display a moderate spread in crystal characteristics and fission track ages (27–16 Ma) compared to some other fields (e.g., New England, 81–6 Ma; Sutherland *et al*., 1993). The unusual {100}-{110} prism combination probably reflects high incompatible element contents in highly evolved alkaline melts. Similar crystal forms in Boat Harbour, Tasmania, zircons (Hollis & Sutherland, 1995; Sutherland, 1996) differ in containing quartz inclusions, while corundum is a rare associate. The zircon-bearing Boat Harbour basalt sequence includes evolved alkaline lavas (Sutherland *et al*., 1996), so that zircon crystallisation within crustal magma chambers remains a feasible process there. Tumbarumba basalts, however, lack extended fractionation, which favours zircon crystallisation from deep, low-volume, mantle-derived salic melts.

Many eastern Australian gemfields, including Tumbarumba, occupy granite-intruded basement rocks (e.g., Grabben Gullen, Oberon, Barrington, New England, NSW; Hoy, Lava Plains, Queensland; Victoria; NE Tasmania). This may just reflect abundant granite generation within the foldbelts, but could signal some genetic connection. A link between the gemfields and hydrous metasomatised mantle sources may involve slab subduction processes prior to granite emplacement as volcanic arc slivers are known along the Gilmore Suture (Scheibner & Basden, 1996). Metasomatised slabs would favour low-volume salic melt generation during initial basaltic thermal input. Ionov & Hofmann (1995) presented a model where vein titanian amphibole (and mica), enriched in Nb and Ta, develop in mantle peridotite above a subduction zone at depths of 50–90 km. Such metasomatic veinings would have different ages, depending on particular subduction/granite emplacement regimes within eastern Australia (Scheibner & Basden, 1996). This fits Sr isotopic studies of eastern Australian basalt fields, which suggest episodic, heterogeneous amphibole (+ mica + apatite) introductions within mantle source regions (O'Reilly & Griffin, 1984, 2000). The amphibole/mica-poor MORB source for the 400 Ma Ruby Creek micro-dolerite suggests amphibole metasomatism either post-dated or lay at deeper mantle levels at that time.

This Tumbarumba gemfield study shows:

1 Australian gem corundum suites not only extend to well-defined bimodal magmatic and metamorphic suites (Barrington), but also include polymodal suites of magmatic, magmatic "exsolution", magmatic-metasomatic and metamorphic origins.

2 Australian magmatic BGY corundum and related zircon typically develop from minor salic melts associated with amphibole-enriched mantle below the host basaltic fields.

3 Some Cr-enriched metasomatic and metamorphic corundum suites may reflect interactions of basaltic melting events with local Cr-bearing serpentinite belts.

ACKNOWLEDGMENTS. Fieldwork and sampling in the Tumbarumba-Kiandra area was assisted by A. Spate and D. Costello, Tumut Office, NSW National Parks & Wildlife, who arranged collecting permits; by G. Martin, Tumbarumba, who provided information and access to his property and west Tumbarumba drilling program, as well as considerable hospitality; by R. Condon, Holdsworthy, who supplied underground water drilling logs and core samples from west Tumbarumba; by J. Law, Tumbarumba Creek Caravan Park, who introduced local prospectors; by S.A. "Bluey" Miller, Adelong Road, for permission to sample on his land and for making his local gem collection available for inspection; by Dr H. Corbella, sabbatical visitor, University of Sydney, who assisted in the January–February 1997 trip; by M. Auybi who assisted in the April 1997 trip; by R. Abell, AGSO, Canberra, who aided the April work by providing radiometric maps and advice on basalt sites related to the Yarrangobilly 1:100 000 mapping projects. Dr L.M. Barron, G. Oakes and S.R. Lishmund provided field and analytical data from NSW Mineral Resources sources.

Further gem materials for the study came from P.J. Brown, Albion Park, who was instrumental in arranging purchase of a large parcel of sapphires collected by the family over 10 years and from K.G. McQueen, Cooperative Research Centre for Landscape Evolution and Mineral Exploration, University of Canberra, and P.W. Millsteed, Canberra, ACT.

Analytical aspects of the study were aided by Prof. W.B. Stern, University of Basel in his joint trace-element analytical gem program with D. Schwarz, Gübelin Gem Lab, Lucerne, Switzerland; by M. Garland, Geology Dept., University of Toronto, Canada who undertook laser Raman spectroscopy on sapphire inclusions; by C. Knockolds, Electron Microscope Unit, University of Sydney, who facilitated electron microprobe studies; and by K.J. Henley, AMDEL, Adelaide, who supervised basalt analyses. B.J. Barron, organised EMP analyses of garnet grains at CSIRO, Sydney.

Geochronology was organised through P.D. Kinny and M.C. Fanning (U-Pb isotope work), SHRIMP facility, Australian National University, ACT, through P. Green (zircon fission track), Geotrack International, Melbourne, and through B. Webb, AMDEL, and H. Zwingmann, CSIRO Petroleum, Sydney (K-Ar dating).

Preparation of the samples, script and diagrams was assisted by S. Folwell, R. Springthorpe, D. Colchester and S. Lindsey, Australian Museum; by R. Hungerford and L. Callan, Environmental Sciences, University of Technology, Sydney and K. Maynard, Sydney. The Australian Museum Trust provided funds for the project. K.G. McQueen read the script, while P.W. Carr, Geology Department, University of Wollongong, NSW and I.C. Roach, Department of Geology, Australian National University, Canberra, ACT provided valuable comments during reviews.

References

Ablay, G.J., M.R. Carroll, M.R. Palmer, J. Marti & S.J. Sparks, 1998. Basanite-phonolite lineages of the Teide-Pico Viejo volcanic complex, Teneriffe, Canary Islands. *Journal of Petrology* 39: 905–936.

Allen, T.C., 1999. Petrogenesis of the Jurassic Igneous Rocks of Southeastern Australia. *PhD thesis*, University of Sydney (unpubl.)

Andrews, E.C., 1901. Report on the Kiandra Lead. *New South Wales Geological Survey—Mineral Resources* 10, pp. 32.

Barron, L.M., 1987. Summary of petrology and chemistry of rocks from the Sapphire Project. *Geological Survey of New South Wales Department of Mineral Resources—Petrological Report* 87/9 (unpublished).

Beccaluva, L., F. Siena, M. Coltorti, A. Di Grande, A. Lo Giudice, G. Macciolta, R. Tassinari & C. Vaccaro, 1998. Nephelinitic to tholeiitic magma generation in a transitional tectonic setting: an integrated model for the Iblean volcanism, Sicily. *Journal of Petrology* 39: 1547–1576.

Benisek, A., & F. Finger, 1993. Factors controlling the development of prism faces in granite zircons: a microprobe study. *Contributions to Mineralogy and Petrology* 114: 441–451.

Birch, W.D., & D.A. Henry, 1997. *Gem Minerals of Victoria*. Special Publication No. 4 of the Mineralogical Society of Victoria, pp. 120. Melbourne: Royal Society of Victoria.

Bishop, P., R.W. Young & I. McDougall, 1985. Stream profile change and longterm landscape evolution: Early Miocene and modern rivers of the east Australian highland crest, central New South Wales, Australia. *Journal of Geology* 93: 455–474.

Brown, M.C., 2000. Cenozoic tectonics and landform evolution of the coast and adjacent highlands of southeast New South Wales. *Australian Journal of Earth Sciences* 47: 245–357.

Chazot, G., M.A. Menzies & B. Harte, 1996. Silicate glasses in spinel lherzolites from Yemen: origin and chemical composition. *Chemical Geology* 134: 159–179.

Chen, Y.D., S.Y. O'Reilly, W.L. Griffin & T.E. Krogh, 1998. Combined U-Pb dating and Sm-Nd studies on lower crustal and mantle xenoliths from the Delegate basaltic pipes, southeastern Australia. *Contributions to Mineralogy and Petrology* 30: 154–161.

Clarke, W.B., 1860. *Researches in the Southern Goldfields of New South Wales*, 2nd edn, vii, pp. 305. Sydney: Reading and Wellbank.

Coenraads, R.R., 1990a. Key areas for alluvial diamond and sapphire exploration in the New England gem fields, New South Wales, Australia. *Economic Geology* 85: 1186–1207.

Coenraads, R.R., 1990b. Palaeogeography of the Braemar deep-lead sapphire deposit, New South Wales. *Journal and Proceedings of the Royal Society of New South Wales* 123: 75–84.

Coenraads, R.R., 1992. Sapphires and rubies associated with volcanic provinces: inclusions and surface features shed light on their origin. *Australian Gemmologist* 18: 70–78.

Coenraads, R.R., 1994. Evaluation of potential sapphire source rocks within the catchments of Kings Plains Creek and Swan Brook, near Inverell, New South Wales. *Records of the Australian Museum* 46: 5–24.

Coenraads, R.R., F.L. Sutherland & P.D. Kinny, 1990. The origin of sapphires: U-Pb dating of zircon inclusions shed new light. *Mineralogical Magazine* 54: 1113–1122.

Coldham, T., 1985. Sapphires from Australia. *Gems & Gemology* 21(3): 130–146.

Coltorti, M., C. Bonadiman, R.W. Hinton, F. Siena & B.G.J. Upton, 1999. Carbonate metasomatism of the oceanic upper mantle: evidence from clinopyroxenes and glasses in ultramafic xenoliths of Grande Comore, Indian Ocean. *Journal of Petrology* 40: 133–165.

Comin-Chiaramonti, P., A. Cundari, E.M. Piccirillo, C.B. Gomes, F. Castorina, P. Censi, A. De Min, A. Marzoli, S. Speziale & V.F. Velazquez, 1997. Potassic and sodic igneous rocks from eastern Paraguay: their origin from the lithospheric mantle and genetic relationships with the associated Parana flood tholeiites. *Journal of Petrology* 38: 495–528.

Compston, W., I.S. Williams, J.L. Kirschvink, Z. Zhang & M.A. Guogan, 1992. Zircon ages for the Early Cambrian time-scale. *Journal of the Geological Society of London* 149: 171–184.

Curran, J.M., 1897. On the occurrence of Precious Stones in New South Wales and the Deposits in which they are found. *Journal and Proceedings of the Royal Society of New South Wales* 30: 214–285.

Dana, E.S., 1932. *A Textbook of Mineralogy*, 4th ed, pp. 851. Boston: F.H. Gilson Co.

Degeling, P.R., 1982. *Wagga Wagga 1:250 000 Metallogenic Map SI 55-15 (plus parts of SI 55-14, SJ 55-2, SJ 55-3) Mine Data Sheets and Metallogenic Study*. Pp. 451. Sydney: Geological Survey of New South Wales.

Draper, D.S., & T.H. Green, 1997. *P-T* phase relations of silicic, alkaline, aluminous mantle-xenolith glasses under anhydrous and C-O-H fluid-saturated conditions. *Journal of Petrology* 38: 1187–1221.

Duncan, R.A., & I. McDougall, 1989. Volcanic Time-Space Relationships. In: *Intraplate Volcanism in Eastern Australia and New Zealand*, ed. R.W. Johnson, pp. 43–54. Cambridge: Cambridge University Press.

Eggins, S.M., R.L. Rudnick & W.F. McDonough, 1998. The composition of peridotites and their minerals: a laser-ablation ICP-MS study. *Earth and Planetary Science Letters* 154: 53–71.

Ewart, A., & B.W. Chappell, 1989. Trace element geochemistry. In: *Intraplate Volcanism in Eastern Australia and New Zealand*, ed. R.W. Johnson, pp. 219–235. Cambridge: Cambridge University Press.

Galbraith, R.F., 1981. On statistical modes for fission track counts. *Mathematical Geology* 13: 471–488.

Galbraith, R.F., 1988. Graphical display of estimates having differing standard errors. *Technometrics* 30: 271–281.

Galbraith, R.F., & P.F. Green, 1990. Estimating the Component Ages in a Finite Mixture. *Nuclear Tracks Radiation Measurement* 17: 197–206.

Gill, E.D., & K.R. Sharp, 1957. The Tertiary rocks of the Snowy Mountains, eastern Australia. *Journal of the Geological Society of Australia* 4: 21–40.

Gleadow, A.J.W., A.J. Hurford & R.D. Quaife, 1976. Fission track dating of zircon: improved etching techniques. *Earth and Planetary Science Letters* 33: 169–187.

Graham, I.T., 2000. The Genesis and Tectonic Significance of Chromitite-bearing Serpentinites in Southern New South Wales, *PhD Thesis*, University of Technology, Sydney (unpubl.) 2 vols.

Graham, I.T., B.J. Franklin, B. Marshall & G. Caparelli, 1998. U/Pb and Nb/Sm geochronology of ophiolitic rocks from the Tumut serpentinite province, southern NSW. *Geological Society of Australia Abstracts Series* 49: 175.

Graham, I.T., B.J. Franklin, B. Marshall, E.C. Leitch & M. Fanning, 1996. Tectonic significance of 400 Ma zircon ages for ophiolitic rocks from the Lachlan Fold Belt, eastern Australia. *Geology* 24(12): 1111–1114.

Green, P.F., 1981. A new look at statistics in fission track dating. *Nuclear Tracks* 76: 148–150.

Green, P.F., 1985. A comparison of zeta calibration baselines in zircon, sphene and apatite. *Chemical Geology (Isotope Geoscience Section)* 58: 1–22.

Guo, J.F., S.Y. O'Reilly & W.L. Griffin, 1996a. Corundum from basaltic terrains: a mineral inclusion approach to the enigma. *Contributions to Mineralogy and Petrology* 122: 368–386.

Guo, J.F., S.Y. O'Reilly & W.L. Griffin, 1996b. Zircon inclusions in corundum megacrysts: I. Trace element geochemistry and clues to the origin of corundum megacrysts in alkali basalts. *Geochimica et Cosmochimica Acta* 60: 2347–2363.

Heaman, L.M., R. Bowins & J. Crocket, 1990. The chemical composition of igneous zircon suites: implications for geochemical tracer studies. *Geochimica et Cosmochimica Acta* 54: 1597–1607.

Hinton, R.W., & B.G.J. Upton, 1991. The chemistry of zircon: Variation within and between large crystals from syenite and alkali basalt xenoliths. *Geochimica et Cosmochimica Acta* 55: 3287–3302.

Hoang, N., & M. Flower, 1998. Petrogenesis of Cenozoic basalts from Vietnam: implication for origins of a "diffuse igneous province". *Journal of Petrology* 39: 369–395.

Hollis, J.D., & F.L. Sutherland, 1985. Occurrences and origins of gem zircons in eastern Australia. *Records of the Australian Museum* 36: 299–311.

Hughes, R.W., 1997. Ruby & sapphire. Pp. 511. Boulder, Colorado: RWH Publishing.

Hurford, A.J., & P.F. Green, 1983. The Zeta age calibrations of fission-track dating. *Isotopic Geoscience* 1: 285–317.

Ionov, D.A., & A.W. Hofmann, 1995. Nb-Ta-rich mantle amphiboles and micas: implications for subduction related metasomatic trace element fractionations. *Earth and Planetary Science Letters* 131: 341–356.

Ionov, D.M., W.L. Griffin & S.Y. O'Reilly, 1997. Volatile-bearing minerals and lithophile trace elements in the upper mantle. *Chemical Geology* 141: 153–184.

Johnson, R.W. & M.B. Duggan, 1989. Rock classification and analytical databases. In: *Intraplate Volcanism in Eastern Australia and New Zealand*, ed. R.W. Johnson, pp. 12–13. Cambridge: Cambridge University Press.

Knutson, J., & M.C. Brown, 1989. Monaro, Snowy Mountains and South Coast. In: *Intraplate Volcanism in Eastern Australia and New Zealand*, ed. R.W. Johnson, pp. 130–131. Cambridge: Cambridge University Press.

Kohn, B.P., A.J.W. Gleadow & S.J.D. Cox, 1999. Denudation history of the Snowy Mountains: constraints from apatite fission track thermochronology. *Australian Journal of Earth Sciences* 46: 181–198.

Kostopoulos, D.K., & K.D. James, 1992. Parameterisation of the melting regime of the shallow upper mantle and the effects of variable lithospheric stretching on mantle model stratification and trace element concentrations in magmas. *Journal of Petrology* 27: 745–750.

Krosch, N.J., & W. Cooper, 1991a. Queensland sapphire. *Australian Gemmologist* 17(11): 460–464.

Krosch, N.J., & W. Cooper, 1991b. Queensland sapphire II. *Australian Gemmologist* 17(12): 511–515.

Kushiro, I., 1990. Partial melting of mantle wedge and evolution of island arc crust. *Journal of Geophysical Research* 95(B10): 15929–15939.

Lafeber, D., 1956. Columnar jointing and intracolumnar differentiation in basaltic rocks. *Verhandelingen. Koninklijke Nederlands Geologisch Mijnbouwkundig Genootschap* 16: 241–245.

Lanyon, R., R. Varne & A.J. Crawford, 1993. Tasmanian Tertiary basalts, the Balleny plume, and opening of the Tasman Sea. *Geology* 21: 555–558.

Le Maitre, R.W., ed., 1989. *A Classification of IGNEOUS ROCKS and Glossary of Terms*, pp. 193 pp. Oxford: Blackwell, Scientific Publications.

Linthout, K., 1984. Alkali-zirconosilicates in peralkaline rocks. *Contributions to Mineralogy and Petrology* 86: 155–158.

Liversidge, A., 1888. *The Minerals of New South Wales, etc.*, pp. 326. London: Trübner & Co.

Lundstrom, C.C., 2000. Rapid diffusive infiltration of sodium into partially molten peridotite. *Nature* 403: 527–530.

Mackenzie, D.E., & A.J.R. White, 1970. Phonolite globules in basanite from Kiandra, Australia. *Lithos* 3: 309–317.

MacNevin, A.A., & G.G. Holmes, 1980. Gemstones. *New South Wales Geological Survey, Mineral Industry of New South Wales* 18, 119 pp.

Malíková, P., 1999. Origin of sapphires from the Jizerská Louka alluvial deposit in North Bohemia, Czech Republic, Europe. *Australian Gemmologist* 20(5): 202–206.

Matson, S.M., & G.R. Rossman, 1988. Fe^{2+}-Ti^{4+} charge transfer in stoichiometric Fe^{2+}, Ti^{4+} minerals. *Physics and Chemistry of Minerals* 16: 76–82.

McDonough, W.F., & F.A. Frey, 1987. Rare earth elements in upper mantle rocks. In: *Geochemistry and Mineralogy of the Rare Earth Elements, Reviews in Mineralogy*, ed. B.R. Lipin & G.A. McKay, vol 21, chapt 5, pp. 99–145. Washington DC: Mineralogical Society of America.

McKenzie, D., & R.K. O'Nions, 1991. Partial melt distributions from inversion of rare earth element concentrations. *Journal of Petrology* 32: 1021–1091.

Morris, P.A., 1986. Constraints on the origin of the mafic alkaline volcanics and included xenoliths from Oberon, New South Wales, Australia. *Contributions to Mineralogy and Petrology* 93: 207–214.

Mumme, I.A., 1988. *The World of Sapphires—Their Occurrence, Discrimination, Synthesis and Valuation*, pp. 189. Sydney: Mumme Publications.

Neumann, E.-R., & E. Wulff-Pedersen, 1997. The origin of highly silicic glass in mantle xenoliths from the Canary Islands. *Journal of Petrology* 39: 1413–1539.

Neville, B.J., & F. von Gnielinski, 1998. Australiens sapphire largestatten. In: *Rubin, Saphir, Korund*, pp. 70–75, Extra Lapis No. 15. Münich: Christian Weise Verlag.

Neville, B.J., & F. von Gnielinski, 1999. Gemstones. Sapphire and ruby in Australia. *Queensland Government Mining Journal* 100 (1171): 6–12.

Nielsen, R., 1998, 12 August. Geochemical earth reference model: trace element partitioning information. Internet address: http://www-ep.es.llnl.gov/germ/partitioning.html.

Oakes, G.M., L.M. Barron & S.R. Lishmund, 1996. Alkali basalt and associated volcaniclastic rocks as a source of sapphire in eastern Australia. *Australian Journal of Earth Sciences* 43: 289–298.

O'Connor, T.K., A.D. Edgar & F.E. Lloyd, 1996. Origin of glass in Quaternary Mantle Xenoliths from Meerfeldermaar, West Eifel, Germany: implications for enrichment in the lithospheric mantle. *The Canadian Mineralogist* 34: 187–200.

Oliver, J.G., & I.J. Townsend, 1993. *Gemstones in Australia*, pp. 72. Canberra: Australian Government Publishing Service.

O'Reilly, S.Y., 1989. Xenolith types distribution and transport. In: *Intraplate Volcanism in Eastern Australia and New Zealand*, ed. R.W. Johnson, pp. 249–253. Cambridge: Cambridge University Press.

O'Reilly, S.Y., & W.L. Griffin, 1984. Sr isotopic heterogeneity in primitive basaltic rocks, south-eastern Australia: correlation with mantle metasomatism. *Contributions to Mineralogy and Petrology* 87: 220–230.

O'Reilly, S.Y., & W.L. Griffin, 1988. Mantle metasomatism beneath western Victoria, Australia: I. Metasomatic processes in Cr-diopside lherzolites. *Geochimica et Cosmochimica Acta* 52: 433–447.

O'Reilly, S.Y., & W.L. Griffin, 2000. Apatite in the mantle: implications for metasomatic processes and high heat production in Phanerozoic mantle. *Lithos* 43: 217–232.

O'Reilly, S.Y., W.L. Griffin & O. Gaul, 1997. Palaeogeothermal gradients in Australia. Key to 4-D lithosphere mapping, *AGSO Journal of Australian Geology and Geophysics* 17: 63–72.

O'Reilly, S.Y., W.L. Griffin & A. Stabel, 1988. Evolution of eastern Australian lithosphere: Isotopic evidence for magmatic and tectonic underplating. In: *Oceanic and continental Lithosphere: Similarities and differences*, ed. M.A. Menzies & K.G. Cox, pp. 89–108. Oxford: Journal of Petrology Special Volume, Oxford University Press.

O'Reilly, S.Y., & M. Zhang, 1995. Geochemical characteristics of lava-field basalts from eastern Australia and inferred sources: connections with the subcontinental lithospheric mantle? *Contributions to Mineralogy and Petrology* 121: 148–170.

Panter, K.S., P.R. Kyle & J.L. Smellie, 1997. Petrogenesis of a phonolite-trachyte succession at Mount Sidley, Marie Byrd Land, Antarctica. *Journal of Petrology* 38: 1225–1253.

Pecover, S.R., 1993. The geology and mining of the Strathdarr sapphire deposit, New England gemfields, northeastern New South Wales. In: *New England Orogen, eastern Australia*, ed. P.G. Flood & J. Aitchison, pp. 83–491. Armidale: Department of Geology and Geophysics, University of New England.

Pecover, S.R., 1996. Sapphire-producing Cretaceous/Tertiary volcano-fluvial deposits in eastern Australia. In: *Mesozoic 96. Mesozoic Geology of the Eastern Australia Plate Conference. Geological Society of Australia Extended Abstracts* 43: 442–449.

Pupin, J.P., 1980. Zircon and granite petrology. *Contributions to Mineralogy and Petrology* 73: 207–220.

Pupin, J.P., & G. Turco, 1974. Contrôle thermique du developpment de la muscovite dans les granitoides et morphologie du zircon. *Compte Rendue de l'Academie des Sciences, Paris* 278 (D): 2719–2722.

Roach, I.C., 1999. The setting, structural control, geochemistry and mantle source of the Monaro Volcanic Province, southeastern New South Wales, Australia, *PhD thesis*, University of Canberra (unpubl.).

Robertson, A.D.C., & F.L. Sutherland, 1992. Possible origins and ages for sapphires and diamond from the central Queensland gemfields. In: *R.O. Chalmers Commemorative papers (Mineralogy, Meteoritics, Geology)*, ed. F.L. Sutherland, pp. 45–54. *Records of the Australian Museum, Supplement* 15.

Roeder, P.L., & R.F. Emslie, 1970. Olivine-liquid equilibrium. *Contributions to Mineralogy and Petrology* 29: 275–289.

Scarrow, J.H., & K.G. Cox, 1995. Basalts generated by decompressive adiabatic melting of a mantle plume: a case study from the Isle of Skye, NW Scotland. *Journal of Petrology* 36: 3–22.

Scheibner, E., & H. Basden, eds., 1996. Geology of New South Wales—Synthesis. Volume 1. Structural Framework. *Geological Survey of New South Wales, Memoir Geology* 13(1), pp. 295.

Schiano, P., & R. Clocchiatti, 1994. World wide occurrence of silica-rich melts in sub-continental and sub-oceanic mantle minerals. *Nature* 368: 621–624.

Schiano, P., R. Clocchiatti, B. Bourdon, K.W. Burton & B. Thellier, 2000. The composition of melt inclusions in minerals at the garnet-spinel transition zone. *Earth and Planetary Science Letters* 174: 375–383.

Schmetzer, K., H.A. Hänni, H.-J. Bernhardt & D. Schwarz, 1996. Trapiche rubies. *Gems & Gemology* 32 (winter issue): 242–250.

Schwarz, D., & W.B. Stern, 2000. Chemical fingerprinting as a tool for the characterization of gem corundums from different genetic environments. *Abstracts Volume* [CD ROM], *31st International Geological Congress* 16–17 August, Rio de Janiero, Brazil.

Schwarz, D., J. Kanis & K. Schmetzer, 2000. Sapphires from Ambondromifehy region, Antisiranana Province, northern Madagascar. *Gems & Gemology* 36(fall issue): 216–233.

Schwarz, D., E.J. Petsch & J. Kanis, 1996. Sapphires from the Andranondambo region, Madagascar. *Gems & Gemology* 32 (summer issue): 80–99.

Shaw D. M., 1970. Trace element fractionation during anatexis. *Geochimica et Cosmochimica Acta* 34: 237–243.

Simons, F.J., A. Zielhuis & R.D. van der Hilst, 1999. The deep structure of the Australian continent from surface wave tomography. *Lithos* 48: 17–43.

Speer, J.A., 1982. Zircon. In: *Reviews in Mineralogy*, vol. 5, Orthosilicates, chapt. 3, ed. P.H. Ribbe, pp. 67–112. Washington DC: Mineralogical Society of America.

Spry, M.J., D.L. Gibson & R.A. Eggleton, 1999. Tertiary evolution of the coastal lowlands and the Clyde River palaeovalley in southeast New South Wales. *Australian Journal of Earth Sciences* 46: 173–180.

Stephenson, P.J., 1989. Northern Queensland. In: *Intraplate Volcanism in Eastern Australia and New Zealand*, ed. R.W. Johnson, pp. 89–97. Cambridge: Cambridge University Press.

Stephenson, P.J., 1990. The geological context of sapphire occurrences in the Anakie region, central Queensland. *Geological Society of Australia Abstracts Series* 25: 232–233.

Stern, W.B., 1984. Zur simultan analyse von silicaten (hauptokomponenenten, spuren) mittels energie-dispersiver Röntgenfluoreszence-spertrometrie (EDS-XFA). *Fresenius Zeitschrift fuer Analytische Chemie* 2560: 1–9.

Stuart-Smith, P.G., 1990. The structure and tectonics of the Tumut region, N.S.W.: data record and summary of investigations 1986–1989. *Bureau of Mineral Resources, Australia, Record* 1990/78, pp. 41 (unpublished).

Sun, S.-S. & W.F. McDonough, 1989. Chemical and isotopic systematics of oceanic basalts; implications for mantle composition and processes. In: *Magmatism in the Ocean Basins*, ed. A.D. Saunders & M.J. Norry. *Geological Society of London Special Publication* 4(2): 313–346.

Sunagawa, I., H.-J. Bernhardt & K. Schmetzer, 1999. Texture formation and element partitioning in trapiche ruby. *Journal of Crystal Growth* 206: 322–330.

Sutherland, F.L., 1996. Alkaline rocks and gemstones, Australia: a review and synthesis. *Australian Journal of Earth Sciences* 43: 323–343.

Sutherland, F.L., 1998. Origin of north Queensland Cenozoic volcanism: Relationships to long lava flow basaltic fields, Australia. *Journal of Geophysical Research* 103(B11): 27347–27358.

Sutherland, F.L., 1999. Volcanism, geotherms, gemstones and lithosphere, since orogenesis, N.E. New South Wales: A Synthesis. In: *New England Orogen; Regional Geology, Tectonics and Metallogenesis*, ed. P.G. Flood, pp. 355–364. Armidale, NSW: Earth Sciences, University of New England.

Sutherland, F.L., & R.R. Coenraads, 1996. An unusual ruby-sapphire-spinel assemblage from the Tertiary Barrington volcanic province, New South Wales. *Mineralogical Magazine* 60: 623–638.

Sutherland, F.L., & C.M. Fanning, 2001. Gem-bearing basaltic volcanism, Barrington, New South Wales: Cenozoic evolution, based on basalt K-Ar ages and zircon fission track and U-Pb isotope dating. *Australian Journal of Earth Sciences* 48: 221–237.

Sutherland, F.L., & D. Schwarz, 2001. Origin of gem corundums from basaltic fields. *Australian Gemmologist* 21(1): 30–33.

Sutherland, F.L., A. Ewart, L.R. Raynor, J.D. Hollis & W.D. McDonough, 1989. Tertiary basalt magmas and the Tasmanian lithosphere. In: *Geology and Mineral Resources of Tasmania*, ed. C.F. Burrett & E.L. Martin. *Geological Society of Australia Special Publication* 15: 386–398.

Sutherland, F.L., D.F. Hendry, B.J. Barron, W.L. Matthews & J.D. Hollis, 1996. An unusual Tasmanian Tertiary basalt sequence, near Boat Harbour, Northwest Tasmania. *Records of the Australian Museum* 48: 131–161.

Sutherland, F.L., P.W.O. Hoskin, C.M. Fanning & R.R. Coenraads, 1998a. Models of corundum origin from alkali basaltic terrains: a reappraisal. *Contributions to Mineralogy and Petrology* 133: 356–372.

Sutherland, F.L., R.E. Pogson & B.J. Barron, 1998b. Discussion and Reply. Palaeogeothermal gradients in Australia: key to 4-D lithosphere mapping, S.Y. O'Reilly, W.L. Griffin & O. Gaul. *Australian Journal of Earth Sciences* 45: 817–821.

Sutherland, F.L., R.E. Pogson & J.D. Hollis, 1993. Growth of the central New England basaltic gemfields, New South Wales, based on zircon fission track dating. In *New England Orogen, Eastern Australia*, ed. P.G. Flood & J. Aitchison, pp. 483–491. Armidale, NSW: Department of Geology and Geophysics, University of New England.

Sutherland, F.L., D. Schwarz, R.R. Coenraads, G. Webb & T. Coldham, 1999. Origin of chromium-coloured gem corundums, Australia. In: *Abstracts. 17th International Gemmological Conference, Goa, India—1999*, pp. 37–39. Bombay: Forum of Indian Gemmologists for Scientific Studies.

Sutherland, F.L., D. Schwarz, E.A. Jobbins, R.R. Coenraads & G. Webb, 1998c. Distinctive gem corundum suites from discrete basalt fields: a comparative study of Barrington, Australia, and West Pailin, Cambodia, gemfields. *Journal of Gemmology* 26: 65–85.

Sweeny, B., 1996. Interesting gems from north-east Tasmania. *Australian Gemmologist* 19: 264–267.

Tera, F., & G.F. Wasserburg, 1972. U-Th-Pb systematics in lunar rocks. *Earth and Planetary Science Letters* 14: 281–304.

Upton, B.G.J., R.W. Hinton, P. Aspen, A. Finch & J.W. Valley, 1999. Megacryst and associated xenoliths: Evidence for migration of geochemically enriched melts in the upper mantle beneath Scotland. *Journal of Petrology* 40: 935–956.

Vallance, T.G., 1953. Studies in the metamorphic and plutonic geology of the Wantabadgery-Adelong-Tumbarumba district, N.S.W. Part I. Introduction and metamorphism of the sedimentary rocks. *Linnean Society of New South Wales—Proceedings* 78(3–4): 90–121.

Vallance, T.G., 1954a. Studies in the metamorphic and plutonic geology of the Wantabadgery-Adelong-Tumbarumba district, N.S.W. Part II. Intermediate basic rocks. *Linnean Society of New South Wales—Proceedings* 78(5–6): 181–196.

Vallance, T.G., 1954b. Studies in the metamorphic and plutonic geology of the Wantabadgery-Adelong-Tumbarumba district, N.S.W. Part III. The granitic rocks. *Linnean Society of New South Wales—Proceedings* 78(5–6): 197–220.

Vavra, G., 1990. On the kinematics of zircon growth and its petrological significance: a cathodoluminesence study. *Contributions to Mineralogy and Petrology* 106: 90–99.

Vavra, G., 1994. Systematics of internal zircon morphology in major Variscan granitoid types. *Contributions to Mineralogy and Petrology* 117: 31–344.

Wass, S.Y., 1980. Geochemistry and origin of xenolith-bearing and related alkali basaltic rocks from the Southern Highlands, New South Wales. *American Journal of Science* 280(A): 639–666.

Watson, E.B., 1979. Zircon saturation in felsic liquids: Experimental results and applications to trace element geochemistry. *Contributions to Mineralogy and Petrology* 70: 407–419.

Wellman, P., & I. McDougall, 1974. Potassium-argon ages of the Cainozoic volcanic rocks of New South Wales, Australia. *Journal of the Geological Society of Australia* 21: 247–272.

White, A.J.R., & B.W. Chappell, 1989. *Geology of the Numbla 1:100,000 Sheet (8624)*. Sydney: Geological Survey of New South Wales, Department of Minerals and Energy.

Wiechert, U., D.A. Ionov & K.H. Wedepohl, 1997. Spinel peridotite xenoliths from the Afsagin-Dush volcano, Darigana lava plateau, Mongolia: a record of partial melting and cryptic metasomatism in the upper mantle. *Contributions to Mineralogy and Petrology* 126: 345–364.

Wilkinson, J.F.G., & H.D. Hensel, 1991. An analcime mugearite-megacryst association from north eastern New South Wales: implications for high-pressure amphibole dominated fractionation of alkaline magmas. *Contributions to Mineralogy and Petrology* 127: 272–290.

Wilkinson, J.F.G., & R.W. Le Maitre, 1987. Upper mantle amphiboles and micas and TiO_2, K_2O and P_2O_5 abundances and 100Mg/(Mg+Fe^{2+}) ratios of common basalts and andesites: Implications for modal mantle metasomatism and undepleted mantle compositions. *Journal of Petrology* 28: 37–73.

Willis, J.L., 1972. Mining History of the Tumbarumba Gold Field. *Geological Survey of New South Wales Bulletin* 23, pp. 633 and 4 maps.

Wilshire, H.G., & A.V. McGuire, 1996. Magmatic infiltration and melting in the lower crust and upper mantle beneath the Cima volcanic field, California. *Contributions to Mineralogy and Petrology* 123: 358–374.

Worden, J.M., H. Baadsgaard, D.N. Cracknell & D. Krstic, 1996. Major extensional events recorded by zircon xenocrysts from the central Queensland gemfields. In *Mesozoic 96. Mesozoic Geology of the Eastern Australia Plate Conference*. *Geological Society of Australia Extended Abstracts* 43: 569–573.

Yaxley, G.M., D.H. Green & V. Kamenetsky, 1998. Carbonatite metasomatism in south eastern Australian lithosphere. *Journal of Petrology* 39: 1917–1930.

Yaxley, G.M., & V. Kamenetsky, 1999. In situ origin for glass in mantle xenoliths from south eastern Australia: insights from trace element compositions of glasses and metasomatic phases. *Earth and Planetary Science Letters* 172: 97–109.

Young, R.W., & M.C. Brown, 2000. Cenozoic tectonics and landform evolution of the coast and adjacent highlands of southeast New South Wales. Discussion [authored by Young]. Reply [authored by Brown]. *Australian Journal of Earth Sciences* 47: 823–826.

Young, R., & I. McDougall, 1993. Long-term landscape evolution: Early Miocene and modern rivers in southern New South Wales, Australia. *Journal of Petrology* 101: 35–49.

Zhang, M., P.J. Stephenson, S.Y. O'Reilly, M.T. McCulloch & M. Norman, 2001. Petrogenesis and geodynamic implications of late Cenozoic basalts in North Queensland, Australia: trace element and Sr-Nd-Pb isotope evidence. *Journal of Petrology* 42: 685–719.

Zhang, M., & S.Y. O'Reilly, 1997. Multiple sources for basaltic rocks from Dubbo, eastern Australia: geochemical evidence for plume-lithosphere mantle interaction. *Chemical Geology* 136: 33–54.

Zielhuis, A., & R.D. van der Hilst, 1996. Upper mantle shear velocity beneath eastern Australia from inversion of wave forms from SKIPPY portable arrays. *Geophysical Journal International* 127: 1–16.

Zou, H., A. Zindler, X. Xu & Q. Qi, 2000. Major, trace element, and Nd, Sr and Pb isotope studies of Cenozoic basalts in SE China: mantle sources, regional variations, and tectonic significance. *Chemical Geology* 171: 33–47.

Manuscript received 6 November 2000, revised 12 March 2001 and accepted 13 March 2001.

Associate Editor: G.E. Edgecombe.